NUMERICAL SIMULATION OF OPTICAL WAVE PROPAGATION THROUGH RANDOM MEDIA

by

Jeongki Pack

Dissertation submitted to the Faculty of the

Virginia Polytechnic Institute and State University

in partial fulfillment of the requirements for the degree of

Doctor of Philosophy

in

Electrical Engineering

APPROVED:

David A. de Wolf, Chairman

Ioannis M. Besieris

Gary S. Brown

Ting C. Poon

Werner E. Kohler

September, 1988

Blacksburg, Virginia

NUMERICAL SIMULATION OF OPTICAL WAVE PROPAGATION THROUGH RANDOM MEDIA

by

Jeongki Pack

David A. de Wolf, Chairman

Electrical Engineering

(ABSTRACT)

The propagation of optical plane waves through a one-dimensional Gaussian phase screen and a two-dimensional Gaussian extended medium are simulated numerically, and wave statistics are calculated from the data obtained by the numerical simulation. For instantaneous realization of a random medium, a simplified version of the random-motion model [77] is used, and for wave-propagation calculation the wave-kinetic numerical method and/or the angular-spectral representation of the Huygens-Fresnel diffraction formula are used. For the wave-kinetic numerical method, several different levels of approximations are introduced, and the region of validity of those approximations is studied by single-realization calculations. Simulation results from the wave-kinetic numerical method are compared, either with those from the existing analytical expressions for the phase-screen problem, or with those from the Huygens-Fresnel diffraction formula for the extended-medium problem. Excellent agreement has been observed. Extension to two-dimensional media with the power-law spectrum or three-dimensional problems is straight-forward. We may also deal with space-time correlations using, for example, Taylor's *frozen-in* hypothesis.

Acknowledgements

I am sincerely grateful to Professor David A. de Wolf for his encouragement, invaluable and timely advice, and guidance throughout this work. I also would like to thank Professor Ioannis M. Besieris and Gary S. Brown for their encouragement and continuous interest in my work. Special thanks are due to Williams Richardson, a consultant in the Computing Center, who introduced me the Array Processor, without which many numerical results presented in this dissertation would not have been possible. Finally, I wish to thank my family for their patience and support during the course of this work.

Table of Contents

List of Illustrations

1. Introduction

When a wave field propagates through a medium with random fluctuations of refractive index, the wavefront and thus the resulting field or irradiance also undergo random fluctuations. Here, we restrict our discussion to continuous random media.

The twinkling of starlight in the turbulent atmosphere and the scintillation of cosmic radio sources due to electron density irregularities in the ionosphere or the interplanetary medium have been of great concern to astronomers. To communication engineers, theoretical prediction concerning the scintillation of radio signals (fading) by the ionosphere is important for the design of communication links between satellites and earth stations. These types of problems can be modeled by means of a phase screen. With the advent of the laser, people have become interested in optical-communication or laser-fusion systems. Thus, optical wave propagation through atmospheric turbulence has also been of great scientific interest since the early 1960s.

A great deal of progress has been made in the last two decades on theoretical studies of wave statistics through a random phase screen [1-28] and an extended medium [29-42], yet the behavior of electromagnetic waves in random media is not fully understood. Much effort has gone into finding analytical solutions of the problems.

The phase screen problem may be formulated rather easily, using the Huygens-Fresnel diffraction formula [43-45]. For lower-order statistical moments of the electric field, the resulting integral representations can be calculated either analytically [1-22] or numerically [23-28]. For higher-order moments, however, there are some difficulties.

In extended media, scalar wave fields are governed by the reduced wave equation (or parabolic equation in the small-angle approximation regime) [See, for example, 32-34]. Several methods have been proposed to solve this problem analytically. They are largely based on two techniques : perturbation theoretical methods (e. g. Born approximation, Rytov method, diagram method) and moment-equation methods. For strong fluctuations, diagram methods and moment-equation methods have been widely used [32-34]. We note that in this analytical approach, to obtain moments or moment equations we need a decoupling assumption for mixed correlations between the refractive index fluctuation and the corresponding wave field. For example, the moment equation for Γ_{nm} in the small-angle approximation regime with the delta correlation assumption (Markov approximation) is given by [32, 34] :

$$\{\frac{\partial}{\partial z} - \frac{i}{2k}[(\Delta_1 + \cdots + \Delta_n) - (\Delta'_1 + \cdots + \Delta'_m)] + \frac{k^2}{2} Q_{nm}\}\ \Gamma_{nm} = 0$$

where Q_{nm} is related to the transverse correlation function of the refractive index, and $\Gamma_{nm} = < u(\vec{\rho}_1, z) \ldots u(\vec{\rho}_n, z) u^*(\vec{\rho}_1', z) \ldots u^*(\vec{\rho}_m', z) >$.

In general, it is difficult to find analytical and even numerical solutions for higher-order moments. For lower-order moments, for example, $\Gamma_4 = < u(\vec{\rho}_1, z) u(\vec{\rho}_2, z) u^*(\vec{\rho}_1, z) u^*(\vec{\rho}_2, z) >$, asymptotic solutions are available in the limit of weak or strong fluctuations. There have also been many efforts to compute integral representations for moments, or to solve moment equations, numerically. The fourth-order moment of the field has been computed successfully [46-50], and the

differential equation for the coherence function or the Fourier transform of it (the second-order moment) has been solved either by the Monte Carlo method or by the finite-difference method [51-59].

In addition to Γ_{nm} (e. g. Γ_{22}, covariance of irradiance), another important statistical quantity is the probability distribution of irradiance $p(I)$, which we need to describe random irradiance fluctuations completely. It would be very difficult to predict $p(I)$ with the analytical approach mentioned above, since for a non-gaussian random process $I(\vec{\rho})$ all the higher-order moments , that is, $< I^n >$, $n = 1, 2, \ldots$, are needed. We note that several probability functions, based on phenomenological models, have been proposed [60-76]. These are not well established, except in the weak fluctuation region where the scintillation index, $\sigma_I^2 = < (I - < I >)^2 > / < I >^2$, is much smaller than 1, and in the saturation region where σ_I^2 is close to 1.

Due to the limitations of the analytical approach, people began to seek solutions by numerical experiments, using fast modern computers. In a numerical experiment, we simulate wave propagation through a random medium by instantaneous realizations of the medium (or by instantaneous realizations of the random phase in case of the phase screen problem), and compute wave statistics *a posteriori*. Once a sufficient data base for random irradiance fluctuations is obtained, any statistical quantity can be calculated in principle. Two things are crucial for the numerical simulation : (i) a model for realizing a random medium; (ii) a method of computing wave propagation through the medium.

The random media we are interested in are usually assumed to be statistically homogeneous Gaussian random processes. In such media, the statistical properties of the media are completely described by the correlation function (or the spectrum) of the fluctuating part of the refractive index, $\delta n = n - < n >$. At least one model for realizing $\delta n(\vec{r})$ with an arbitrary spectrum exists. In the random-motion model intro-

duced by de Wolf [77], a random medium can be represented as a weighted sum of Gaussians the centers of which are moving around randomly. The number density of the Gaussian eddies for each scale size can be calculated analytically for a given spectrum. This model can also be used to generate a random phase $\phi(\vec{r})$.

Note that linear-systems methods are also available for generating random phase fluctuations. The key ideas are as follows. First, we generate Gaussian white noise, and then introduce arbitrary correlations appropriately, for example by using linear system theory [78-84]. Such methods may be useful for one-dimensional random processes, but extension to higher-dimensional problems would not be easy.

Numerical studies of the one-dimensional phase screen exist [85-88]. The electromagnetic field behind a random phase screen can be represented by the Huygens-Fresnel formula with the corresponding initial random phase. (Note that for a very thick phase screen we have to use less well-understood techniques for extended media.) In preceding studies, the random phase $\phi(x)$ is generated appropriately (Franke et al. use the random-motion model [88], and Knepp and Rino et al. utilize the linear-system theory [86-87]), and the diffraction integral (or the angular-spectral representation of it) is computed using a fast Fourier transform algorithm.

At the completion of the present project, our attention was directed towards several numerical simulations in the area of underwater acoustics, which concern the fluctuations of acoustic signals due to random variations in the sound-speed field (internal waves) [89-90]. DeFerrari used a simplified model for sound-speed fluctuation $\delta c/c$, and computed the propagation of the acoustic field by the ray theory. Flatte et al. generated $\delta c/c$ for each predetermined rectangular mesh using a somewhat sophisticated algorithm, and then solved the corresponding parabolic equation of the acoustic field by the *split-step-Fourier* algorithm [91] which is equivalent to one of our

simulation schemes, i. e. the method utilizing the angular-spectral representation of the Huygens-Fesnel formula.

In this thesis, we present new simulation schemes and numerical results for both phase screen and extended medium. We are primarily interested in optical wave propagation in almost transparent refractive-index media with a large scale such that the smallest scale size of the medium is much larger than the wave length (e. g. atmosphere). The medium will also be assumed to be statistically homogeneous and Gaussian.

The methods and models used for simulation are discussed in Chap. 2. We choose the random-motion model mentioned before [77] to realize a random medium, since our preliminary work has indicated that it is more efficient than the method utilizing the linear-system theory [78-84]. (It should be mentioned here that initially we used the latter method to generate one-dimensional random angle fluctuations which result from a random Gaussian phase function.) We will neglect space-time correlations which can be incorporated in the random-motion model in its most general form, and thus different realizations are independent of each other. This general model is still complicated, numerically, and to reduce the computing time, we have to simplify it. In the simplified model, the entire volume of a medium is divided into thin slabs, and each slab is squeezed in such a way that all the Gaussian eddies in the slab are contained in a single transverse layer.

To compute irradiance for each realization of the medium we use the wave-kinetic numerical method [110-112] and/or the angular-spectral representation of the Huygens-Fresnel diffraction formula [43, 85]. There were specific reasons for using both methods. At first, the simulations involved only the wave-kinetic numerical method, since the usefulness of the Huygens-Fresnel formula for extended media appeared to be limited. Later, we found that the latter could be applied to extended

media with the simplified model mentioned above. (We notice in retrospect that this turns out to be equivalent to the *split-step-Fourier* algorithm applied directly to the parabolic equation [90,91].) This gives us a means of comparing usefulness (or efficiency) of both methods to each other.

The wave-kinetic theory has been introduced by Besieris and Tappert [93-100]. Related studies can be found elsewhere [101-108]. In the wave-kinetic theory, we describe the propagation of a wave in configuration space as the evolution of the Wigner distribution function (WDF) [92] in phase space (joint configuration-wavenumber space), which is governed by a wave-kinetic equation (or a transport equation).

In general, it is not possible to solve the kinetic equation for an arbitrary inhomogeneous media analytically. A method for numerical implementation of the wave kinetic theory (which we call the wave-kinetic numerical method) has been developed and tested for simple canonical problems by de Wolf and Pack [109-112]. The essential points are the following. The initial WDF which corresponds to an input beam or a plane wave is discretized into a sum of elementary Gaussian beamlets. If each beamlet is narrow enough, then the calculation of beamlet propagation may be simplified. Finally in the observation plane, all beamlets are put together again to yield the output WDF.

The Liouville approximation facilitates the calculation of beamlet propagation, even though it has a certain limited region of validity. In the Liouville approximation, the trajectory of each beamlet is governed by the classical G. O. (Geometrical Optics) trajectory equations [44-45], and the WDF is conserved along the ray trajectories. It follows that a closed-form expression for the output WDF (as a weighted sum of the elementary beamlets) can be found easily. The advantage of the wave kinetic approach over the conventional G. O. method, is that even for this lowest-order approximation some of the diffraction effects are incorporated. We wish to apply the

lower-order approximations, whenever applicable, especially, the Liouville approximation. Its regime of validity is somewhat limited, however, it is the simplest, and it is applicable to any configuration of inhomogeneities. A third or higher-order approximation can be made if necessary.

As we mentioned before, the well-known Huygens-Fresnel diffraction formula is very useful for a phase screen problem [1-28], since simulations for this problem can be done in various ways, simply by generating the random phase $\phi(\vec{\rho})$. In this research, the angular-spectrum approach will be used, instead of direct application of the formula. We note that for a one-dimensional phase screen we need two Fourier transform operations, which can be done by the fast Fourier transform. The angular-spectral representation allows more efficient computation, especially for a plane wave, since the angular spectrum of a plane wave is very narrow. This may also applied to extended media by proper rearrangement of the Gaussian eddies, namely, by using the simplified model. This method is a good simulation algorithm in itself, and it can also be used as a check for the wave-kinetic numerical method.

We have applied the simulation schemes to plane-wave propagation through a one-dimensional Gaussian phase screen and a two-dimensional Gaussian extended medium. The numerical results and discussions are presented in Chap. 3 and Chap. 4, respectively. To obtain data for wave statistics, we put receivers across the observation plane, and store the data from each receiver for many realizations (approximately 1000 realizations). To compute statistical quantities, we will use standard estimators for the quantities [114]. Sometimes, there appear extraordinary samples, so called *outliers*, for some realizations. If that happens, then those outliers may be removed by techniques generally used for statistical estimations.

We note that the Gaussian correlation function (or spectrum) is not physical. A power-law spectrum is generally accepted as a more realistic model for atmospheric

turbulence. For the Kolmogorov spectrum, it is proportional to $K^{-11/3}$ (or $K^{-8/3}$ for the two-dimensional problem). For the Gaussian spectrum, however, there is only one scale size, which permits simple formulations and a reduction in computation time. In addition, for the Gaussian phase screen an analytical expression for the covariance of irradiance $C_I(x)$ which can be integrated numerically without any difficulty is available [26]. Thus, the results from the numerical simulation may be compared easily to a known analytical result. The numerical simulation for the power-law spectrum can be done similarly, because it may also be represented as a weighted sum of Gaussians.

The simplified model mentioned above has certain advantages. It allows easier corrections to the lower-order approximations for the wave-kinetic numerical method, and application of the Huygens-Fresnel formula to extended media. In addition, the model (together with the linear interpolation scheme used for phase and angle calculations) reduces computing time considerably, and thus it permits the numerical simulation for extended media within a reasonable time.

2. Methods and Models for Simulation

In this chapter, methods and models for simulation will be discussed in their general context. The detailed discussions and calculations for specific applications will be presented in subsequent chapters.

As mentioned in the introduction, we choose the random-motion model and use a simplified version, to simulate refractive-index fluctuations numerically. To compute a wave field or irradiance for each realization, the wave-kinetic numerical method and the Huygens-Fresnel diffraction formula will be used. The usefulness of both methods will be compared to each other later.

2.1 Assumptions for Refractive-Index Fluctuations

Consider a wave propagating through a continuous random medium. The behavior of the wave field in this type of medium is entirely determined by refractive-index fluctuations. Let us define the fluctuating part of the refractive index as

$$\delta n(\vec{r}) = n(\vec{r}) - < n(\vec{r}) > \tag{2.1}$$

We assume that $\delta n(\vec{r})$ is a statistically homogeneous Gaussian random function. The statistical properties of such a medium are adequately described by the correlation function of $\delta n(\vec{r})$,

$$B_n(\vec{r}) = < \delta n(\vec{r} + \vec{r}\,') \, \delta n(\vec{r}\,') > \ , \tag{2.2}$$

or more conveniently by the corresponding spectrum,

$$\Phi_n(\vec{K}) = \frac{1}{(2\pi)^3} \int_{-\infty}^{\infty} d^3r \ e^{-i\vec{K}\cdot\vec{r}} \ B_n(\vec{r}) \ . \tag{2.3}$$

Further, we assume that the smallest scale size ℓ of the medium is much larger than the wavelength λ , and that the fluctuation is weak, $|\delta n| \ll 1$. In such a medium, an input wave scatters predominantly in the forward direction and the (backward) reflections are negligible, so that a small angle approximation (or a quasi-optical approximation) will hold.

The electric field of a monochromatic optical wave satisfies the vector wave equation [33],

$$\nabla^2\vec{E} + k^2 n^2 \vec{E} + 2\nabla(\vec{E}\cdot\nabla \ln n) = 0 \ , \tag{2.4}$$

where the convention, $e^{-i\omega t}$, is used for time dependence, and the medium is assumed to be isotropic. With the aforementioned assumption, $\ell \gg \lambda$, one may neglect the depolarization term, i. e. , the last term in (2.4). Since the resulting equation may be decomposed into three scalar equations, the wave equation reduces to the Helmholtz equation

$$\nabla^2 E + k^2 n^2 E = 0 \ . \tag{2.5}$$

For a wave propagating in the positive z- direction, it is convenient to let

$$E(\vec{r}) = u(\vec{\rho}, \ z) e^{ikz} \ . \tag{2.6}$$

Substitution of (2.6) and (2.1) with $< n(\vec{r}) > = 1$ in (2.5) leads to

$$\frac{\partial^2 u}{\partial z^2} + 2ik\frac{\partial u}{\partial z} + \Delta u + 2k^2 \delta n\, u = 0 \ , \quad (\Delta = \frac{\partial^2}{\partial x^2} + \frac{\partial^2}{\partial y^2}) \ , \tag{2.7}$$

where the condition, $|\delta n| \ll 1$, is used.

If the spectral content of the refractive-index fluctuation, $\Phi_n(K)$, is contained well within the wavenumber k, i. e., $\ell \gg \lambda$, then $u(\vec{\rho}, z)$ is a slowly varying function of z, and one can assume that $|\partial^2 u/\partial z^2| \ll 2k\,|\partial u/\partial z|$. It follows that the scalar wave equation becomes a parabolic wave equation [32-34, 116]:

$$\left[\frac{\partial}{\partial z} - \frac{i}{2k}\nabla - ik\,\delta n(\vec{\rho}, z)\right] u(\vec{\rho}, z) = 0 \ , \tag{2.8}$$

with an initial condition $u(\vec{\rho}, z = 0) = u_0(\vec{\rho})$. This is our starting equation.

2.2 Random-Motion Model

In the random-motion model [77], a random medium can be simulated with a weighted sum of Gaussian eddies:

$$\delta n(\vec{r}, t) = \sum_{j=1}^{M} \sum_{i=1}^{N_j} q_{ij}\, A(\ell_j)\, e^{-|\vec{r} - \vec{R}_{ij}(t)|^2/\ell_j^2}, \tag{2.9}$$

where $q_{ij} = \pm 1$ in a random fashion, $A(\ell_j)$ is a weight for each eddy with size ℓ_j, and $R_{ij}(t)$ are eddy centers which are moving around randomly [cf. Fig. 2.1]. We note that ℓ_j may be continuous. In the following, we will neglect space-time correlations, and thus different realizations are independent of each other.

To calculate statistics of the medium, it is more convenient to write (2.9) at any fixed time t as:

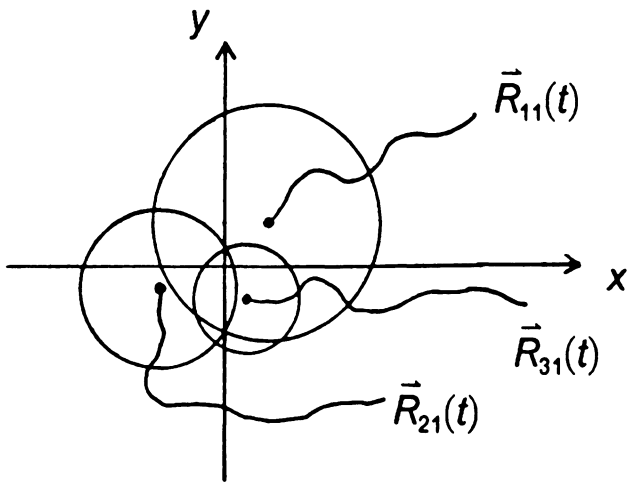

Figure 2.1 Random-motion model.

$$\delta n(\vec{r}) = \sum_{i=1}^{N} q_i \psi_i(\vec{r} - \vec{R}_i, \ell_i) \ , \tag{2.10}$$

where

$$\psi_i(\vec{r}, \ell_i) = A\, e^{-r^2/\ell_i^2} \ . \tag{2.11}$$

Here, the weight for each Gaussian eddy, $A(\ell_j)$, is assumed to be constant. For convenience, we let $A^2 = < \delta n^2 >$ in the following. Using this expression, one may show that [77]:

$$< \delta n(\vec{r}) > = 0 \ , \tag{2.12}$$

and

$$B_n(\vec{r}) = (2\pi)^3 \sum_i \frac{1}{V} \int_{-\infty}^{\infty} d^3K \ |\Psi_i(\vec{K}, \ell_i)|^2 \, e^{i\vec{K}\cdot\vec{r}} \ , \tag{2.13}$$

where V is the volume to which the Gaussian eddies are confined, and $\Psi_i(\vec{K}, \ell_i)$ is the Fourier transform of $\psi_i(\vec{r}, \ell_i)$, which is defined as

$$\psi_i(\vec{r} - \vec{R}_i, \ell_i) = \int_{-\infty}^{\infty} d^3K \ \Psi_i(\vec{K}, \ell_i) \, e^{i\vec{K}\cdot(\vec{r} - \vec{R}_i)} \ . \tag{2.14}$$

We now assume that the scale lengths $\ell_i = s$ are continuous, with s being the corresponding size parameter. Let $n(s)ds$ be the number density of eddies (per unit volume), the size of which lies between s and $s + ds$. It follows then that

$$B_n(\vec{r}) = \int_{-\infty}^{\infty} d^3K \ \Phi_n(\vec{K}) \, e^{i\vec{K}\cdot\vec{r}} \ , \tag{2.15}$$

with

$$\Phi_n(\vec{K}) \equiv (2\pi)^3 \int_0^{\infty} ds \ n(s) \, |\Psi(\vec{K}, s)|^2 \ . \tag{2.16}$$

In (2.16), $\Psi(\vec{K},\ s)$ is the Fourier transform of $\psi(\vec{r},\ s) = <\delta n^2>^{1/2} e^{-r^2/s^2}$:

$$\Psi(\vec{K},\ s) = (2\sqrt{\pi})^{-3} <\delta n^2>^{1/2} s^3\, e^{-K^2 s^2/4} \ . \tag{2.17}$$

Let us now define $p = K^2$ and $\zeta = \frac{1}{2} s^2$. Equation (2.16) then becomes

$$G(p) = \int_0^\infty d\zeta\ F(\zeta)\, e^{-p\zeta} \ , \tag{2.18}$$

where $G(p)$ and $F(\zeta)$ are related to $\Phi_n(K)$ and $n(s)$, respectively, by $G(p = K^2) = \Phi_n(K)$ and $F(\zeta = \frac{1}{2} s^2) = 2^{-3} <\delta n^2> s^5\, n(s)$. Thus, for a given spectrum $\Phi_n(K)$ we may compute $F(\zeta)$, and therefore $n(s)$, by the inverse Laplace transform of $G(p)$.

For a two-dimensional problem, this can be done similarly. We define a two-dimensional spectrum as

$$\Phi_{n,2}(\vec{\kappa}) = \int_{-\infty}^{\infty} dK_y\ \Phi_n(\vec{\kappa},\ K_y) \ , \quad \vec{\kappa} = (K_x, K_z) \ . \tag{2.19}$$

Let $\psi_2(\vec{r},\ s) = <\delta n^2>^{1/2} e^{-r^2/s^2}$ as in the three-dimensional case, where $\vec{r} = (x, z)$. Following the same procedure, we can show that

$$\Phi_{n,2}(\vec{\kappa}) = (2\pi)^2 \int_0^\infty ds\ n(s)\, |\Psi_2(\vec{\kappa},\ s)|^2 \ , \tag{2.20}$$

where $\Psi_2(\vec{\kappa},\ s) = (2\sqrt{\pi})^{-2} <\delta n^2>^{1/2} s^2\, e^{-\kappa^2 s^2/4}$. As in the three-dimensional case, this may also be rewritten as the inverse Laplace transform relation,

$$G_2(p) = \int_0^\infty d\zeta\ F_2(\zeta)\, e^{-p\zeta} \ , \tag{2.21}$$

where $G_2(p = \kappa^2) = \Phi_{n,2}(\kappa)$ and $F_2(\zeta = \frac{1}{2} s^2) = 2^{-2} < \delta n^2 > s^3 n(s)$.

We are interested mainly in two spectral models: the Kolmogorov spectrum and the Gaussian spectrum. Atmospheric turbulence is usually described by the Kolmogorov spectrum [32-34]:

$$\Phi_n(K) = \alpha C_n^2 K^{-11/3} \qquad \text{for } 2\pi/L_0 \ll K \ll 2\pi/\ell_0 , \tag{2.22}$$

where $\alpha \simeq 0.033$, and ℓ_0, L_0 are the inner- and the outer-scale of turbulence, respectively. The *structure constant* C_n^2 is related to the variance of refractive-index fluctuations $< \delta n^2 >$ by [34]:

$$C_n^2 \simeq 1.91 \ < \delta n^2 > L_0^{-2/3} \ . \tag{2.23}$$

Since the Kolmogorov spectrum is valid only for the so called *inertial subrange*, another mathematical model, i. e., the von Karman spectrum, which is valid for all K, is often used [33, 34]:

$$\Phi_n(K) = \alpha C_n^2 (K^2 + L_0^{-2})^{-11/6} e^{-K^2/k_m^2} , \tag{2.24}$$

where $k_m = 5.92/\ell_0$. We note that this reduces to the Kolmogorov spectrum in the inertial subrange, but is mathematically more convenient in a number of relevent integrals.

Although the Gaussian spectrum has little physical significance, it is often used due to its mathematical simplicity. It is given by

$$\Phi_n(K) = (2\sqrt{\pi})^{-3} \ell^3 < \delta n^2 > \ e^{-K^2 \ell^2/4} , \tag{2.25}$$

which is obtained by taking the Fourier transform [cf. Eq. (2.3)] of the Gaussian correlation function,

$$B_n(r) = <\delta n^2> \; e^{-r^2/\ell^2} \; . \tag{2.26}$$

The corresponding two-dimensional spectra can be calculated using the relation given by (2.19) [cf. Appendix A2.1]. The two-dimensional von Karman spectrum is then given by

$$\Phi_{n,2}(\kappa) \simeq \frac{\sqrt{\pi}\,\Gamma(4/3)}{\Gamma(11/6)} \; \alpha \, C_n^2 \, (\kappa^2 + L_0^{-2})^{-4/3} \, e^{-\kappa^2/k_m^2} \; , \tag{2.27}$$

for $\kappa \ll k_m$, and the two-dimensional Gaussian spectrum becomes

$$\Phi_{n,2}(\kappa) = (2\sqrt{\pi})^{-2} \, \ell^2 <\delta n^2> \; e^{-\kappa^2 \ell^2/4} \; . \tag{2.28}$$

By taking the inverse Laplace transforms properly, we can calculate the number densities of the eddies per unit volume (per unit area in case of two-dimensional problems) per unit scale length, $n(s)$, for the spectrums given above [cf. Appendix A2.2]. For the three-dimensional von Karman spectrum, we obtain

$$n(s) = \frac{2^{13/6} \, \alpha \, C_n^2}{\Gamma(11/6) <\delta n^2>} \; (s^2 - 2\ell_m^2)^{5/6} \, s^{-5} \, e^{-(s^2 - 2\ell_m^2)/2L_0^2} \quad \text{for } s^2 \geq 2\ell_m^2 \; , \tag{2.29}$$

where $\ell_m = 1/k_m$. We note that $n(s) = 0$ for $s^2 < 2\ell_m^2$. Substituting the values for α and C_n^2, we get

$$n(s) \simeq 0.3 \, L_0^{-2/3} \, s^{-10/3} \left[1 - 2(\ell_m/s)^2\right]^{5/6} e^{-s^2/2L_0^2} \quad \text{for } s^2 \geq 2\ell_m^2 \; , \tag{2.30}$$

where the term $e^{-\ell_m^2/L_0^2}$ is neglected since $\ell_m \ll L_0$.

For the two-dimensional von Karman spectrum, similar calculations lead to

$$n(s) = \frac{2^{5/3}\sqrt{\pi}\ \alpha\ C_n^2}{\Gamma(11/6) < \delta n^2 >} (s^2 - 2\ell_m^2)^{1/3} s^{-3} e^{-(s^2 - 2\ell_m^2)/2L_0^2}$$
$$\simeq 0.377\ L_0^{-2/3}\ s^{-7/3} [1 - 2(\ell_m/s)^2]^{1/3}\ e^{-s^2/2L_0^2} \qquad \text{for } s^2 \geq 2\ell_m^2\ , \tag{2.31}$$

and $n(s) = 0$ for $s^2 < 2\ell_m^2$.

The calculations for Gaussian spectra are straightforward:

$$n(s) = \frac{8}{\pi^{3/2}} \ell^{-3}\ \delta(s - \ell/\sqrt{2})\ , \tag{2.32}$$

for the three-dimensional Gaussian spectrum, and

$$n(s) = \frac{4}{\pi} \ell^{-2}\ \delta(s - \ell/\sqrt{2})\ , \tag{2.33}$$

for the two-dimensional Gaussian spectrum, where $\delta(s)$ is the Dirac delta function.

Notice that there is only one scale size, $\ell/\sqrt{2}$, for the Gaussian spectrum. The corresponding number density per unit volume (or per unit area in case of two-dimensional problems) can be calculated by integrating $n(s)$ with respect to the scale size s:

$$N_V = \int_0^\infty n(s)\ ds\ . \tag{2.34}$$

For the von Karman spectrum (or for the Kolmogorov spectrum), however, the scale sizes are continuously distributed, the dependence on s being $s^{-10/3}$ (or $s^{-7/3}$ for the two-dimensional spectrum) in the inertial subrange. To implement this, one may discretize the scale size s , linearly with a spacing Δs (or in logarithmic scale) [cf. Eq. (2.9)]:

$$N_{V,j} = \int_{s_j - \Delta s/2}^{s_j + \Delta s/2} n(s)\ ds\ , \tag{2.35}$$

phase screen

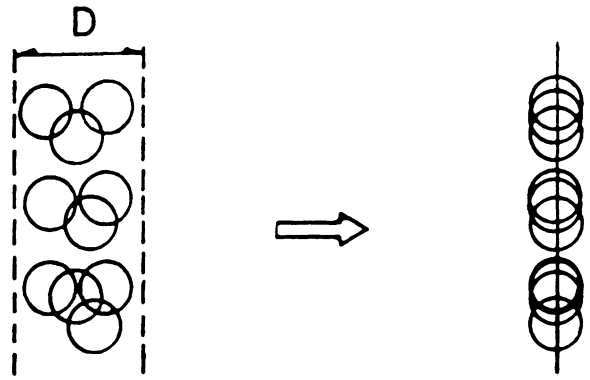

extended medium

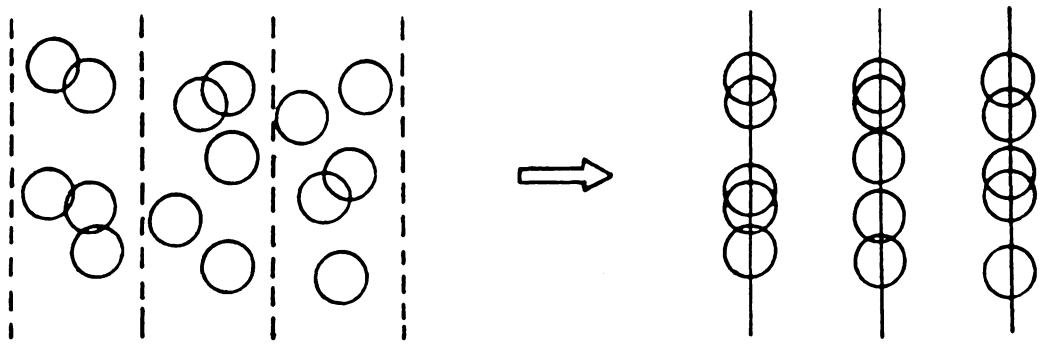

Figure 2.2 Simplified model.

where $s_j = s_{min} + (j - 1/2)\,\Delta s$, $(j = 1, 2, \ldots, M)$, with $s_{min} = \sqrt{2}\,\ell_m$ and $s_{max} = s_M + \Delta s/2 \sim O(L_0)$.

We can easily implement this general model directly. However, it is still complicated, numerically. To reduce the computing time, we have to simplify it. In the simplified model, we treat a phase screen as a thin slab if possible (if it exceeds a critical thickness, then it has to be treated as an extended medium), and for an extended medium we divide the entire volume of the medium into thin slabs. All the eddies in each slab are projected into a single transverse plane (or a line in case of two-dimensional problems), as shown in Fig. 2.2. Here it is assumed that the refractive-index fluctuation is weak enough, i. e., $|\delta n| \ll 1$, so that the above simplification is valid. If not, we have to use the general form of the random-motion model (with the detailed calculations for refractive effects), for which vastly more computing time would be required.

2.3 Wave-Kinetic Numerical Method

2.3.1 Kinetic Equation for the Wigner Distribution Function

In the wave-kinetic theory [93-100], we describe the wave propagation in configuration space as the evolution of the Wigner distribution function (WDF) [92] in phase space [See below]. Here we define the WDF as

$$F(\vec{\rho},\ \vec{\theta};\ z) = \frac{1}{(2\pi)^2} \int_{-\infty}^{\infty} d^2s\ e^{-ik\vec{\theta}\cdot\vec{s}}\ u(\vec{\rho} + \frac{\vec{s}}{2},\ z)\ u^*(\vec{\rho} - \frac{\vec{s}}{2},\ z)\ , \tag{2.36}$$

where the parameter $\vec{\theta}$ is related to the corresponding wavevector $\vec{K}$ by $\vec{K} = k\vec{\theta}$ (i. e., θ really corresponds to an angle in the small-angle approximation regime mentioned in Sec. 2.1). In the following, we will thus use wavevector and angle interchangeably.

Two important properties of the WDF are:

$$k\int_{-\infty}^{\infty} d^2\theta\ F(\vec{\rho},\ \vec{\theta};z) = |u(\vec{\rho},\ z)|^2 \equiv I(\vec{\rho},\ z)\ , \tag{2.37}$$

and

$$\int_{-\infty}^{\infty} d^2\rho\ F(\vec{\rho},\ \vec{\theta};z) = \frac{1}{(2\pi)^2}\ |U(\vec{\theta},\ z)|^2\ , \tag{2.38}$$

where $I(\vec{\rho},\ z)$ represents irradiance at z and $U(\vec{\theta},\ z)$ is the Fourier transform of $u(\vec{\rho},\ z)$. In other words, wavenumber (or angle) integration of the WDF yields irradiance, and coordinate integration gives rise to power spectral density. We note that equations (2.37) and (2.38) may be combined to yield Parseval's theorem, i. e.,

$$\begin{aligned}\int_{-\infty}^{\infty} d^2\rho\ |u(\vec{\rho},\ z)|^2 &= \frac{k}{(2\pi)^2}\int_{-\infty}^{\infty} d^2\theta\,|U(\vec{\theta},\ z)|^2 \\ &= k\int_{-\infty}^{\infty} d^2\rho \int_{-\infty}^{\infty} d^2\theta\ F(\vec{\rho},\ \vec{\theta};z)\ .\end{aligned} \tag{2.39}$$

The kinetic equation of the WDF, which describe the evolution of $F(\vec{\rho},\ \vec{\theta};z)$ in the four-dimensional $\vec{\rho}-\vec{\theta}$ phase space, can be found from the parabolic wave equation (2.8). Substituting (2.8) in the definition of the WDF given by (2.36) and using the relation

$$\begin{aligned}&\frac{\partial}{\partial z}\left[u(\vec{\rho}+\frac{\vec{s}}{2},\ z)\,u^*(\vec{\rho}+\frac{\vec{s}}{2},\ z)\right] \\ &= \frac{i}{2k}\nabla_\rho\cdot(u_-^*\nabla_\rho u_+ - u_+\nabla_\rho u_-^*) + ik\,(\delta n_+ - \delta n_-)\,u_+u_-^*\ ,\end{aligned} \tag{2.40}$$

we obtain

$$\begin{aligned}\frac{\partial F}{\partial z} &= \frac{i}{2k}\frac{1}{(2\pi)^2}\,\nabla_\rho\cdot\int_{-\infty}^{\infty} d^2s\ e^{-ik\vec{\theta}\cdot\vec{s}}(u_-^*\nabla_\rho u_+ - u_+\nabla_\rho u_-^*) \\ &\quad + ik\frac{1}{(2\pi)^2}\int_{-\infty}^{\infty} d^2s\ e^{-ik\vec{\theta}\cdot\vec{s}}(\delta n_+ - \delta n_-)\,u_+u_-^*\ ,\end{aligned} \tag{2.41}$$

where $u_+ = u(\vec{\rho} + \frac{\vec{s}}{2}, z)$, $u_-^* = u^*(\vec{\rho} - \frac{\vec{s}}{2}, z)$, $\delta n_+ = \delta n(\vec{\rho} + \frac{\vec{s}}{2}, z)$, and $\delta n_- = \delta n(\vec{\rho} - \frac{\vec{s}}{2}, z)$. After some manipulation, we find [112]:

$$\left\{ \frac{\partial}{\partial z} + \vec{\theta}\cdot\nabla_\rho - ik\left[\delta n(\vec{\rho} + \frac{i}{2k}\nabla_\theta, z) - \delta n(\vec{\rho} - \frac{i}{2k}\nabla_\theta, z) \right] \right\} F(\vec{\rho}, \vec{\theta}; z) = 0. \quad (2.42)$$

This equation can be written symbolically as

$$\left[\frac{\partial}{\partial z} + \vec{\theta}\cdot\nabla_\rho + 2k\,\delta n(\vec{\rho}, z)\ \sin\left(\frac{1}{2k} \overleftarrow{\nabla}_\rho \cdot \vec{\nabla}_\theta \right) \right] F(\vec{\rho}, \vec{\theta}; z) = 0\ , \quad (2.43)$$

where $\overleftarrow{\nabla}_\rho = \partial/\partial\vec{\rho}$ operates only to the left and $\vec{\nabla}_\theta = \partial/\partial\vec{\theta}$ operates only to the right. The sine operator is merely a shorthand notation for a series expansion of the operator $\frac{1}{2k} \overleftarrow{\nabla}_\rho \cdot \vec{\nabla}_\theta$. To obtain irradiance, we solve the above kinetic equation for F with an initial condition, $F(\vec{\rho}, \vec{\theta}; z = 0) = F_0(\vec{\rho}, \vec{\theta})$, and perform the wavenumber integration given by (2.37).

It is interesing to note that the ensemble average of the WDF is the Fourier transform of the field coherence function. Let us introduce $\hat{\Gamma}_2(\vec{\rho}, \vec{s}; z) = u(\vec{\rho} + \frac{\vec{s}}{2}, z)\, u^*(\vec{\rho} - \frac{\vec{s}}{2}, z)$. The coherence function is usually defined as $\Gamma_2(\vec{\rho}, \vec{s}; z) = \langle \hat{\Gamma}_2(\vec{\rho}, \vec{s}; z) \rangle$. From the definition, we have

$$\langle F(\vec{\rho}, \vec{\theta}; z) \rangle = \frac{1}{(2\pi)^2} \int_{-\infty}^{\infty} d^2s\ e^{-ik\vec{\theta}\cdot\vec{s}}\ \Gamma_2(\vec{\rho}, \vec{s}; z)\ . \quad (2.44)$$

The equation for $\hat{\Gamma}_2$, which is equivalent to (2.42), can be shown to be [See, for example, Refs. 121 and 122]:

$$\left\{ \frac{\partial}{\partial z} - \frac{i}{k}\nabla_\rho\cdot\nabla_s - ik\left[\delta n(\vec{\rho} + \frac{\vec{s}}{2}, z) - \delta n(\vec{\rho} - \frac{\vec{s}}{2}, z) \right] \right\} \hat{\Gamma}_2(\vec{\rho}, \vec{s}; z) = 0\ . \quad (2.45)$$

The kinetic equation derived above is valid only in the parabolic approximation regime. More general forms of kinetic equations can be found elsewhere [93-104].

2.3.2 Liouville Approximation

In general, the kinetic equation of the WDF given by (2.42) or (2.43) is difficult to solve. Expanding the sine operator in the Taylor series, we may rewrite (2.43) as

$$\left\{ \frac{\partial}{\partial z} + \vec{\theta}\cdot\nabla_\rho + 2k\,\delta n(\vec{\rho},\, z)\left[\frac{1}{2k}\overleftarrow{\nabla}_\rho\cdot\vec{\nabla}_\theta - \frac{1}{3!}\left(\frac{1}{2k}\overleftarrow{\nabla}_\rho\cdot\vec{\nabla}_\theta\right)^3 + \cdots \right] \right\} F = 0 \ . \quad (2.46)$$

In the Liouville approximation, we take only the first term of the series expansion, which results in

$$\frac{\partial F}{\partial z} + \vec{\theta}\cdot\nabla_\rho F + \nabla_\rho \delta n(\vec{\rho},\, z)\cdot\nabla_\theta F = 0 \ . \quad (2.47)$$

This equation is exact only for inhomogeneities whose spatial dependence is linear or quadratic, since in (2.46) the third and the higher-order derivatives of δn vanishes. However, for general higher-order inhomogeneities, say, cubic or exponential inhomogeneities, it is only an approximate equation. The validity of the Liouville approximation will be discussed in the next chapter.

The kinetic equation (2.47) can be solved easily using the method of characteristic equations [119]. The characteristic equations are given by

$$\frac{d\vec{\rho}(z)}{dz} = \vec{\theta}(z) \ , \quad (2.48)$$

$$\frac{d\vec{\theta}(z)}{dz} = \nabla_\rho \delta n[\vec{\rho}(z),\, z] \ , \quad (2.49)$$

and the WDF is conserved along the characteristics, i. e.,

$$F[\vec{\rho}(z),\, \vec{\theta}(z);\, z] = F_0[\vec{\rho}(0),\, \vec{\theta}(0);\, 0] \ . \quad (2.50)$$

For notational convenience, we will use the following notations in what follows: $\vec{\rho}$, $\vec{\theta}$, $\vec{\rho}_0$ and $\vec{\theta}_0$ for $\vec{\rho}(z)$, $\vec{\theta}(z)$, $\vec{\rho}(0)$ and $\vec{\theta}(0)$; x, y, θ_x and θ_y for $x(z)$, $y(z)$, $\theta_x(z)$ and $\theta_y(z)$; x_0, y_0, θ_{x0} and θ_{y0} for $x(0)$, $y(0)$, $\theta_x(0)$ and $\theta_y(0)$.

In optics, the conservation of the WDF F along ray trajectories is often referred to as the Liouville theorem, which states, alternatively, that phase space volume is conserved along the direction of propagation z [44]. In other words, the Jacobian determinant, which is related to phase space volume by

$$d\vec{\rho}\, d\vec{\theta} = J\left(\frac{\partial\vec{\rho}\,\partial\vec{\theta}}{\partial\vec{\rho}_0\,\partial\vec{\theta}_0}\right) d\vec{\rho}_0\, d\vec{\theta}_0 \ , \tag{2.51}$$

becomes unity in the Liouville approximation. This, in turn, may be viewed as the conservation of energy.

We note that the characteristic equations (2.48) and (2.49) are the geometrical-optics (G.O.) ray equations. They are, however, different from the classical G.O. approximation in two respects. The WDF and other quantities concerned (e. g. irradiances, etc.) can be computed through caustics or ray crossings, and some diffraction effects are included in the Liouville approximation. The WDF $F(\vec{\rho}, \vec{\theta}; z)$ is not a fully geometrical-optical quantity, and the second term in (2.47) [or (2.43)] represents diffraction.

As a simple example, consider a Gaussian beam propagating in free space [99]. For an input beam-wave with beam width W_0,

$$u_0(\vec{\rho}_0) = e^{-\rho_0^2/W_0^2} \ , \tag{2.52}$$

the input WDF can be calculated from its definition (2.36):

$$F_0(\vec{\rho}_0,\ \vec{\theta}_0) = \frac{W_0^2}{2\pi}\, e^{-2\rho_0^2/W_0^2}\, e^{-k^2 W_0^2\, \theta_0^2/2} \quad . \tag{2.53}$$

In free space, $\delta n = 0$ and the trajectory equations become linear:

$$\vec{\theta} = \vec{\theta}_0 = \text{const.} \ , \tag{2.54}$$

$$\vec{\rho} = \vec{\rho}_0 + \vec{\theta}_0 z \ . \tag{2.55}$$

Thus, the output WDF is given by [cf. Eq. (2.50)]:

$$\begin{aligned} F(\vec{\rho},\ \vec{\theta}; z) &= F_0(\vec{\rho} - \vec{\theta} z,\ \vec{\theta}) \\ &= \frac{W_0^2}{2\pi}\, e^{-2(\vec{\rho} - \vec{\theta} z)^2/W_0^2}\, e^{-k^2 W_0^2\, \theta^2/2} \ . \end{aligned} \tag{2.56}$$

After some manipulation, we find

$$F(\vec{\rho},\ \vec{\theta}; z) = \frac{W_0^2}{2\pi}\, e^{-2\rho^2/W^2}\, e^{-k^2 W^2 (\vec{\theta} - \vec{\rho}/R)^2/2} \ , \tag{2.57}$$

where

$$\begin{aligned} W^2 &= W_0^2 \left[1 + 4z^2/k^2 W_0^4\right] \ , \\ R &= (z^2 + 4k^2 W_0^4)/z \ . \end{aligned} \tag{2.58}$$

The evolution of the WDF described by (2.57) is plotted in Fig. 2.3. The r.m.s. spreading of ray angles is $1/k^2W^2$, which indicates diffraction effects. Notice that it goes to zero as $k \to \infty$ in the classical G.O. approximation (which fails to include diffraction effects).

Up to now, we have discussed three-dimensional problems. For two-dimensional problems, all the formulations remain the same except that $\vec{\rho}$, $\vec{\theta}$ are replaced by

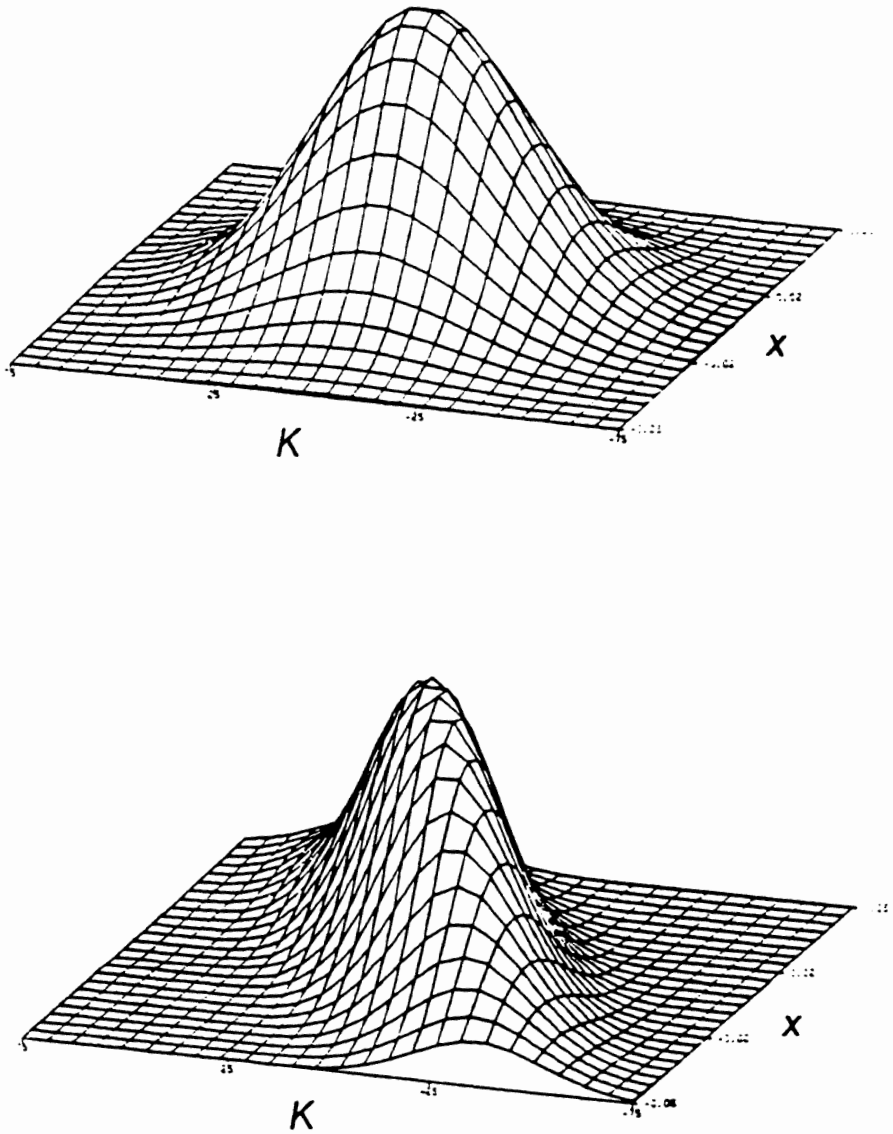

Figure 2.3 Evolution of WDF in phase space: beam wave propagation in free space.

x, θ_x, and the corresponding operations (e. g. differentiation or integration) should be modified appropriately. The details will be shown in the relevant chapters.

2.3.3 Wave Propagation Calculation with Gaussians

In order to obtain the output WDF from (2.50), we need to integrate the characteristic equations, (2.48) and (2.49), from 0 to z. If they can be integrated analytically, then we obtain the characteristic curves:

$$\begin{aligned} \vec{\rho} &= f_\rho(\vec{\rho}_0,\ \vec{\theta}_0)\ , \\ \vec{\theta} &= f_\theta(\vec{\rho}_0,\ \vec{\theta}_0)\ . \end{aligned} \tag{2.59}$$

If f_ρ and f_θ are invertible functions to give

$$\begin{aligned} \vec{\rho}_0 &= f_\rho^{-1}(\vec{\rho},\ \vec{\theta})\ , \\ \vec{\theta}_0 &= f_\theta^{-1}(\vec{\rho},\ \vec{\theta})\ , \end{aligned} \tag{2.60}$$

then $F(\vec{\rho},\ \vec{\theta};z)$ can be easily obtained from $F_0(\vec{\rho}_0,\ \vec{\theta}_0)$ as in the free-space case discussed before. In inhomogeneous media, however, f_ρ and f_θ are nonlinear functions of $\vec{\rho}_0$ and $\vec{\theta}_0$, and hence they can not be inverted in general. We may overcome this difficulty by a method that includes Gaussian decomposition of the input WDF.

The first step of the wave-kinetic numerical method is to discretize $F_0(\vec{\rho}_0,\ \vec{\theta}_0)$ into a sum of Gaussians, utilizing the Poisson sum formula for a Gaussian function [78, 112]:

$$\frac{\Delta x}{\sqrt{2\pi}\ s}\sum_{m=-\infty}^{\infty} e^{-(x-m\,\Delta x)^2/2s^2} = 1 + 2\sum_{m=1}^{\infty} e^{-2(\pi m s/\Delta x)^2}\cos(2\pi m x/\Delta x)\ . \tag{2.61}$$

If $\Delta x \leq s$, then we may drop the summation term in the right-hand side with error less than 10^{-8}. By multiplying both sides of the resulting equation by an arbitrary function $f(x)$, we obtain

$$f(x) \simeq \frac{\Delta x}{\sqrt{2\pi}\, s} \sum_n f(n\Delta x)\, e^{-(x-n\Delta x)^2/2s^2} , \quad (\Delta x \leq s) . \tag{2.62}$$

This discretization formula (or Gaussian interpolation) turns out to work very well for a smooth function $f(x)$, if Δx is sufficiently small. We may choose different values for s and Δx, but our experience indicates that the choice $\Delta x = s$ is optimal[112].

After discretization with Gaussians, an input WDF $F_0(\vec{\rho}_0, \vec{\theta}_0)$ can be formally represented as

$$F_0(\vec{x}_0^4) = \sum_i \Lambda^i \exp\left[- \sum_{m,n=1}^{4} \alpha_{mn}^i (x_{m0} - x_{m0}^i)(x_{n0} - x_{n0}^i) \right] , \tag{2.63}$$

where $\vec{x}_0^4 \equiv (x_{10}, x_{20}, x_{30}, x_{40}) = (x_0, y_0, \theta_{x0}, \theta_{y0})$ represents the four-vector at $z = 0$ in the four-dimensional phase space, and $\vec{x}_{0i}^4 \equiv (x_{10}^i, x_{20}^i, x_{30}^i, x_{40}^i) = (x_0^i, y_0^i, \theta_{x0}^i, \theta_{y0}^i)$ correspond to Gaussian centers.

Now, let us introduce new variables for difference coordinates, $\delta\vec{x}_0^4 = \vec{x}_0^4 - \vec{x}_{0i}^4$ and $\delta\vec{x}^4 = \vec{x}^4 - \vec{x}_i^4$, where $\vec{x}^4 = (x, y, \theta_x, \theta_y)$ represents the four-vector at $z = L$ and $\vec{x}_i^4 = (x^i, y^i, \theta_x^i, \theta_y^i)$ are Gaussian centers. Since x_m and x_m^i $(m = 1, 4)$ satisfy the same trajectory equations, (2.48) and (2.49), $\delta\vec{x}^4$ can be found as a function of $\delta\vec{x}_0^4$, a nonlinear relationship in general. If for each Gaussian beamlet, α_{mn}^i $(m, n = 1, 4)$ are sufficiently large, then the beamlet is confined within a very small *patch* in four-dimensional space around its center, and an inhomogeneous medium can be approximated as a locally homogeneous one within the corresponding region along the trajectory (of the Gaussian center in configuration space). Under this condition, $\delta\vec{x}_0^4$ transforms linearly into $\delta\vec{x}^4$ as each beamlet moves along a ray trajectory, i. e.,

$$\vec{\delta x}^4 = P^i \, \vec{\delta x}_0^4 \ , \tag{2.64}$$

where P^i is a constant-coefficient matrix which will be referred to as a propagation matrix for convenience. Since energy is conserved in the Liouville approximation, $|P^i| = J(\vec{\delta x}^4 / \vec{\delta x}_0^4) = 1$, and thus P^i has its inverse. Let us introduce a transformation matrix which is defined as $T^i = (P^i)^{-1}$. It follows that

$$\vec{\delta x}_0^4 = T^i \, \vec{\delta x}^4 \ . \tag{2.65}$$

Substitution of this into the discretized input WDF (2.63) results in the desired output WDF:

$$F_L(\vec{x}^4) = \sum_i \Lambda^i \exp\left[- \sum_{m,n=1}^{4} \hat{\alpha}^i_{mn} (x_m - x^i_m)(x_n - x^i_n) \right] , \tag{2.66}$$

where $\hat{\alpha}^i_{mn} = [(T^i)^{-1} A^i T^i]_{mn}$ with $A^i = [\alpha^i_{mn}]$, and the Gaussian centers, $\vec{x}_i^4$, can be calculated (either analytically or numerically) from the trajectory equations.

Once $F_L(\vec{x}^4)$ is obtained, the expression for irradiance at $z = L$ can be found analytically by wavenumber integration of $F_L(\vec{x}^4)$ as in (2.37). The result will express that the irradiance $I_L(\vec{\rho})$ as a weighted sum of Gaussians in configuration space, which can be computed numerically without any difficulty.

Errors introduced by the discretization and the linearization (i. e., approximations for linear propagation matrices T^i) will tend towards zero as $\Delta x \to 0$. [Note that we chose $\Delta x = s$ in the discretization formula (2.62).] As will be seen in the following chapters, Δx can be made relatively large for moderate accuracy. More importantly, errors involved in the Liouville approximation (which will be referred to as the first-order approximation in what follows) become significant as the refraction effects get large. When (r.m.s.) ray bending due to refraction (usually represented by r.m.s.

refractive angle fluctuation multiplied by distance) is large, we need higher-order approximations. Discussions concerning higher-order approximations and the validity of the first-order approximation will be presented in the following chapters.

2.4 Huygens-Fresnel Diffraction Formula

Let us consider a plane wave incident normally on an infinite screen at $z = 0$, which has a plane aperture. The field at z can be found from a diffraction integral. Scalar diffraction theory was first developed by Huygens and Fresnel. A more rigorous mathematical approach was made by Kirchhoff with two crucial assumptions about boundary conditions, which turned out to be inconsistent [43-45, 120]. The mathematical inconsistencies were removed by Rayleigh and Sommerfeld by making use of a proper Green's function for the scalar Helmholtz wave equation (2.5). The resulting expression takes the form of [43-45, 120]:

$$E(\vec{r}) = \frac{k}{2\pi i} \int_{S'} d^2\rho' \ \frac{e^{ikR}}{R} \left(1 + \frac{i}{kR}\right) E_0(\vec{\rho}\,') \ , \tag{2.67}$$

where $R = |\vec{r} - \vec{\rho}\,'|$, $\vec{r} = (\vec{\rho}, z)$, and S' represents the aperture plane. Assuming that $R \gg \lambda$ (i. e., $z \gg \lambda$) and $E_0(\vec{\rho}\,') = 0$ outside of the aperture, we may write (2.67) as

$$E(\vec{r}) = \frac{k}{2\pi i} \int_{-\infty}^{\infty} d^2\rho' \ \frac{e^{ikR}}{R} E_0(\vec{\rho}\,') \ . \tag{2.68}$$

Now consider a random phase screen (or a thin slab of random inhomogeneities). In the thin-screen approximation, only the random phase fluctuations through the screen are considered, with neglect of other scattering (e. g. refraction) effects. We may then apply the diffraction integral to the phase-screen problem with $E_0(\vec{\rho}) = e^{i\phi(\vec{\rho})}$, where $\phi(\vec{\rho})$ is the random phase fluctuation at $z = 0$ introduced by the screen

of thickness D. In this case, S' in (2.67) corresponds to the output plane of the phase screen. (If the above approximation does not hold, then we have to treat the thin slab as an extended medium.)

If the smallest scale size ℓ of a phase screen (or the minimum aperture size of a conventional diffraction problem) is much less than the distance z, then R in the denominator of the integrand of the diffraction integral (2.68) may be replaced by z. The phase factor kR can be expanded as

$$kR = k\sqrt{z^2 + (\vec{\rho} - \vec{\rho}\,')^2} \simeq kz + \frac{(\vec{\rho} - \vec{\rho}\,')^2}{2z} - \frac{(\vec{\rho} - \vec{\rho}\,')^4}{8z^3} + \cdots$$

If the third and higher terms are negligible compared to unity (i. e., $k\ell^4/z^3 \ll 1$), then we may keep only the first two terms (the Fresnel approximation). Using the definition for $u(\vec{\rho}, z)$ given by (2.6), i. e., $u(\vec{\rho}, z) = E(\vec{r})\, e^{-ikz}$, we obtain the Huygens-Fresnel diffraction formula:

$$u(\vec{\rho}, z) = \frac{k}{2\pi i z} \int_{-\infty}^{\infty} d^2\rho'\ e^{ik(\vec{\rho} - \vec{\rho}\,')^2/2z}\, u_0(\vec{\rho}\,') \ , \tag{2.69}$$

where $u_0(\vec{\rho}) = e^{i\phi(\vec{\rho})}$ with $\phi(\vec{\rho})$ being the random phase fluctuation introduced by a phase screen. Here we note the following. First, this expression is a formal solution of the parabolic wave equation with $\delta n = 0$ [cf. Eq. (2.8)] for an initial condition $u_0(\vec{\rho})$, i. e., this can be obtained directly from the corresponding Green's function. Secondly, if $k\ell^2/z \ll 1$, then this Huygens-Fresnel diffraction formula reduces to the Fraunhofer diffraction formula.

Let us now reformulate scalar diffraction theory using the angular-spectral representation. We define a two-dimensional Fourier transform as

$$U_0(\vec{q}) = \frac{1}{(2\pi)^2} \int_{-\infty}^{\infty} d^2\rho \; u_0(\vec{\rho})\, e^{-i\vec{q}\cdot\vec{\rho}} \;, \tag{2.70}$$

which is called the angular spectrum of the field $u_0(\vec{\rho})$. It is noted that angular spectrum is usually represented by direction cosines (α, β, γ) such that $\vec{q} = (k\alpha, k\beta)$ and $\gamma = \sqrt{1-\alpha^2-\beta^2}$, where $\vec{q}$, α and β are equivalent to $\vec{K}$, θ_x and θ_y defined in the previous section. (For small-angle diffraction, the direction cosines α, β become angles.) We now want to represent the field at z, $E(\vec{\rho}, z)$, as a superposition of plane waves propagating in different directions,

$$E(\vec{\rho}, z) = \int_{-\infty}^{\infty} d^2q \; \tilde{E}(\vec{q}, z)\, e^{i\vec{q}\cdot\vec{\rho}} \;. \tag{2.71}$$

Since E must satisfy the scalar Helmholtz equation (2.5), $\tilde{E}$ must also satisfy the corresponding differential equation

$$\frac{\partial^2}{\partial z^2}\tilde{E} + (k^2 - q^2)\,\tilde{E} = 0 \;. \tag{2.72}$$

A unit-amplitude plane wave travelling with direction cosines (α, β, γ) is then simply given by

$$e^{ik(\alpha x+\beta y+\gamma z)} = e^{i(\vec{q}\cdot\vec{\rho} + \sqrt{k^2-q^2}\, z)} \;. \tag{2.73}$$

If we choose

$$\tilde{E}(\vec{q}, z) = U_0(\vec{q})\, e^{i\sqrt{k^2-q^2}\, z} \;, \tag{2.74}$$

then $\tilde{E}$ satisfies the differential equation (2.72). Substitution of (2.74) in (2.71) results in

$$E(\vec{\rho}, z) = \int_{-\infty}^{\infty} d^2q \; e^{i\vec{q}\cdot\vec{\rho}}\, e^{i\sqrt{k^2-q^2}\, z}\, U_0(\vec{q}) \;. \tag{2.75}$$

For small-angle diffraction, $q^2 \ll k^2$ (or $\alpha^2 + \beta^2 \ll 1$). We note here that if $\alpha^2 + \beta^2 > 1$, then the components of the angular spectrum becomes *evanescent waves*. By taking only the first two terms in the binomial expansion of the term, $\sqrt{1-(q/k)^2}$, we obtain the angular-spectral representation of the Huygens-Fresnel diffraction integral:

$$u(\vec{\rho},\ z) = \int_{-\infty}^{\infty} d^2q\ e^{i\vec{q}\cdot\vec{\rho}}\, e^{-izq^2/2k}\, U_0(\vec{q}) \ . \tag{2.76}$$

This expression can also be obtained directly from the Huygens-Fresnel formula (2.69), by applying the convolution theorem for the two-dimensional Fourier transform to the diffraction integral, which is in the form of the convolution integral. The above derivation, however, gives us more physical insight.

For the two-dimensional problem, this can be done similarly [See, for example, Ref. 85]. In the small-angle approximation regime, the Huygens-Fresnel diffraction formula and its angular-spectral representation are given by:

$$u(x,\ z) = \sqrt{\frac{k}{2\pi i z}} \int_{-\infty}^{\infty} dx'\ e^{ik(x-x')^2/2z}\, u_0(x') \ , \tag{2.77}$$

and

$$u(x,\ z) = \int_{-\infty}^{\infty} dq\ e^{iqx}\, e^{-izq^2/2k}\, U_0(q) \ , \tag{2.78}$$

where the one-dimensional Fourier transform is defined as

$$U_0(q) = \frac{1}{2\pi} \int_{-\infty}^{\infty} dx\ e^{-iqx}\, u_0(x) \ . \tag{2.79}$$

In our numerical simulation, the angular-spectral representation will be used. The reason is that it allows more efficient computation than the direct application of the diffraction integral [cf. Eq. (2.69) or (2.77)], since the chosen input spectrum U_0 (which is the Fourier transform of $e^{i\phi}$ for a phase screen problem) will be band limited. To compute $u(\vec{\rho}, z)$ [or $u(x, z)$] for a given u_0 using the angular-spectral representation (2.76) [or (2.78)], we need two Fourier transform operations. We note that the Huygens-Fresnel formula may also be applied to an extended medium, by using the simplified model where an extended medium is approximated by many equally-spaced phase screens. More details for implementation (with a fast Fourier transform) and application to extended media will be discussed in the following chapters.

Appendix A2.1 Calculation of Two-Dimensional Spectra

For the von Karman spectrum, we have from (2.19) and (2.24):

$$\Phi_{n,2}(\kappa) = \int_{-\infty}^{\infty} dK_y \; \alpha \, C_n^2 \, (\kappa^2 + L_0^{-2} + K_y^2)^{-11/6} \, e^{-(\kappa^2 + K_y^2)/k_m^2} \; . \tag{A2.1}$$

After some manipulation, this may be rewritten as

$$\Phi_{n,2}(\kappa) = \alpha \, C_n^2 \, (\kappa^2 + L_0^{-2})^{-4/3} \, e^{-\kappa^2/k_m^2} \int_0^{\infty} dt \; t^{-1/2} \, (1+t)^{-11/6} \, e^{-\beta^2 t} \; , \tag{A2.2}$$

where $\beta^2 = (\kappa^2 + L_0^{-2})/k_m^2$. Using the integral representation for the Kummer function [cf. 13.2.5 in Ref. 117], we obtain

$$\Phi_{n,2}(\kappa) = \sqrt{\pi} \; \alpha \, C_n^2 \, \psi\left(\frac{1}{2}, \; -\frac{1}{3}, \; \beta^2\right) (\kappa^2 + L_0^{-2})^{-4/3} e^{-\kappa^2/k_m^2} \; . \tag{A2.3}$$

For small β (i. e., $\kappa \ll k_m$), this may be simplified as

$$\Phi_{n,2}(\kappa) \simeq \frac{\sqrt{\pi} \; \Gamma(4/3)}{\Gamma(11/6)} \; \alpha \, C_n^2 \, (\kappa^2 + L_0^{-2})^{-4/3} e^{-\kappa^2/k_m^2} \; , \tag{A2.4}$$

where the asymptotic expansion of the Kummer function is used:

$$\psi(a, \; b, \; z) \sim \frac{\Gamma(b-1)}{\Gamma(a)} \; z^{1-b} \qquad \text{as} \quad |z| \to 0 \; . \tag{A2.5}$$

For the Gaussian spectrum, equations (2.19) and (2.25) lead to the expression

$$\Phi_{n,2}(\kappa) = \int_{-\infty}^{\infty} dK_y \; (2\sqrt{\pi})^{-3} \, \ell^3 < \delta n^2 > \; e^{-(\kappa^2 + K_y^2)\ell^2/4} \; . \tag{A2.6}$$

A trivial integration of the Gaussian function results in

$$\Phi_{n,2}(\kappa) = (2\sqrt{\pi})^{-2}\, \ell^2 < \delta n^2 > \; e^{-\kappa^2 \ell^2/4} \; . \qquad (A2.7)$$

Appendix A2.2 Calculation of Number Densities of the Gaussian Eddies

von Karman spectrum (3-D):

By replacing K in (2.24) by $\sqrt{p}$, we obtain

$$G(p) = \alpha\, C_n^2\, (p + L_0^{-2})^{-11/6}\, e^{-p\ell_m^2} \; , \qquad (A2.8)$$

where $\ell_m = 1/k_m$. The inverse Laplace transform is given by the following Bromwich integral [118]:

$$F(\zeta) = \frac{1}{2\pi i} \int_{\beta - i\infty}^{\beta + i\infty} dp \;\; G(p)\, e^{p\zeta} \; , \qquad (A2.9)$$

where β is a real number such that $\beta > -L_0^{-2}$. We note that $p = -L_0^{-2}$ is the only branch point (or singularity) in $G(p)$. Let $z = -(p + L_0^{-2})$. Substituting (A2.8) in (A2.9) and changing the integration variable to z in the resulting expression, we can show that

$$F(\zeta) = \alpha\, C_n^2\, e^{-(\zeta - \ell_m^2)/L_0^2}\; \frac{i}{2\pi} \int_{C'} dz \;\; (-z)^{-11/6}\, e^{-z(\zeta - \ell_m^2)} \; , \qquad (A2.10)$$

where the contour C' runs from $\beta' - i\infty$ to $\beta' + i\infty$ with $\beta' < 0$. Now we may deform the contour C' to the Hankel contour C, which *starts at* $+\infty$ *on the real axis, circles the origin in the counterclockwise direction and returns to the starting point* [cf. 6.1.4 in Ref. 117]. It follows then that $F(\zeta)$ becomes

$$F(\zeta) = \begin{cases} \dfrac{\alpha\, C_n^2}{\Gamma(11/6)}\,(\zeta - \ell_m^2)^{5/6}\, e^{-(\zeta-\ell_m^2)/L_0^2} , & \zeta \geq \ell_m^2 \\ 0 , & \zeta < \ell_m^2 . \end{cases} \qquad (A2.11)$$

Using the relation,

$$F(\zeta = \frac{1}{2}s^2) = 2^{-3} < \delta n^2 > s^5\, n(s) , \qquad (A2.12)$$

we obtain

$$n(s) = \begin{cases} \dfrac{2^{13/6}\,\alpha\, C_n^2}{\Gamma(11/6) < \delta n^2 >}\,(s^2 - 2\ell_m^2)^{5/6}\, s^{-5}\, e^{-(s^2-2\ell_m^2)/2L_0^2} , & s^2 \geq 2\ell_m^2 \\ 0 , & s^2 < 2\ell_m^2 . \end{cases} \qquad (A2.13)$$

von Karman spectrum (2-D):

From (2.27), we have

$$G_2(p) = \frac{\sqrt{\pi}\ \Gamma(4/3)}{\Gamma(11/6)}\ \alpha\, C_n^2\,(p + L_0^{-2})^{-4/3}\, e^{-p\ell_m^2} . \qquad (A2.14)$$

The same procedure as in the three-dimensional case leads to [cf. Eq. (2.21)]:

$$F_2(\zeta) = \frac{\sqrt{\pi}\ \Gamma(4/3)}{\Gamma(11/6)}\ \alpha\, C_n^2\, e^{-(\zeta-\ell_m^2)/L_0^2}\ \frac{i}{2\pi}\int_{C'} dz\ (-z)^{-4/3}\, e^{-z(\zeta-\ell_m^2)} . \qquad (A2.15)$$

After deforming the contour C' to the Hankel contour C, we obtain

$$F_2(\zeta) = \begin{cases} \dfrac{\sqrt{\pi}\ \alpha\, C_n^2}{\Gamma(11/6)}\,(\zeta - \ell_m^2)^{1/3}\, e^{-(\zeta-\ell_m^2)/L_0^2} , & \zeta \geq \ell_m^2 \\ 0 , & \zeta < \ell_m^2 . \end{cases} \qquad (A2.16)$$

Using the relation,

$$F_2(\zeta = \frac{1}{2}s^2) = 2^{-2} < \delta n^2 > s^3\, n(s) \ , \qquad (A2.17)$$

we obtain

$$n(s) = \begin{cases} \dfrac{2^{5/3}\sqrt{\pi}\ \alpha\, C_n^2}{\Gamma(11/6) < \delta n^2 >} (s^2 - 2\ell_m^2)^{1/3}\, s^{-3}\, e^{-(s^2 - 2\ell_m^2)/2L_0^2} \ , & s^2 \geq 2\ell_m^2 \\ 0 \ , & s^2 < 2\ell_m^2 \ . \end{cases} \qquad (A2.18)$$

Gaussian spectrum (3-D):

For $\Phi_n(K)$ given by (2.25), we have

$$G(p) = (2\sqrt{\pi})^{-3}\, \ell^3 < \delta n^2 >\ e^{-p\ell^2/4} \ . \qquad (A2.19)$$

From the relation (2.18), one can see easily that

$$F(\zeta) = (2\sqrt{\pi})^{-3}\, \ell^3 < \delta n^2 >\ \delta(\zeta - \ell^2/4) \ . \qquad (A2.20)$$

Using (A2.12), we obtain

$$n(s) = \frac{8}{\pi^{3/2}}\ \ell^{-3}\, \delta(s - \ell/\sqrt{2}) \ . \qquad (A2.21)$$

Gaussian spectrum (2-D):

For $\Phi_{n,2}(\kappa)$ given by (2.28), we have

$$G_2(p) = (2\sqrt{\pi})^{-2}\, \ell^2 < \delta n^2 >\ e^{-p\ell^2/4} \ . \qquad (A2.22)$$

The relation (2.21) gives rise to

$$F_2(\zeta) = (2\sqrt{\pi})^{-2}\, \ell^2 < \delta n^2 > \, \delta(\zeta - \ell^2/4) \ . \qquad (A2.23)$$

From (A2.17), we obtain

$$n(s) = \frac{4}{\pi}\, \ell^{-2}\, \delta(s - \ell/\sqrt{2}) \ . \qquad (A2.24)$$

3. One-Dimensional Gaussian Phase Screen

The simulation schemes discussed in the previous chapter are applied to the problem of a one-dimensional Gaussian phase screen with a (unit amplitude) plane-wave input. The simulation model and the wave propagation calculations with the wave-kinetic numerical method and the Huygens-Fresnel diffraction formula for this specific problem are discussed in detail. An available analytical expression for the covariance of irradiance is also presented, and the results are compared with those from numerical simulations.

In this and following chapters, we will normalize all the length parameters with respect to the scale size ℓ [See Sec. 3.1 for its definition], whenever convenient, and denote them by putting bars on top of the original variables, for example, $\bar{k} = k\ell$, $\bar{x} = x/\ell$, $\bar{z}$ (or $\bar{L}$) $= z/\ell$ (or L/ℓ).

3.1 Simulation Model

Let us consider a plane wave propagating through a one-dimensional phase screen with a Gaussian correlation function given by

$$B_n(x,\ z) = \eta_0^2\, e^{-(x^2+z^2)/\ell^2}\ , \tag{3.1}$$

where η_0^2 is the variance of the refractive index, i. e., $\eta_0^2 = <\delta n^2>$, and ℓ is the correlation length or scale size. (Note that there is only one scale size, $\ell/\sqrt{2}$, in this

case as was shown in Sec. 2.1.) The geometry for this problem is sketched in Fig. 3.1. Using the results from Sec. 2.1 [cf. Eqs. (2.10), (2.33), and (2.34)], the fluctuating part of the refractive-index fluctuation $\delta n(x, z)$ can be modeled by

$$\delta n(x, z) = \eta_0 \sum_{m=1}^{N_E} q_m \, e^{-2[(x - x_m^c)^2 + (z - z_m^c)^2]/\ell^2} \quad , \tag{3.2}$$

where $q_m = \pm 1$, and eddy centers, (x_m^c, z_m^c), are uniformly distributed over the rectangular region of thickness D and width W. (Later in this chapter, we will discuss criteria for choosing the values of these parameters D and W in our simulation.) The number density of Gaussian eddies (with the scale size $\ell/\sqrt{2}$) per unit area can be found from (2.33):

$$N_S = 4/\pi\ell^2 \quad . \tag{3.3}$$

It follows then that the total number of eddies N_E in (3.2) is given by

$$N_E = N_x N_z \quad , \qquad N_x = \frac{2}{\sqrt{\pi}} \frac{W}{\ell} \quad , \quad N_z = \frac{2}{\sqrt{\pi}} \frac{D}{\ell} \quad , \tag{3.4}$$

where N_x and N_z represent the average number of eddies along the x- and the z- axis, respectively.

For a phase screen problem, we usually assume a *thin-screen* approximation, i. e. that through a layer of thickness D with random inhomogeneities all other scattering effects except phase fluctuations are negligible [cf. Sec. 2.4]. The phase screen problem is then simply described by a phase correlation function,

$$B_\phi(x) = \phi_0^2 \, e^{-x^2/\ell^2} \quad , \tag{3.5}$$

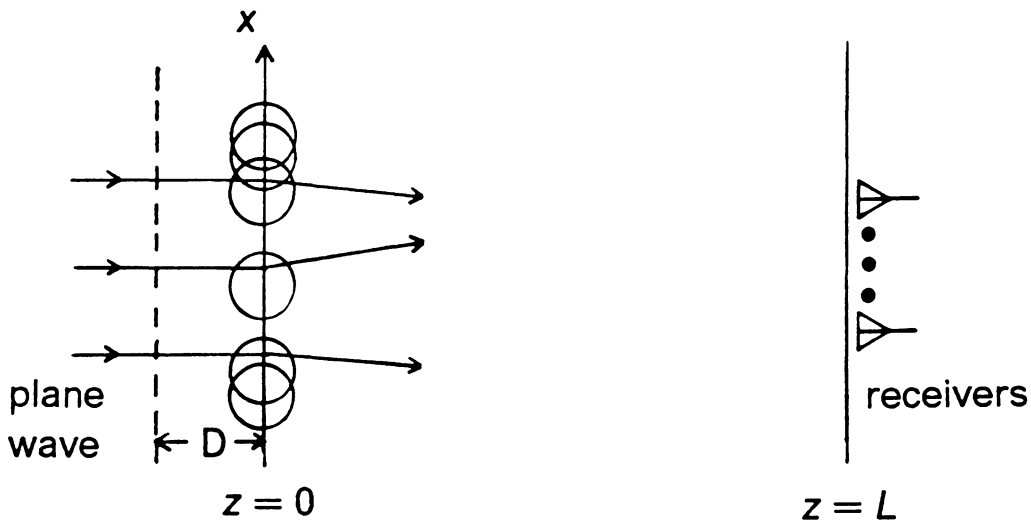

Figure 3.1 Geometry for numerical simulation of one-dimensional Gaussian phase screen.

where ϕ_0 is the r.m.s. phase fluctuations in the layer of thickness D at $z = 0$. With the thin-screen approximation, the expression for $\phi(x)$ may be found from,

$$\phi(x) = k\int_{-D}^{0} dz\ \delta n(x,\ z)\ . \tag{3.6}$$

Provided that $D \gg \ell$, we obtain

$$\phi(x) \simeq \phi_{0E}\sum_{m=1}^{N_E} q_m\, e^{-2(x-x_m^c)^2/\ell^2}\ , \tag{3.7}$$

with

$$\phi_{0E} = \sqrt{\frac{\pi}{2}}\, k\ell\eta_0\ . \tag{3.8}$$

Using this expression, we can generate a Gaussian random phase with an arbitrary ϕ_0.

The relationship between the correlation functions, $B_n(x)$ and $B_\phi(x)$, can be found from (3.6):

$$B_\phi(x) \simeq k^2 D\int_{-\infty}^{\infty} dz\ B_n(x,\ z)\ . \tag{3.9}$$

From this equation or directly from (3.7), we can show that the phase correlation function from this model results in the expression (3.5), with the variance of phase fluctuations at $z = 0$ being given by

$$\phi_0^2 = \phi_{0E}^2\, N_z = \sqrt{\pi}\, k^2\ell D\eta_0^2\ . \tag{3.10}$$

Since we are interested only in the resulting phase fluctuations at $z = 0$, $\delta n(x, z)$ given by (3.2) may be simplified as

$$\delta n(x, z) = \eta_0 \sum_{m=1}^{N_E} q_m \, e^{-2[(x - x_m^c)^2 + z^2]/\ell^2} \quad , \tag{3.11}$$

which would be valid if the displacement of eddy centers $\Delta z \lesssim D/2$ does not change results at $z = L$ appreciably, i. e. $D \ll k\ell^2$. (If the condition does not hold, then we have to treat the phase screen as an extended medium.) This leads to the simplified model for the phase screen, which is shown in Fig. 3.1. This simplified model will be used in our numerical simulation. The continuous random variable x_m^c is generated by a continuous uniform random number generator. The discrete random variable q_m ($= \pm 1$) can be generated either by a discrete random number number generator or by a continuous random number generator. [When we use a continuous random number generator, we assign $+ 1$ if the generated number is greater than 0.5 and $- 1$ otherwise.] We note that this simplified model reduces computing time considerably, since we have only a single layer of Gaussian eddies. If the observation distance L is much larger than ℓ, then this simplified model will give rise to the same results as the original model given by (3.2), asymptotically. In keeping with this notion, equation (3.11) may be simplified further:

$$\delta n(x, z) \simeq \sqrt{\frac{\pi}{2}} \, \eta_0 \ell \sum_{m=1}^{N_E} q_m \, e^{-2(x - x_m^c)^2/\ell^2} \, \delta(z) \quad . \tag{3.12}$$

This will be referred to as an impulse approximation: an impulse in phase or angle is introduced at $z = 0$ [See Sec. 3.2 for similar treatment, i. e., equivalent approximation, for trajectory calculations in the wave-kinetic numerical method]. Note that this approximation is consistent with the thin-screen approximation mentioned before.

Another important quantity is a random angle which results from a random phase fluctuation $\phi(x)$. Previously [cf. definitions for the WDF and the trajectory equations: Eqs. (2.36), (2.48), and (2.49)], we have defined θ at a given point (x, z), as $\theta = k_x/k$, where k_x is the x-component of the wavevector $\vec{k} = (k_x, k_z)$. In the small-angle approximation regime such that $k_x \ll k$, this quantity is approximately an angle in radians, as well as a tangent of the angle. From the relation $k_x = \partial\phi/\partial x$, we obtain

$$\theta(x) = \frac{1}{k}\frac{d\phi(x)}{dx} \quad . \tag{3.13}$$

Using this, one can show that [See, for example, Ref. 78]:

$$B_\theta(x) = -\frac{1}{k^2}\frac{d^2}{dx^2} B_\phi(x) \quad . \tag{3.14}$$

Substituting (3.5) in (3.14), we find

$$B_\theta(x) = \vartheta_0^2 (1 - 2x^2/\ell^2)\, e^{-x^2/\ell^2} \quad , \tag{3.15}$$

where ϑ_0^2 is the variance of angle fluctuations at $z = 0$,

$$\vartheta_0^2 = 2\phi_0^2\ell^2/k^2 \quad . \tag{3.16}$$

Let us now introduce several important parameters which are very convenient for describing phase screen (or extended medium) problems. We define

$$\begin{aligned} \gamma &= L_F/L \quad , \\ \zeta &= L/f = 2\phi_0/\gamma \quad , \end{aligned} \tag{3.17}$$

where $L_F = k\ell^2$ is the distance at which diffraction effects become significant (it is often referred to as the Fresnel distance), and $f \equiv L_F/2\phi_0$ represents the focal length of a Gaussian phase lens [3, 85]. Note that any two of the three parameters,

γ, ζ, and ϕ_0, describe a phase screen problem completely [See the analytical expression for $C_I(x)$ in Sec. 3.5]. The parameter γ is a measure of diffraction. Diffraction effects are negligible (G.O. region) when $\gamma \gg 1$. In the Fraunhofer region, where diffraction effects are important, this parameter is much less than 1 ($\gamma \ll 1$). Next, the parameter ζ is a measure of refraction. When $\zeta \sim 1$, we are in the random focusing region, and irradiance fluctuations are dominated by random spikes. In the limit of $\zeta \ll 1$, rays do not cross each other, and thus interference effects due to refraction becomes small, which results in weak irradiance fluctuations. When $\zeta \gg 1$, we are in a highly-saturated Rayleigh-statistics regime.

The effects of ζ (with γ or ϕ_0 fixed) on the scintillation index σ_I^2 [cf. see Eq. (3.87) for its definition] are shown in Fig. 3.2. The curves are obtained by numerical integration of the analytical expression for σ_I^2, which will be discussed in Sec. 3.5. The curves for σ_I^2 reach at their maxima (due to focusing effects) in the region, $0.5 < \zeta < 1.0$, for given values of γ and ϕ_0 , which are greater than certain lower limits. As γ or ϕ_0 increases, random focusing effects appear at the values of ζ close to 0.5. We are interested in the random focusing region, since the wave statistics in the two limiting cases, $\zeta \ll 1$ (weak fluctuation regime, where $\sigma_I^2 \ll 1$) and $\zeta \gg 1$ (saturation region, where $\sigma_I^2 \simeq 1$), are rather well understood. Thus, in our numerical simulation, it is convenient to choose $\gamma = 13.856$ (G.O. region), and the values for ζ will be chosen between 0.0 and 1.0.

Even though γ and ϕ_0 (or ζ) determine a phase screen completely, we will assume some specific values for the physical parameters, k and ℓ, throughout this and the following chapter. We let $k = 1.0472 \times 10^7$ (which corresponds to the wavelength of the He-Ne laser, $\lambda = 0.6\,\mu m$), and $\ell = 10^{-2}\,m$. (Notice that in ground-level atmospheric turbulence, typical values for the inner- and the outer-scale of turbulence are given

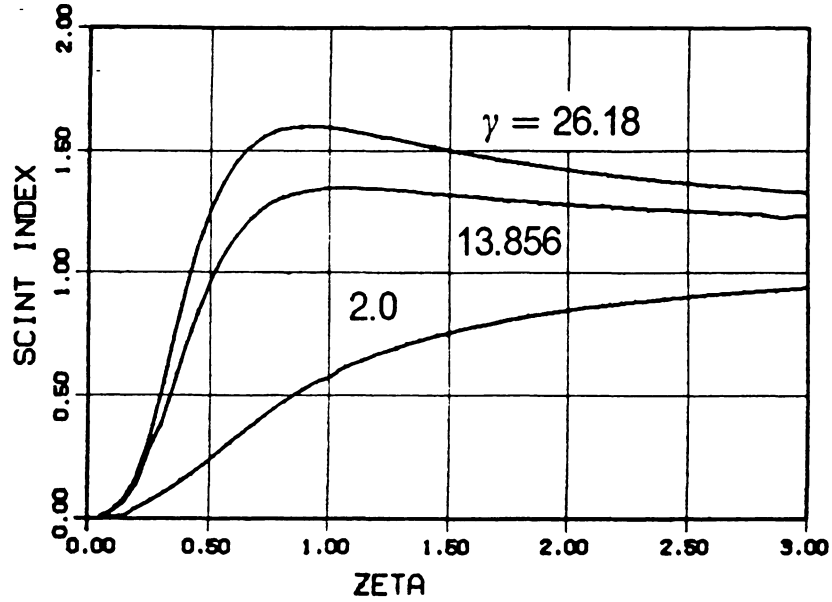

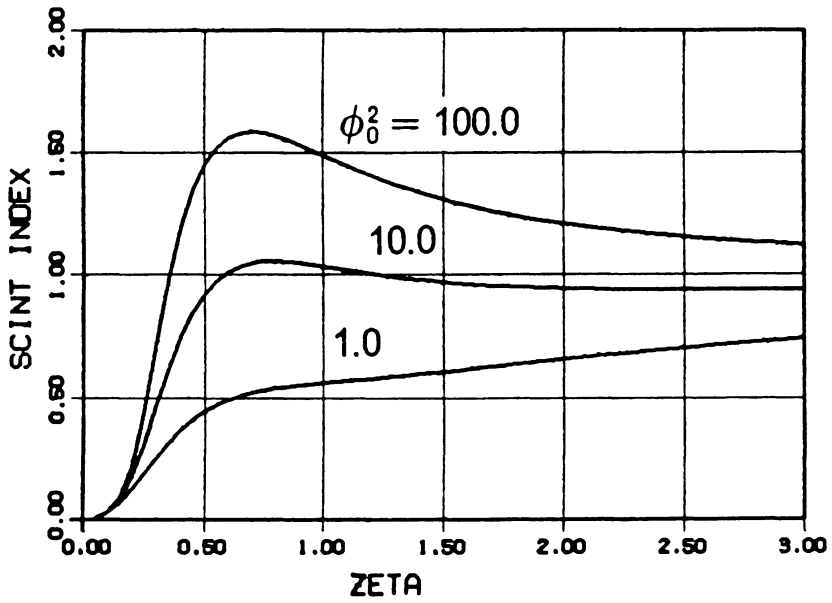

Figure 3.2 The effects of ζ on σ_I^2: with γ (or z) fixed; with ϕ_0 fixed [see Eq. (3.87) for the definition of the scintillation index σ_I^2].

respectively by $l_0 = 10^{-3}\,m$ and $L_0 = 10\,m$.) It follows that $\ell \gg \lambda$ and the small-angle approximation can be applied.

3.2 Wave-Kinetic Numerical Method

Consider an input beam wave,

$$u_0(x_0) = e^{-x_0^2/W_0^2} \ , \tag{3.18}$$

where W_0 is the beam width, and for a plane wave we let $W_0 \to \infty$. As before, we use the following shorthand notations for $\theta(z)$ and $x(z)$: $\theta = \theta(L)$ and $x = x(L)$; $\theta_0 = \theta(0)$ and $x_0 = x(0)$. For two-dimensional problems, we have [cf. Eqs. (2.36) and (2.37)]:

$$\bar{F}(\bar{x},\ \theta;\bar{z}) = \frac{1}{2\pi}\int_{-\infty}^{\infty} d\bar{s}\ e^{-i\bar{k}\theta\bar{s}}\ u(\bar{x}+\frac{\bar{s}}{2},\ \bar{z})u^*(\bar{x}-\frac{\bar{s}}{2},\ \bar{z}) \ , \tag{3.19}$$

and

$$I(\bar{x},\ \bar{z}) = \bar{k}\int_{-\infty}^{\infty} d\theta\ \bar{F}(\bar{x},\ \theta;\bar{z}) \ , \tag{3.20}$$

where the bar notations are used for the dimensionless parameters $\bar{k}$, $\bar{x}$, $\bar{z}$, and $\bar{s}$, as mentioned before, and $\bar{F} = F/\ell$. From this definition, the input WDF is given by

$$\bar{F}_0(\bar{x}_0,\ \theta_0) = \frac{\bar{W}_0}{\sqrt{2\pi}}\, e^{-2\bar{x}_0{}^2/\bar{W}_0{}^2}\, e^{-\bar{k}^2\bar{W}_0{}^2\theta_0{}^2/2} \ . \tag{3.21}$$

Now we wish to compute the output WDF $\bar{F}_L(\bar{x},\ \theta)$ and the irradiance $I_L(\bar{x})$ at $\bar{z} = \bar{L}$ for a given realization of the screen [cf. Fig. 3.1], using the wave-kinetic numerical

method. We will discuss the Liouville approximation first, and then the third- and higher-order approximations.

3.2.1 Liouville Approximation

We first discretize the input WDF given by (3.21) with Gaussian beamlets to obtain

$$\bar{F}_0(\bar{x}_0,\ \theta_0) = \sum_{n=1}^{N_r} \Lambda_n\, e^{-(\bar{x}_0 - n\,\overline{\Delta x})^2/2\overline{\Delta x}^2}\, e^{-\bar{k}^2\bar{W}_0{}^2\theta_0{}^2/2}\ , \tag{3.22}$$

where we let the beamlet spacing $\overline{\Delta x}$ and the r.m.s. spread of each beamlet $\bar{s}$ be the same [cf. Eq. (2.62)]. The constant coefficient Λ_n is given by

$$\Lambda_n = \frac{\overline{W}_0}{2\pi}\, e^{-2(n\,\overline{\Delta x})^2/\bar{W}_0{}^2}\ , \tag{3.23}$$

and N_r represents the number of rays. Here, $\bar{F}_0$ is discretized only for $\bar{x}_0$, since we are interested in a plane wave for which $\overline{W}_0 \to \infty$ and the term $e^{-\bar{k}^2\bar{W}_0{}^2\theta_0{}^2/2}$ is already sharply peaked around $\theta_0 = 0$. The trajectory equations for this two-dimensional problem are given by [cf. Eqs. (2.48) and (2.49)]:

$$\begin{aligned} \frac{d\,x(z)}{dz} &= \theta(z)\ , \\ \frac{d\,\theta(z)}{dz} &= \frac{\partial}{\partial x}\ \delta n[x(z),\ z]\ . \end{aligned} \tag{3.24}$$

First we consider a single Gaussian eddy centered at $(x_c,\ z_c)$ so that $\delta n(x,\ z) = \eta_0\, e^{-2[(x-x_c)^2 + (z-z_c)^2]/\ell^2}$. For weak refractive-index fluctuations ($\eta_0 \leq 10^{-6}$, typical in the atmosphere), we may integrate the trajectory equations by an iteration-perturbation method [111, 112]:

$$\theta = \theta_0 + \Delta(L)$$
$$x = x_0 + \theta_0 L + \int_0^L dz\ \Delta(z)\ , \tag{3.25}$$

where

$$\Delta(z) = \int_0^z dz'\ \frac{\partial}{\partial x}[\delta n(x, z')]_{x = x_0 + z'\theta_0}\ . \tag{3.26}$$

We note that $\Delta(L)$ is very small compared to unity. For a beam wave with $W_0 \geq \ell \sim O(10^{-2}\, m)$, we have $\theta \sim 1/kW_0 \ll 1$ since k is of $O(10^7\, m^{-1})$ in optics. Thus, for $L - z_c \gg \ell$, we obtain [111, 112]:

$$\theta = \theta_0 + \Delta$$
$$x = x_0 + \theta_0 L + (L - z_c)\,\Delta\ , \tag{3.27}$$

where

$$\Delta = -2\sqrt{2\pi}\,\eta_0 \bar{d}\, e^{-2\bar{d}^2}\ , \tag{3.28}$$

with $\bar{d} = [x(z_c) - x_c]/\ell = (x_0 + z_c\theta_0 - x_c)/\ell$. We now assume that the expressions for θ and x given above hold for $z \geq z_c$, and $\theta = \theta_0$, $x = x_0$ for $z < z_c$. This will be called the impulse approximation [cf. Eq. (3.12)], i. e., we assume that impulses in phase or angle are introduced at $z = z_c$. This approximation does not describe accurately what happens to a ray within a few lengths ℓ of the eddy center (x_c, z_c), but it is asymptotically accurate (within the validity of the approximations made for trajectory calculations).

Now, consider the Gaussian eddies lined up along the x-axis as shown in Fig. 3.3, so that $\delta n(x, z)$ can be represented by (3.11). Using results for a single Gaussian eddy and the bar notations, we obtain (with the impulse approximation):

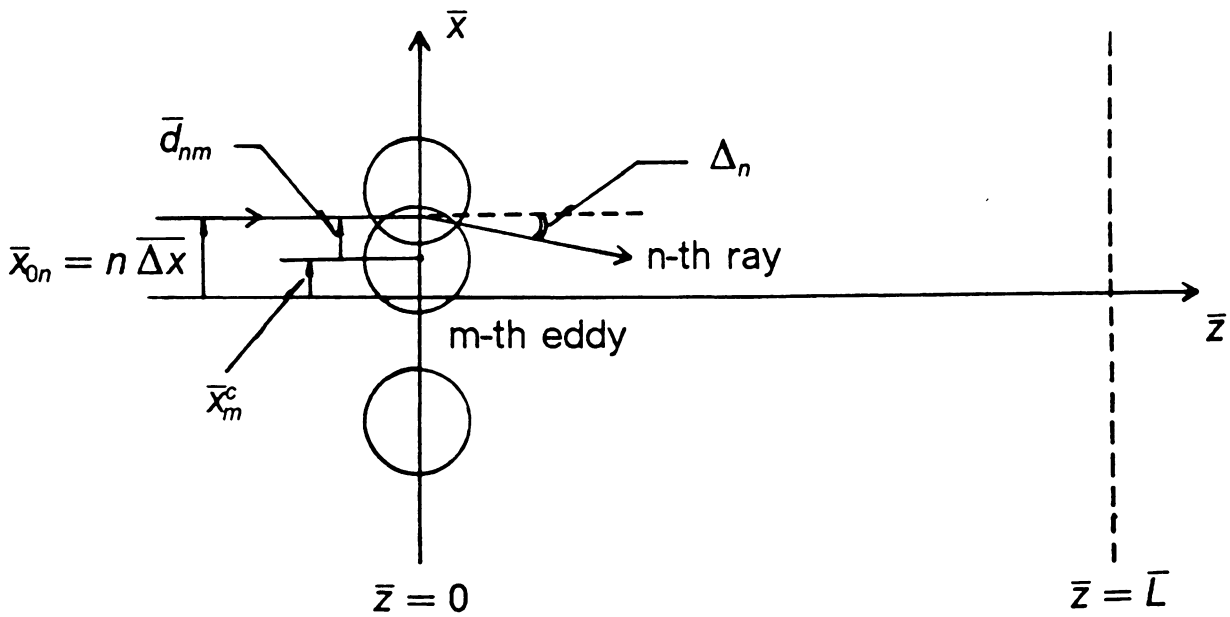

Figure 3.3 Two-dimensional Gaussian eddies lined up along the x-axis. Parameters for wave-kinetic numerical method are shown.

$$\theta = \theta_0 + \Delta$$
$$\bar{x} = \bar{x}_0 + \bar{z}\,\theta_0 + \bar{z}\,\Delta \ , \tag{3.29}$$

where

$$\Delta = -2\sqrt{2\pi}\,\eta_0 \sum_{m=1}^{N_E} q_m\,\bar{d}_m\,e^{-2\bar{d}_m^2} \ , \quad (\bar{d}_m = \bar{x}_0 - \bar{x}_m^c) \ . \tag{3.30}$$

We note here that $\Delta(\bar{x}_0) = \frac{1}{\bar{k}} \frac{d\phi(\bar{x}_0)}{d\bar{x}_0}$. Similarly for the center of the n-th beamlet, we have

$$\theta_n = \theta_{n0} + \Delta_n$$
$$\bar{x}_n = \bar{x}_{n0} + \bar{z}\,\theta_{n0} + \bar{z}\,\Delta_n \ , \tag{3.31}$$

where $\Delta_n = \Delta(\bar{x}_0 = \bar{x}_{n0})$, i. e.,

$$\Delta_n = -2\sqrt{2\pi}\,\eta_0 \sum_{m=1}^{N_E} q_m\,\bar{d}_{nm}\,e^{-2\bar{d}_{nm}^2} \ , \quad (\bar{d}_{nm} = \bar{x}_{n0} - \bar{x}_m^c) \ . \tag{3.32}$$

Let us introduce new variables for difference coordinates in two-dimensional phase space: $\overline{\delta x_0} = \bar{x}_0 - \bar{x}_{n0}$, $\delta\theta_0 = \theta_0 - \theta_{n0}$; $\overline{\delta x} = \bar{x} - \bar{x}_n$, $\delta\theta = \theta - \theta_n$. It follows then from (3.29) and (3.31) that

$$\delta\theta = \delta\theta_0 - 2\sqrt{2\pi}\,\eta_0 \sum_{m=1}^{N_E} q_m\,(\bar{d}_m\,e^{-2\bar{d}_m^2} - \bar{d}_{nm}\,e^{-2\bar{d}_{nm}^2}) \ . \tag{3.33}$$

By expanding the first exponential in a Taylor series around $\bar{d}_m = \bar{d}_{nm}$, we obtain

$$\delta\theta \simeq \delta\theta_0 - 2\sqrt{2\pi}\,\eta_0 \sum_{m=1}^{N_E} q_m (1 - 4\bar{d}_{nm}^2)\, e^{-2\bar{d}_{nm}^2} (\bar{d}_m - \bar{d}_{nm})$$
$$= \delta\theta_0 + \Delta_n' \,\overline{\delta x_0} \ , \tag{3.34}$$

where Δ_n' is the derivative of the angle impulse for the n-th ray, i. e.,

$$\Delta_n' = \frac{d}{d\bar{x}_0}\, \Delta(\bar{x}_0)\,|_{\bar{x}_0 = \bar{x}_{n0}} \ . \tag{3.35}$$

Similarly for $\overline{\delta x}$, we obtain

$$\overline{\delta x} = (1 + \bar{L}\Delta_n')\,\overline{\delta x_0} + \bar{L}\,\delta\theta_0 \ . \tag{3.36}$$

Equations (3.34) and (3.36) may be combined in a convenient matrix form:

$$\begin{bmatrix} \overline{\delta x} \\ \delta\theta \end{bmatrix} = P_n \begin{bmatrix} \overline{\delta x_0} \\ \delta\theta_0 \end{bmatrix} , \tag{3.37}$$

with

$$P_n = \begin{bmatrix} 1 + \bar{L}\Delta_n' & \bar{L} \\ \Delta_n' & 1 \end{bmatrix} . \tag{3.38}$$

Note the similarity between the propagation matrix T_n and the *ABCD* matrix in Gaussian optics. We note that $|T_n| = 1$ as mentioned before, which indicates that energy is conserved in the Liouville approximation. Now the initial coordinates $\overline{\delta x_0}$ and $\delta\theta_0$ can be related to the final coordinates $\overline{\delta x}$ and $\delta\theta$:

$$\begin{bmatrix} \overline{\delta x_0} \\ \delta\theta_0 \end{bmatrix} = T_n \begin{bmatrix} \overline{\delta x} \\ \delta\theta \end{bmatrix} , \tag{3.39}$$

with

$$T_n = P_n^{-1} = \begin{bmatrix} 1 & -\bar{L} \\ -\Delta_n' & 1 + \bar{L}\,\Delta_n' \end{bmatrix} . \tag{3.40}$$

Substituting (3.39) in (3.22), where $\bar{x}_0 - n\,\overline{\Delta x} = \overline{\delta x}_0$ and $\theta_0 = \delta\theta_0$ (since $\bar{x}_{n0} = n\,\Delta x$ and $\theta_{n0} = 0$ in this case), we obtain the output WDF:

$$F_L(\bar{x}, \theta) = \sum_{n=1}^{N_r} \Lambda_n \, e^{-[\hat{\alpha}_x \overline{\delta x}^2 - 2\hat{\alpha}_{x\theta} \overline{\delta x}\, \delta\theta + \hat{\alpha}_\theta \delta\theta^2]} \ , \tag{3.41}$$

where

$$\begin{aligned} \hat{\alpha}_x &= \alpha_x + \alpha_\theta \, \Delta_n'^2 \\ \hat{\alpha}_{x\theta} &= \alpha_x \, \bar{L} + \alpha_\theta \, \Delta_n' \, (1 + \bar{L}\Delta_n') \\ \hat{\alpha}_\theta &= \alpha_x \, \bar{L}^2 + \alpha_\theta \, (1 + \bar{L}\Delta_n')^2 \end{aligned} \tag{3.42}$$

with

$$\alpha_x = 1/2\overline{\Delta x}^2 \ , \quad \alpha_\theta = \bar{k}^2 \overline{W}_0{}^2/2 \ . \tag{3.43}$$

Finally, the expression for the irradiance at $z = L$ can be obtained by the wavenumber integration given by (3.20):

$$I_L(\bar{x}) = \frac{1}{\sqrt{2\pi}} \sum_{n=1}^{N_r} \frac{1}{|S_n|} \, e^{-2(n\overline{\Delta x})^2/\overline{W}_0{}^2} \, e^{-(\bar{x} - \bar{x}_n)^2/2S_n^2\overline{\Delta x}^2} \ , \tag{3.44}$$

where

$$S_n^2 = \left(\frac{\bar{L}}{\bar{k}\,\overline{W}_0 \overline{\Delta x}} \right)^2 + C_n^2 \ , \tag{3.45}$$

with

$$C_n = 1 + \Delta_n' \, \bar{L} \ , \tag{3.46}$$

and the ray center $\bar{x}_n$ is given by (with $\theta_{n0} = 0$):

$$\bar{x}_n = \bar{x}_{n0} + \Delta_n \bar{L} \ , \quad (\bar{x}_{n0} = n\,\overline{\Delta x}) \ . \tag{3.47}$$

Notice that C_n^2 in (3.45) is not the structure constant defined in Sec. 2.1. The expression for Δ_n and Δ_n' are given by (3.32) and (3.35), respectively. Now for a plane wave, $W_0 \to \infty$ and thus S_n in (3.44) may be replaced by C_n. It follows that (3.44) becomes

$$I_L(\bar{x}) \simeq \frac{1}{\sqrt{2\pi}} \sum_{n=1}^{N_r} \frac{1}{|C_n|}\, e^{-(\bar{x}-\bar{x}_n)^2/2C_n^2\overline{\Delta x}^2} \ , \tag{3.48}$$

which is the final expression for the irradiance at $z = L$ from the Liouville approximation (or the first-order approximation). In the following section, the third- and higher-order approximations will be introduced, and the region of validity of the lower-order approximations will be discussed.

3.2.2 Higher-Order Approximations

First, we wish to re-derive the result of the previous section in a slightly different way. Using the idea of the thin-screen approximation, we let $u(x,\ z = 0^+) = e^{i\phi(x)}$ where $\phi(x)$ is given by (3.7), as in the Huygens-Fresnel diffraction integral formulation [cf. Secs. 2.3 and 3.3]. It follows then from the definition that the WDF at $z = 0^+$ for a plane wave input can be represented as [cf. Fig. 3.4]:

$$\bar{F}_0^+(\bar{x}_0,\ \theta_0) = \frac{1}{2\pi} \int_{-\infty}^{\infty} d\bar{s}\ e^{-ik\bar{\theta}_0\bar{s}}\, e^{i[\phi(\bar{x}_0 + \frac{\bar{s}}{2}) - \phi(\bar{x}_0 - \frac{\bar{s}}{2})]} \ . \tag{3.49}$$

The phase difference in the above equation can be expanded in the Taylor series:

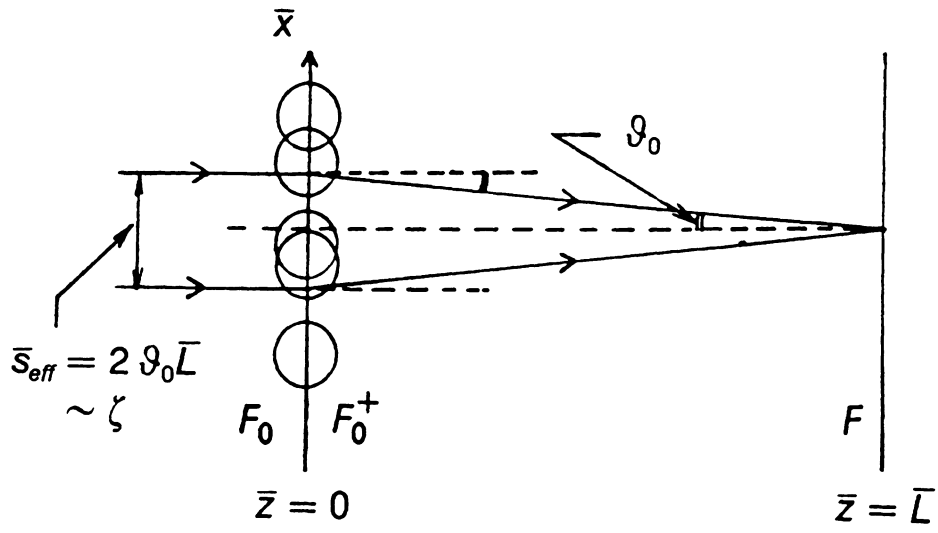

Figure 3.4 Validity of lower-order approximations.

$$\phi(\bar{x}_0 + \frac{\bar{s}}{2}) - \phi(\bar{x}_0 - \frac{\bar{s}}{2}) = 2\bar{k}\sum_{m=0}^{\infty} \frac{\Delta^{(2m)}(\bar{x}_0)}{(2m+1)!}\left(\frac{\bar{s}}{2}\right)^{2m+1} , \tag{3.50}$$

where $\Delta^{(2m)}(\bar{x}_0) = d^{2m}\Delta/d\bar{x}_0^{2m}$ with

$$\Delta(\bar{x}_0) = \frac{1}{\bar{k}}\frac{d\phi(\bar{x}_0)}{d\bar{x}_0} . \tag{3.51}$$

If we take only the first term in the series expansion of the phase difference and apply the discretization scheme, using the approximate equation (with error $\lesssim 10^{-7}$),

$$1 \simeq \frac{1}{\sqrt{2\pi}}\sum_n e^{(\bar{x}_0 - \bar{x}_{n0})^2/2\overline{\Delta x}^2} , \quad (\bar{x}_{n0} = n\,\overline{\Delta x}) , \tag{3.52}$$

then (3.49) becomes

$$\bar{F}_0^+(\bar{x}_0,\ \theta_0) \simeq \frac{1}{2\pi}\frac{1}{\sqrt{2\pi}}\sum_n \int_{-\infty}^{\infty} d\bar{s}\ e^{-i\bar{k}\bar{s}[\theta_0 - \Delta(\bar{x}_0)]}\, e^{-(\bar{x}_0 - \bar{x}_{n0})^2/2\overline{\Delta x}^2} . \tag{3.53}$$

Since each Gaussian beamlet is sharply peaked around $\bar{x}_{n0}$, $\Delta(\bar{x}_0) \simeq \Delta_n + \Delta_n'\,(\bar{x}_0 - \bar{x}_{n0})$, where $\Delta_n = \Delta(\bar{x}_{n0})$ and $\Delta_n' = \Delta'(\bar{x}_{n0})$ are given by (3.32) and (3.35). With this approximation, we obtain

$$\bar{F}_0^+(\bar{x}_0,\ \theta_0) \simeq \frac{1}{2\pi}\frac{1}{\sqrt{2\pi}}\sum_n \int_{-\infty}^{\infty} d\bar{s}\ e^{-i\bar{k}\bar{s}(\delta\theta_0 - \Delta_n'\overline{\delta x_0})}\, e^{-\overline{\delta x_0}^2/2\overline{\Delta x}^2} , \tag{3.54}$$

where $\delta\theta_0 \equiv \theta_0 - \Delta_n$ and $\overline{\delta x_0} \equiv \bar{x}_0 - \bar{x}_{n0}$ as before.

The coordinate transformation in free space is described by [cf. Eq. (3.39)]:

$$\begin{bmatrix} \overline{\delta x}_0 \\ \delta\theta_0 \end{bmatrix} = T_n^f \begin{bmatrix} \overline{\delta x} \\ \delta\theta \end{bmatrix} , \tag{3.55}$$

with

$$T_n^f = \begin{bmatrix} 1 & -\bar{L} \\ 0 & 1 \end{bmatrix} . \tag{3.56}$$

Combination of (3.54) and (3.55) results in

$$\bar{F}_L(\bar{x},\ \theta) = \frac{1}{2\pi}\frac{1}{\sqrt{2\pi}}\sum_n \int_{-\infty}^{\infty} d\bar{s}\ e^{-i\bar{k}\bar{s}[\delta\theta - \Delta_n'(\overline{\delta x} - \bar{L}\,\delta\theta)]}\, e^{-(\overline{\delta x} - \bar{L}\,\delta\theta)^2/2\overline{\Delta x}^2} . \tag{3.57}$$

Now the irradiance can be calculated from the wavenumber integration of (3.57) as in (3.20). After a simple manipulation, it is given by

$$I_L(\bar{x}) = \frac{\gamma}{2\pi}\frac{1}{\sqrt{2\pi}}\sum_n \int_{-\infty}^{\infty} d\bar{s} \int_{-\infty}^{\infty} d\xi\ \left[e^{-i\gamma\bar{s}\xi}\right]\left[e^{i\bar{k}\bar{s}\Delta_n'(\overline{\delta x} - \xi)}\, e^{-(\overline{\delta x} - \xi)^2/2\overline{\Delta x}^2}\right] , \tag{3.58}$$

where $\gamma = \bar{k}/\bar{L} = k\ell^2/L$ [cf. Eq. (3.17)]. We note that the inner integral is in the form of a convolution integral. (Here we should mention the following. In this specific case, i. e., in the first-order approximation, it would be easier to do $\bar{s}$-integration first, which will yield the expression (3.48) in the previous section. In the higher-order approximations which will be discussed in this and the next chapters, however, the resulting expressions for $I_L(\bar{x})$ [cf. (A3.3), (3.68) and (A4.9)] can not be integrated with respect to $\bar{s}$ first. Since all the expressions include the same convolution integrals in their inner integrals, we utilize the convolution theorem which leads directly to closed form expressions for the irradiance spectrum $\tilde{I}_L(\Omega)$ [see below]. Thus, we use the convolution theorem even in this first-order approximation to find an expression for $\tilde{I}_L(\Omega)$, which will be compared with those from the higher-order approximations.) Let us define the Fourier transform of a function $g(\bar{x})$ as

$$\tilde{g}(\Omega) = \frac{1}{2\pi} \int_{-\infty}^{\infty} d\bar{x}\ e^{-i\Omega\bar{x}}\, g(\bar{x}) \ . \tag{3.59}$$

(We put the factor $\frac{1}{2\pi}$ here to be consistent with the usual definition for the Fourier transform in the theory of random wave propagation [cf. Defs. (2.3), (2.36), (2.70), and (3.19)].) By replacing the terms in the brackets by their Fourier transforms, we obtain

$$I_L(\bar{x}) = \frac{\overline{\Delta x}}{2\pi} \sum_n \int_{-\infty}^{\infty} d\Omega\ e^{i\Omega(\bar{x} - \bar{x}_n)} \int_{-\infty}^{\infty} d\bar{s}\ \delta(\bar{s} + \frac{\Omega}{\gamma}) \times e^{-\overline{\Delta x}^2(\bar{k}\Delta_n'\bar{s} - \Omega)^2/2} \ . \tag{3.60}$$

After the integration with respect to $\bar{s}$, this becomes

$$I_L(\bar{x}) = \int_{-\infty}^{\infty} d\Omega\ e^{i\Omega\bar{x}}\, \tilde{I}_L(\Omega) \ , \tag{3.61}$$

with

$$\tilde{I}_L(\Omega) = \frac{\overline{\Delta x}}{2\pi} \sum_n e^{-i\bar{x}_n\Omega}\, e^{-\overline{\Delta x}^2 C_n^2 \Omega^2/2} \ . \tag{3.62}$$

Here, C_n and $\bar{x}_n$ are given by (3.46) and (3.47), respectively. We note that this expression for $I_L(\bar{x})$ reduces to (3.48) in the previous section. Thus, the Liouville approximation is equivalent to the first-order approximation in the phase difference.

Similarly, we can show that if we take the first two terms (the third-order approximation) in the series expansion of the phase difference, (3.50), then the spectrum of irradiance $\tilde{I}_L(\Omega)$ is given by [cf. Appendix A3.1]:

$$\tilde{I}_L(\Omega) = \frac{\overline{\Delta x}}{2\pi} \sum_n \left[e^{-i\bar{x}_n\Omega} e^{-\overline{\Delta x}^2 C_n^2 \Omega^2/2} \right] \left[e^{-i\beta_n^3\Omega^3/3} \right] , \tag{3.63}$$

where

$$\beta_n = (\bar{k}\Delta_n'')^{1/3}/2\gamma = [\phi^{(3)}(\bar{x}_{n0})]^{1/3}/2\gamma \ . \tag{3.64}$$

It is interesting to note that this expression can also be obtained by applying the two-scale expansion (which is introduced by Frankenthal et al. [121]) to our problem with the discretization scheme [Appendix A3.2]. Notice that the third-order approximation has the correction factor $e^{-i\beta_n^3\Omega^3/3}$. Since $\beta_n^3 \sim \phi_0/\gamma^3 \sim \zeta/\gamma^2$, for a given $\gamma = \bar{k}/\bar{L}$ this reduces to the first-order approximation if ζ is sufficiently small. We can see this more clearly from Fig. 3.4. The irradiance at $\bar{z} = \bar{L}$ results from the field components $u(\bar{x}_0 \pm \frac{\bar{s}}{2})$ at $z = 0$ [cf. Eqs. (3.49) and (3.50)], where $\bar{s} \le \bar{s}_{eff}$. For a given phase screen with r.m.s. angle fluctuation ϑ_0, $\bar{s}_{eff} \simeq 2\vartheta_0\bar{L}$ ($\simeq \zeta$) as shown in Fig. 3.4. Thus, in order for the lower-order approximations (in the phase difference) to be valid, we need $\zeta \ll 1$ (or beamwidth must be small if the beamwidth is smaller than $\bar{s}_{eff}$) [cf. Eq. (3.50)]. Numerical results, which are presented in Sec. 3.6, indicate that the first-order approximation is valid for $\zeta \le 0.2$. Since we are interested in the random focusing region where $\zeta \sim 1$ [cf. Sec. 3.1], we need a more accurate expression for $I_L(\bar{x})$, i. e., a higher-order approximation, which is valid for all ζ (or at least for $\zeta \lesssim 1$).

Now, we wish to introduce approximations of higher order than third. Rewrite the phase difference given by (3.50) as:

$$\phi(\bar{x}_0 + \frac{\bar{s}}{2}) - \phi(\bar{x}_0 - \frac{\bar{s}}{2}) = \bar{k}\Delta(\bar{x}_0)\bar{s} + h(\bar{x}_0, \bar{s}) \ , \tag{3.65}$$

where

$$h(\bar{x}_0,\ \bar{s}) = 2\bar{k}\sum_{m=1}^{\infty} \frac{\Delta^{(2m)}(\bar{x}_0)}{(2m+1)!}\left(\frac{\bar{s}}{2}\right)^{2m+1} . \tag{3.66}$$

Following the same procedure as in the first-order approximation [cf. Eqs. (3.53)-(3.57)], we can show that

$$\bar{F}_L(\bar{x},\ \theta) = \frac{1}{2\pi}\frac{1}{\sqrt{2\pi}}\sum_n \int_{-\infty}^{\infty} d\bar{s}\ e^{ih_n(\bar{s})} e^{-i\bar{k}\bar{s}[\delta\theta - \Delta_n'(\overline{\delta x} - \bar{L}\,\delta\theta)]} \times e^{-(\overline{\delta x} - \bar{L}\,\delta\theta)^2/2\overline{\Delta x}^2} , \tag{3.67}$$

where $h_n(\bar{s}) = h(\bar{x}_0 = \bar{x}_{n0},\ \bar{s})$. As before [cf. Eq. (3.58)], the wavenumber integration of $\bar{F}_L(\bar{x},\ \theta)$ leads to:

$$I_L(\bar{x}) = \frac{\gamma}{2\pi}\frac{1}{\sqrt{2\pi}}\sum_n \int_{-\infty}^{\infty} d\bar{s}\ e^{ih_n(\bar{s})} \int_{-\infty}^{\infty} d\xi \left[e^{-i\gamma\bar{s}\xi}\right]\left[e^{i\bar{k}\bar{s}\Delta_n'(\overline{\delta x} - \xi)} \times e^{-(\overline{\delta x} - \xi)^2/2\overline{\Delta x}^2}\right] . \tag{3.68}$$

The inner integral is again in the form of the convolution integral. After the same manipulations as in the first-order approximation, we obtain

$$\tilde{I}_L(\Omega) = \frac{\overline{\Delta x}}{2\pi}\sum_n \left[e^{-i\bar{x}_n\Omega}\, e^{-\overline{\Delta x}^2 C_n^2\Omega^2/2}\right]\left[e^{-ih_n(\bar{s}\,=\Omega/\gamma)}\right] , \tag{3.69}$$

where the oddness of the function $h_n(\bar{s})$ is used, and $\bar{x}_n$ and C_n are given by (3.47) and (3.46), respectively. Compare this with the expression (3.62) from the first-order approximation. The second term in the square bracket, $e^{ih_n(\bar{s}\,=\Omega/\gamma)}$, is the correction term. Using the fact that $\bar{x}_n = \bar{x}_{n0} + \bar{L}\,\Delta_n$, we may rewrite the above equation as [cf. Eq. (3.65)]:

$$\tilde{I}_L(\Omega) = \frac{\overline{\Delta x}}{2\pi} \sum_n e^{-i\bar{x}_{n0}\Omega} e^{-i[\phi(\bar{x}_{n0} + \frac{\Omega}{2\gamma}) - \phi(\bar{x}_{n0} - \frac{\Omega}{2\gamma})]} e^{-\overline{\Delta x}^2 C_n^2 \Omega^2/2} , \tag{3.70}$$

where the random phase $\phi(\bar{x})$ is given by (3.7). For the purpose of numerical calculation, we compute only the scattered part of the spectrum, i. e.,

$$\begin{aligned} \tilde{I}_{Ls}(\Omega) &= F\{I_L(\bar{x}) - 1\} \\ &= \frac{\overline{\Delta x}}{2\pi} \sum_n e^{-i\bar{x}_{n0}\Omega} \left\{ e^{-i[\phi(\bar{x}_{n0} + \frac{\Omega}{2\gamma}) - \phi(\bar{x}_{n0} - \frac{\Omega}{2\gamma})]} e^{-\overline{\Delta x}^2 C_n^2 \Omega^2/2} - e^{-\overline{\Delta x}^2 \Omega^2/2} \right\}, \end{aligned} \tag{3.71}$$

where F represents the Fourier transform operation. Numerical results for various diffent values of γ (or ϕ_0) indicate that $\Omega_{max} \sim \gamma$. (We note that $\bar{x}_{n0} \sim O(1)$, $C_n^2 \simeq 1$, and thus $\tilde{I}_{Ls}(\Omega) \simeq \{e^{-i[\phi(\frac{\Omega}{2\gamma}) - \phi(-\frac{\Omega}{2\gamma})]} - 1\} e^{-\overline{\Delta x}^2 \Omega^2/2} \delta(\Omega) = 0$ for $\Omega/\gamma \gg 1$, where $\delta(\Omega)$ represents the Dirac delta function.) Notice that the Gaussian terms $e^{-\overline{\Delta x}^2 C_n^2 \Omega^2/2}$ and $e^{-\overline{\Delta x}^2 \Omega^2/2}$ may be replaced by unity for sufficiently small $\overline{\Delta x}$ such that $\overline{\Delta x} \ll 1/\gamma$. Once the spectrum of irradiance is computed, irradiance $I_L(\bar{x})$ can be calculated by taking the inverse Fourier transform of $\tilde{I}_{Ls}(\Omega)$ using a fast Fourier transform algorithm [cf. Eq. (3.61)].

To check the validity of the higher-order approximation (3.70) [or (3.71)], we now wish to find the analytical expression for $\tilde{I}_L(\Omega)$, starting off with the initial WDF $\bar{F}_0^+$ given by (3.49). Using the coordinate transformation in free space [cf. (3.55)]:

$$\begin{bmatrix} \bar{x}_0 \\ \theta_0 \end{bmatrix} = \begin{bmatrix} 1 & -\bar{L} \\ 0 & 1 \end{bmatrix} \begin{bmatrix} \bar{x} \\ \theta \end{bmatrix} , \tag{3.72}$$

we obtain

$$\bar{F}_L(\bar{x}, \theta) = \frac{1}{2\pi} \int_{-\infty}^{\infty} d\bar{s} \; e^{-i\bar{k}\theta\bar{s}} e^{i[\phi(\bar{x} - \bar{L}\theta + \frac{\bar{s}}{2}) - \phi(\bar{x} - \bar{L}\theta - \frac{\bar{s}}{2})]} . \tag{3.73}$$

The wavenumber integration of the output WDF (i. e., integration with respect to $\bar{k}\theta$) leads to

$$I_L(\bar{x}) = \frac{\gamma}{2\pi}\int_{-\infty}^{\infty} d\bar{s}\int_{-\infty}^{\infty} d\xi\ e^{-i\gamma(\bar{x}-\xi)\bar{s}}\, e^{i[\phi(\xi+\frac{\bar{s}}{2})-\phi(\xi-\frac{\bar{s}}{2})]}\ , \tag{3.74}$$

from which we find

$$\tilde{I}_L(\Omega) = \frac{\gamma}{(2\pi)^2}\int_{-\infty}^{\infty} d\bar{s}\ F_x\left\{e^{-i\gamma\bar{s}\bar{x}}\right\} F_x\left\{e^{i[\phi(\bar{x}+\frac{\bar{s}}{2})-\phi(\bar{x}-\frac{\bar{s}}{2})]}\right\}\ , \tag{3.75}$$

where F_x is the Fourier transform operator for the variable $\bar{x}$. After performing the Fourier transforms with respect to $\bar{x}$ [See Eq. (3.59) for its definition], we obtain

$$\tilde{I}_L(\Omega) = \frac{i}{2\pi}\int_{-\infty}^{\infty} d\bar{x}\ e^{-i\bar{x}\Omega}\, e^{-i[\phi(\bar{x}+\frac{\Omega}{2\gamma})-\phi(\bar{x}-\frac{\Omega}{2\gamma})]}\ . \tag{3.76}$$

For sufficiently small $\overline{\Delta x}$, the Gaussian term in (3.70), $e^{-\overline{\Delta x}^2 c_n^2 \Omega^2/2}$, becomes unity, and the higher-order approximation (3.70) is essentially the trapezoidal-rule integration (or Riemann sum) of the analytical expression (3.76), which is exact within the validity of the thin-screen approximation, $u_0(\bar{x}) = e^{i\phi(\bar{x})}$ [cf. Eqs. (3.49) and (2.69)]. Thus, the higher-order approximation in the wave-kinetic numerical method is equivalent to the Huygens-Fresnel diffraction integral formulation.

3.3 Huygens-Fresnel Diffraction Formula

For a one-dimensional phase screen, by introducing the bar notations in the angular-spectral representation of the Huygens-Fresnel diffraction integral (2.78), we have

$$u(\bar{x}) = \int_{-\infty}^{\infty} dq \; e^{iq\bar{x}} \, e^{-iq^2/2\gamma} \, U_0(q) \;, \tag{3.77}$$

where $\gamma = \bar{k}/\bar{L} = k\ell^2/L$, and

$$U_0(q) = \frac{1}{2\pi} \int_{-\infty}^{\infty} d\bar{x} \; e^{-iq\bar{x}} \, e^{i\phi(\bar{x})} \;. \tag{3.78}$$

Here, $\phi(\bar{x})$ is given by (3.7) with x/ℓ and x_n/ℓ being replaced by $\bar{x}$ and $\bar{x}_n$, respectively. The irradiance at $\bar{z} = \bar{L}$ is then calculated from $I_L(\bar{x}) = |u(\bar{x})|^2$ [cf. Eq. (2.37)]. Note that for the spatial angular frequency q the bar notation is not used since this would not cause any confusion in the following. Thus, q in the above equations is a dimensionless quantity. In the expression (3.77), two Fourier transform operations are involved. A little manipulation facilitates a direct application of an existing fast Fourier transform algorithm (i. e., it allows us to avoid operations involved in an FFT like shift and flip around the $(\frac{N}{2} + 1)$-th data point, where N is the number of discrete data points for FFT) [85].

We may introduce the following discrete data points:

$$\bar{x}_n = (n - 1 - \frac{N}{2})\overline{\Delta x} \;, \quad q_m = (m - 1 - \frac{N}{2})\Delta q \;, \tag{3.79}$$

where $\Delta q = 2\pi/N\,\overline{\Delta x}$. It follows then that

$$
\begin{aligned}
u_n &= \Delta q \sum_{m=1}^{N} e^{iq_m \bar{x}_n} e^{-iq_m^2/2\gamma} \left[\frac{\overline{\Delta x}}{2\pi} \sum_{k=1}^{N} e^{i\phi_k} e^{-iq_m \bar{x}_k} \right] \\
&= \frac{1}{N} \sum_{m=1}^{N} e^{2\pi i (m-1-\frac{N}{2})(n-1-\frac{N}{2})/N} e^{-i(\Delta q)^2 (m-1-\frac{N}{2})/2\gamma} \\
&\times \left[\sum_{k=1}^{N} e^{i\phi_k} e^{-2\pi i (m-1-\frac{N}{2})(k-1-\frac{N}{2})/N} \right] ,
\end{aligned}
\tag{3.80}
$$

where $u_n = u(\bar{x} = \bar{x}_n)$ and $\phi_k = \phi(\bar{x} = \bar{x}_k)$. Let $m' = m - N/2$. Then (3.80) becomes

$$
u_n = \frac{1}{N} \left(\sum_{m'=1}^{N/2} + \sum_{m'=1-N/2}^{0} \right) \left(e^{2\pi i (m'-1)(n-1)/N} e^{-i(\Delta q)^2 (m'-1)^2/2\gamma} \hat{U}_{m'} \right) , \tag{3.81}
$$

where

$$
\hat{U}_{m'} = \sum_{k=1}^{N} e^{-2\pi i (m'-1)(k-1)/N} e^{i\phi_k} . \tag{3.82}
$$

We note that $\hat{U}_{m'}$ is periodic in m' with period N, i. e., $\hat{U}_{m'+N} = \hat{U}_{m'}$ and similarly so for the first exponential term in (3.81). Thus, by shifting the summation index m' in the second summation term in (3.81) by N, we obtain:

$$
u_n = \frac{1}{N} \sum_{m=1}^{N} e^{2\pi i (m-1)(n-1)/N} e^{-i(\Delta q)^2 M^2/2\gamma} \hat{U}_m , \tag{3.83}
$$

where

$$
M = \begin{cases} m - 1 , & m \leq N/2 \\ N + 1 - m , & m > N/2 . \end{cases} \tag{3.84}
$$

This expression can be written more compactly as

$$u_n = F_m^{-1}\left\{ e^{-i(\Delta q)^2 M^2/2\gamma}\ F_k\left[e^{i\phi_k} \right] \right\} , \tag{3.85}$$

where F_k and F_m^{-1} represent a forward FFT with respect to index k and an inverse FFT with respect to index m, respectively.

3.4 Calculation of Statistics

To compute wave statistics from many realizations, we put a number of receivers across the observation plane, which are equally spaced with a distance Δs [cf. Fig. 3.1]. (In fact, the number of receivers is equal to the number of irradiance points for each realization.) In our numerical simulation, we put 11 receivers separated by $\Delta s \simeq 0.1\,\ell$ [cf. Sec. 3.6].) The data from each receiver (for many realizations) are stored, and the statistics are computed *a posteriori*. Let us denote the number of receivers and the number of realizations by N_s and N_l, respectively. For each receiver, we have N_l sample data. In this section, we denote the irradiance at $\bar{z} = \bar{L}$ by $I(\bar{x})$ (which was denoted by $I_L(\bar{x})$ in the preceding).

First, we wish to define the statistical quantities of interest. The normalized covariance of irradiance is defined as

$$C_I(\bar{x}) = \frac{< [I(\bar{x}') - < I >][I(\bar{x} + \bar{x}') - < I >] >}{< I >^2} , \tag{3.86}$$

where the bar notations are used, and $< I >$ is the mean of irradiance fluctuation, which is set to be unity in our numerical simulation. The normalized variance of irradiance, which is usually referred to as the scintillation index, is then given by

$$\sigma_I^2 = C_I(0) = \frac{< [I - < I >]^2 >}{< I >^2} . \tag{3.87}$$

It is more convenient to use a differently normalized covariance, instead of the normalized covariance (3.86). We define the normalized covariance as

$$c_I(\bar{x}) = C_I(\bar{x})/\sigma_I^2 \ . \tag{3.88}$$

The statistical quantities given above can be computed using the following estimators.

Since we have a discrete set of data, we denote the covariance $C_I(k\,\overline{\Delta s})$ simply by $C_I(k)$. We use an estimator for $C_I(k)$ defined as

$$\hat{C}_I(k) = \frac{1}{N_I} \sum_{i=1}^{N_I} \frac{[I_1(i) - \bar{I}_1][I_{k+1}(i) - \bar{I}_{k+1}]}{(\bar{I}_1)^2} \ , \tag{3.89}$$

where

$$\bar{I}_{k+1} = \frac{1}{N_I} \sum_{i=1}^{N_I} I_{k+1}(i) \ , \quad (k = 0, 1, 2, \ldots, N_s - 1) \ . \tag{3.90}$$

In the above equation, we used $\bar{I}_{k+1}$ just for convenience. We may replace $\bar{I}_{k+1}$ by $\bar{I}_1$, or we may use $\frac{1}{N_s} \sum_{k=0}^{N_s-1} \bar{I}_{k+1}$ for $\bar{I}_1$ and $\bar{I}_{k+1}$. Since $< I > = 1.0$ in our case, for large N_I ($\gtrsim$1000), we may simply set $\bar{I}_1 = \bar{I}_{k+1} \simeq 1.0$ as well. Using this estimator, the scintillation index and the normalized covariance can be computed [cf. Eqs. (3.87) and (3.88)]:

$$\hat{\sigma}_I^2 = \hat{C}_I(0) \ , \quad \hat{c}_I(\bar{x}) = \hat{C}_I(\bar{x})/\hat{\sigma}_I^2 \ . \tag{3.91}$$

Here, we need to mention the problem of *outliers* briefly. In numerical simulation, sometimes there appear unusually large or small samples for some realizations, which are often referred to as *outliers*. There are often statistical reasons for removing those outliers. More details will be discussed in Sec. 3.6.

To obtain error bounds of the estimators, we need analytical expressions for the variances of the estimators. The standard error of an estimator, which is used as a convenient measure for error bounds, can be calculated from the corresponding variance by taking its square root. To compute the variances of the estimators exactly, we have to know the probability distribution (of irradiance), which is of course unknown (except a few limiting cases). Thus, to get crude error bounds, which seem to be sufficient for our purpose, we assume that $I(\bar{x})$ is a homogeneous Gaussian random function with a variance σ_I^2. We note here that $I(\bar{x})$ is homogeneous, but not Gaussian, in general. (Several probability distribution functions for irradiance have been proposed, which include log-normal, Rayleigh, Rice-Nakagami, K, I-K, etc. [cf. Refs. 60-76].) Under the assumption, one can show that [114]

$$Var(\bar{I}) = \sigma_I^2 / N_I \ , \tag{3.92}$$

$$Var(\hat{\sigma}_I^2) = \frac{2(N_I - 1)}{N_I^2} \sigma_I^4 \simeq \frac{2}{N_I} \sigma_I^4 \ . \tag{3.93}$$

To get some idea of error bounds for $\hat{c}_I(k)$, let us now consider a standard type of (normalized) covariance estimator,

$$\hat{r}_k = \hat{R}_k / \hat{R}_0 \ , \tag{3.94}$$

with

$$\hat{R}_k = \frac{1}{N_s} \sum_{j=1}^{N_s - k} (I_j - \bar{I})(I_{j+k} - \bar{I}) \ , \quad (k = 0, 1, 2, \dots) \ , \tag{3.95}$$

where I_j, $j = 1, \dots, N_s$, correspond to irradiance samples for a single realization. The covariance estimator $\hat{R}_k$ is different from $\hat{C}_I(k)$. However, if ergodicity holds (and N_s for $\hat{R}_k$ and N_I for $\hat{C}_I(k)$ are large enough), then $\hat{R}_k$ becomes equivalent to $\hat{C}_I(k)$ [78, 114, 123]. We could then use $\hat{R}_k$ with large N_s (or take an average of $\hat{R}_k$ for a relatively large

number of realizations), but our preliminary numerical study indicates that it is more efficient to use $\hat{C}_l(k)$ (with small N_s and large N_l). In other words, it turns out that simulations with small number of sample points and many realizations are preferable to simulations with more sample points and fewer realizations. According to Box et al. [123], the variance of $\hat{r}_k$ for large N_s is given by (with the same assumptions for $I(\bar{x})$ as mentioned before):

$$Var(\hat{r}_k) \simeq \frac{1}{N_s} \sum_{v=-\infty}^{\infty} \{r_v^2 + r_{v+k} r_{v-k} - 4 r_k r_v r_{v-k} + 2 r_v^2 r_k^2\} . \tag{3.96}$$

This can be used as a crude estimate for the variance of $\hat{c}_l(k)$. To see the behavior of $Var(\hat{r}_k)$, consider an exponential covariance function, $r_k = e^{-\alpha |k|}$. One can show that [123]:

$$Var(\hat{r}_k) \simeq \frac{1}{N_s} \left[\frac{(1+\beta^2)(1-\beta^{2k})}{1-\beta^2} - 2k \beta^{2k} \right] , \quad (\beta = e^{-\alpha}) . \tag{3.97}$$

It is informative to note that the standard error of the normalized covariance estimator is zero at $k = 0$, it becomes maximum at $k \simeq 1/(1-\beta^2)$ (i. e., a corresponding integer value), and it approaches $\sqrt{(1+\beta^2)/N_s(1-\beta^2)}$ as k goes to infinity. (We can see this behavior from the simulation results in Sec. 3.6, i. e., the errors become maximum around $\bar{x}$ for which $c_l(\bar{x})$ is close to zero.)

We note that the covariance estimator $\hat{R}_k$ (equivalently $\hat{C}_l(k)$) is a biased estimator, but the variance of $\hat{R}_k$ is much smaller than the variance of the corresponding unbiased estimator $\hat{R}_k'$ $[= \hat{R}_k N_s/(N_s - k)]$ for $k > 0$ [114].

3.5 Analytical Expression for Covariance of Irradiance

From the Huygens-Fresnel formula (2.77), we have

$$u(x, z) = \sqrt{\frac{k}{2\pi i z}} \int_{-\infty}^{\infty} dx_1 \; e^{i\phi(x_1)} \, e^{ik(x - x_1)^2/2z} \; , \tag{3.98}$$

where $\phi(x)$ is a random phase fluctuation at $z = 0$ [cf. Eq. (3.7)]. Thus, irradiance at $z = L$ is given by

$$I(x, z) = \frac{k}{2\pi L} \int_{-\infty}^{\infty} dx_1 \int_{-\infty}^{\infty} dx_2 \; e^{i[\phi(x_1) - \phi(x_2)]} \, e^{ik[(x - x_1)^2 - (x - x_2)^2]/2L} \; . \tag{3.99}$$

The correlation of irradiance can be found from this expression, i. e.,

$$\begin{aligned} B_I(x) &\equiv \langle I(x/2)\, I(-x/2) \rangle \\ &= \int_{-\infty}^{\infty} dx_1 \int_{-\infty}^{\infty} dx_2 \int_{-\infty}^{\infty} dx_3 \int_{-\infty}^{\infty} dx_4 \; \Gamma_{40}(x_1, x_2, x_3, x_4) \\ &\times e^{i\left(\frac{k}{2L}\right)\left[\left(\frac{x}{2} - x_1\right)^2 - \left(\frac{x}{2} - x_2\right)^2 + \left(\frac{x}{2} + x_3\right)^2 - \left(\frac{x}{2} + x_4\right)^2\right]} \; , \end{aligned} \tag{3.100}$$

where

$$\Gamma_{40}(x_1, x_2, x_3, x_4) = \langle e^{i(\phi_1 - \phi_2 + \phi_3 - \phi_4)} \rangle \; , \tag{3.101}$$

with $\phi_j = \phi(x_j)$.

Since $\phi(x)$ is a Gaussian random function with zero mean, Γ_{40} can be represented as

$$\begin{aligned} \Gamma_{40}(x_1, x_2, x_3, x_4) &= e^{-\frac{1}{2}\langle(\phi_1 - \phi_2 + \phi_3 - \phi_4)^2\rangle} \\ &= e^{-2\phi_0^2 + \langle\phi_1\phi_2\rangle + \langle\phi_3\phi_4\rangle + \langle\phi_1\phi_4\rangle + \langle\phi_2\phi_3\rangle - \langle\phi_1\phi_3\rangle - \langle\phi_2\phi_4\rangle} \; , \end{aligned} \tag{3.102}$$

with $\langle \phi_i \phi_j \rangle = \phi_0^2 \, e^{-(x_i - x_j)^2/\ell^2}$ [cf. Eq. (3.5)]. Let us introduce new variables:

$$
\begin{aligned}
X &= \frac{1}{4}\,[(x_1 + x_3) + (x_2 + x_4)] \\
\xi &= (x_1 + x_3) - (x_2 + x_4) \\
\xi_1 &= \frac{1}{2}\,[(x_1 - x_3) + (x_2 - x_4)] \\
\xi_2 &= \frac{1}{2}\,[(x_1 - x_3) - (x_2 - x_4)] \ .
\end{aligned}
\tag{3.103}
$$

We note that $dx_1\,dx_2\,dx_3\,dx_4 = dX\,d\xi\,d\xi_1\,d\xi_2$. For a statistically homogeneous medium, Γ_{40} is independent of X. Since the exponential term in (3.100) becomes

$$
e^{i\left(\frac{k}{L}\right)[\xi_2(\xi_1 - x) + \xi X]} \ , \tag{3.104}
$$

with the new variables, we obtain, after performing integration with respect to X:

$$
\begin{aligned}
B_I(x) = \left(\frac{k}{2\pi L}\right)^2 \int_{-\infty}^{\infty} d\xi_1 \int_{-\infty}^{\infty} \xi_2 \int_{-\infty}^{\infty} d\xi \left[2\pi\,\delta\left(\frac{k}{L}\,\xi\right)\right] \Gamma_{40}(\xi_1,\ \xi_2,\ \xi = 0) \\
\times\, e^{i\left(\frac{k}{L}\right)\xi_2(\xi_1 - x)} \ .
\end{aligned}
\tag{3.105}
$$

From (3.103), we have, for $\xi = 0$: $x_1 - x_2 = -(x_3 - x_4) = \xi_2$, $x_1 - x_4 = x_2 - x_3 = \xi_1$, $x_1 - x_3 = \xi_1 + \xi_2$, and $x_2 - x_4 = \xi_1 - \xi_2$. It follows then that

$$
B_I(x) = \frac{k}{2\pi L} \int_{-\infty}^{\infty} d\xi_1 \int_{-\infty}^{\infty} d\xi_2\, e^{-\phi_0^2 f(\xi_1,\ \xi_2)}\, e^{i\left(\frac{k}{L}\right)\xi_2(\xi_1 - x)} \ , \tag{3.106}
$$

where

$$
f(\xi_1,\ \xi_2) = 2 - 2\,e^{-\xi_1^2/\ell^2} - 2\,e^{-\xi_2^2/\ell^2} + e^{-(\xi_1 + \xi_2)^2/\ell^2} + e^{-(\xi_1 - \xi_2)^2/\ell^2} \ . \tag{3.107}
$$

We may rewrite $B_I(x)$ as

$$B_I(x) = \frac{k}{2\pi L}\left[\int_0^\infty d\xi_1 \int_{-\xi_1}^{\xi_1} d\xi_2 + \int_{-\infty}^0 d\xi_1 \int_{\xi_1}^{-\xi_1} d\xi_2 + \int_0^\infty d\xi_2 \int_{-\xi_2}^{\xi_2} d\xi_1 + \int_{-\infty}^0 d\xi_2 \int_{\xi_2}^{-\xi_2} d\xi_2\right] e^{-\phi_0^2 f(\xi_1,\ \xi_2)}\, e^{i\left(\frac{k}{L}\right)\xi_2(\xi_1 - x)} \quad . \tag{3.108}$$

By letting $\xi_1' = -\xi_1$ and $\xi_2' = -\xi_2$ in the second and the fourth term, respectively, and by using the fact that $f(\xi_1,\ \xi_2) = f(\xi_2,\ \xi_1) = f(-\xi_1,\ \xi_2) = f(\xi_1,\ -\xi_2)$, we obtain, after a simple manipulation for trigonometric functions:

$$B_I(x) = \frac{2k}{\pi L}\int_0^\infty d\xi_1 \int_0^{\xi_1} d\xi_2\, e^{-\phi_0^2 f(\xi_1,\ \xi_2)}\left[\cos\left(\frac{kx\xi_1}{L}\right) + \cos\left(\frac{kx\xi_2}{L}\right)\right] \times \cos\left(\frac{k\xi_1\xi_2}{L}\right) \quad . \tag{3.109}$$

If we let $u = \xi_1/\ell$, $v = \xi_2/\ell$, and $\bar{x} = x/\ell$, then the correlation of irradiance becomes

$$B_I(\bar{x}) = \frac{2\gamma}{\pi}\int_0^\infty du \int_0^u dv\ e^{-\phi_0^2 f(u,\ v)}\left[\cos(\gamma\bar{x}u) + \cos(\gamma\bar{x}v)\right]\cos(\gamma uv), \tag{3.110}$$

where

$$f(u,\ v) = 2 - 2e^{-u^2} - 2e^{-v^2} + e^{-(u+v)^2} + e^{-(u-v)^2} \quad . \tag{3.111}$$

For numerical calculation, it is more convenient to rewrite this as

$$B_I(\bar{x}) = \frac{\gamma}{\pi}\int_0^\infty du \int_0^u dv\ e^{-\phi_0^2 f(u,\ v)}\left\{2\cos(\gamma\bar{x}u)\ \cos(\gamma uv) + \cos[\gamma v(u+\bar{x})] + \cos[\gamma v(u-\bar{x})]\right\} \quad . \tag{3.112}$$

The covariance of irradiance and the scintillation index can be calculated from

$$C_I(\bar{x}) = B_I(\bar{x}) - 1.0 \quad , \quad \sigma_I^2 = C_I(0) \quad . \tag{3.113}$$

We notice that when $\phi_0^2 \gg 1$ (good even for $\phi_0^2 \gtrsim 6$), $f(u, v)$ can be approximated as

$$f(u, v) \simeq \frac{1}{2}\left(\frac{\partial^2 f}{\partial v^2}\right)_{v=0} v^2 = 2\,\beta(u)\,v^2 \ , \tag{3.114}$$

where

$$\beta(u) = 1 - (1 - 2u^2)\,e^{-u^2} \ . \tag{3.115}$$

To compute the integral given by (3.112), we use an adaptive quadrature (a truncated Chebyshev series) algorithm useful for integrals with strongly oscillating integrand, introduced by Piessens et al. [113]. Using this algorithm, we can compute one or both of the integrals,

$$\begin{bmatrix} S(\omega) \\ C(\omega) \end{bmatrix} = \int_a^b dt\ f(t) \begin{bmatrix} \sin(\omega t) \\ \cos(\omega t) \end{bmatrix} \ , \tag{3.116}$$

to within a user-specified absolute tolerance ε_a, or relative tolerance ε_r.

3.6 Numerical Simulation

We first discuss some important input parameters for numerical simulation. The input parameters are defined, and general criteria for choosing the values of those parameters are discussed, in Sec. 3.6.1. The implementations of the wave-kinetic numerical method and the Huygens-Fresnel diffraction formula are studied by single-realization calculations, and results for single realizations from both methods are compared to each other, in Sec. 3.6.2. Finally in Sec. 3.6.3, we present simulation results for σ_I^2 and $c_I(\bar{x})$ from the wave-kinetic numerical method. The results are

compared with those obtained from analytical expressions given by Eqs. (3.112) and (3.113).

3.6.1 Important Input Parameters for Numerical Simulation

As shown in Fig. 3.5, in numerical simulation the width of the screen W must be finite, which can cause edge effects.

First, we wish to discuss the edge effects in view of the wave-kinetic numerical method. Let the width of the region occupied by the receivers at $z = L$ be W_s. Let us also introduce the *spread* parameter L_e such that

$$L_e = \vartheta_0 L \ . \tag{3.117}$$

Since we are realizing a medium with Gaussian eddies, although the eddy centers are confined within the region of width W (and thickness D, or along the x_0-axis in case of the simplified model), the numerically generated inhomogeneity is rather smooth (not very sharp) around both edges at $x_0 = \pm W/2$, but statistically it is highly inhomogeneous in the region within a scale size ℓ from the edges. It follows that irradiance data within several L_e 's ($\simeq 3 L_e$) from the edges in the observation plane ($x = \pm W/2$), where rays from the edge regions arrive, include errors. From preliminary numerical simulations, we found the following rule of thumb:

$$W - W_s \gtrsim 10 L_e \ . \tag{3.118}$$

Using the relations for ϑ_0 and ζ given by (3.16) and (3.17), this also may be written as

$$\overline{W} - \overline{W}_s \gtrsim 5\sqrt{2}\ \zeta \ , \tag{3.119}$$

where the bar notations are used (i. e., $\overline{W} = W/\ell$, $\overline{W}_s = W_s/\ell$).

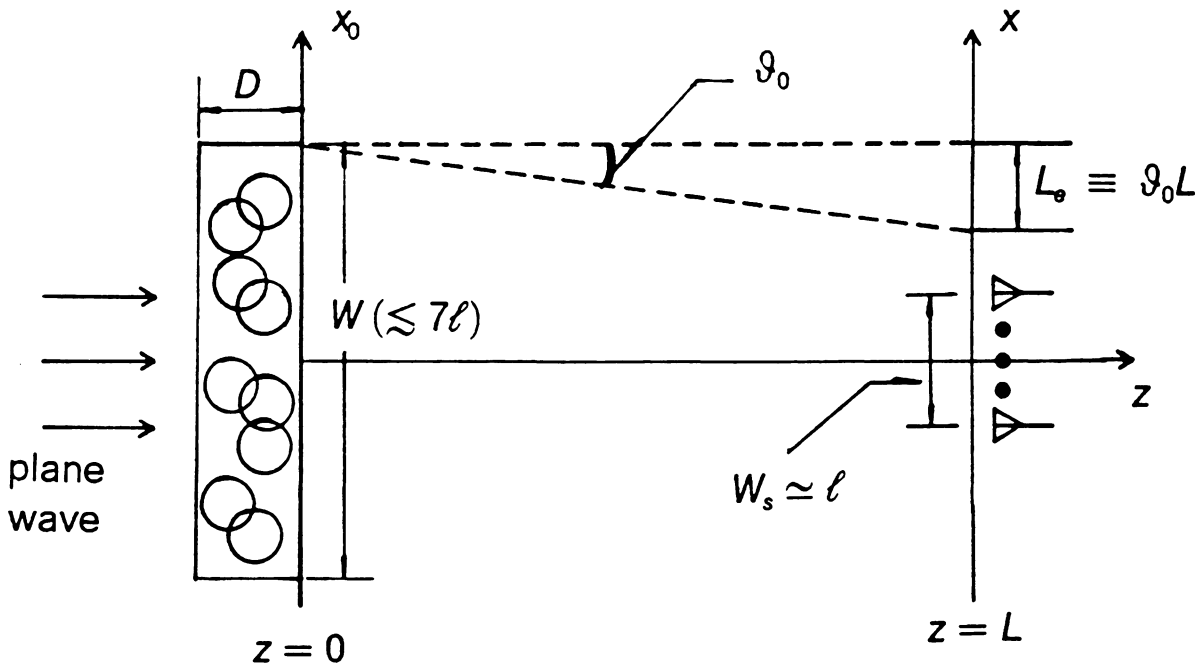

Figure 3.5 Geometry for numerical simulation, which explains edge effects. Relevant parameters are indicated.

In the Huygens-Fresnel diffraction integral formulation, edge effects may be explained in terms of edge diffraction. Suppose now that the edges are very sharp, for convenience. Using the Huygens-Fresnel formula, we can derive (more systematically) a similar criterion for the margin of the screen width, $\overline{W} - \overline{W}_s$. Substituting the angular-spectral representation for $u_0(x)$ given by (2.78) in the Huygens-Fresnel formula (2.76), we obtain [cf. Appendix A3.3 or Ref. 85]:

$$u(\bar{x},\ \bar{L}) = \int_{-\infty}^{\infty} dq\ e^{iq\bar{x}}\, e^{-i\bar{L}q^2/2\bar{k}}\, U_0(q)\, G(\bar{x},\ \bar{L},\ q)\ , \tag{3.120}$$

with

$$\begin{aligned} G(\bar{x},\ \bar{L},\ q) = \frac{1}{\sqrt{2i}} \Bigg\{ & g_F\left[\sqrt{\frac{\bar{k}}{\pi\bar{L}}}\left(\frac{\overline{W}}{2} - \bar{x} + \frac{\bar{L}}{\bar{k}}q\right)\right] \\ & + g_F\left[\sqrt{\frac{\bar{k}}{\pi\bar{L}}}\left(\frac{\overline{W}}{2} + \bar{x} - \frac{\bar{L}}{\bar{k}}q\right)\right]\Bigg\}\ . \end{aligned} \tag{3.121}$$

Here, the bar notations are used, and the function g_F represents the Fresnel integral, defined as

$$g_F(\bar{x}) = \int_0^{\bar{x}} d\xi\ e^{i\pi\xi^2/2}\ . \tag{3.122}$$

Since the scale of $u_0(\bar{x})$ [$= e^{i\phi(\bar{x})}$] is of order $1/\phi_0$ for $\phi_0 > 1$ [85], most of the spectrum of $U_0(q)$ is contained within $|q| \le 2\pi\phi_0$. Now, compare (3.120) with the angular-spectral representation for an infinite phase screen, (3.77). It follows that G must be close to unity within the bandwidth (BW). Since $g_F(\bar{x}) \simeq \sqrt{i/2}$ for $\bar{x} \ge 2$, using the BW given above, we obtain the condition

$$\overline{W} - \overline{W}_s \gtrsim 2\,\bar{L}_{HF}\ , \quad \bar{L}_{HF} = 2\sqrt{\frac{\pi\bar{L}}{\bar{k}}} + 2\phi_0\,\frac{\pi\bar{L}}{\bar{k}}\ . \tag{3.123}$$

Using the parameters γ and ζ [cf. Eq. (3.17)], this may be written as

$$\overline{W} - \overline{W}_s \geq 4\sqrt{\frac{\pi}{\gamma}} + 2\pi\zeta \ . \tag{3.124}$$

In our numerical simulation, $\gamma = 13.856 \gg 1$ and $0 < \zeta < 1$, since we are interested in the random focusing region [See the discussions following (3.17) in Sec. 3.1]. Hence it is certainly true that

$$\overline{W} - \overline{W}_s \gtrsim 2\pi\zeta \ . \tag{3.125}$$

We will therefore use (3.119) [or (3.118)] as the condition for the margin of the screen width $\overline{W}$, which is required for avoiding edge effects.

For a given $\overline{W}_s$ (in our numerical simulation, we put 11 receivers separated by approximately $0.1\,\ell$ so that $\overline{W}_s \simeq 1.0$ [cf. Sec. 3.4]), we have to choose a $\overline{W}$ which satisfies the relation (3.119). As mentioned before, the two important parameters, by which a phase screen problem is completely determined, are γ $(= k\ell^2/L = \bar{k}/\bar{L})$ and ϕ_0 [cf. analytical expression for $C_I(\bar{x})$, Eq. (3.112)]. For these two, the parameter ζ is determined by the relation, $\zeta = 2\,\phi_0/\gamma$. Thus, we have three important parameters, γ, ϕ_0, and $\overline{W}$, assuming that $\overline{W}_s$ and $\bar{k}$ are fixed ($\overline{W}_s \simeq 1.0$, and $\bar{k} = 1.0472\times10^5$ [cf. Secs. 3.4 and 3.1]).

For a given ϕ_0, we are free to choose the number of eddies, i. e., the average number of eddies along the z-axis, N_z , or thickness of the screen D [cf. Eqs. (3.4) and (3.10)]. In other words, if we change $\overline{D}$ $(= D/\ell)$ for a given ϕ_0, then the number of eddies changes and thus the r.m.s. value of refractive-index fluctuations, η_0, also changes for a given $\bar{k}$. A large $\overline{D}$ is required for enough randomness for each realization. The results for numerical simulation of random phase fluctuations [Eq. (3.7) is used to simulate a Gaussian random phase with the correlation function given by (3.5)], showed that $\overline{D} \geq 100$ seems to be enough.

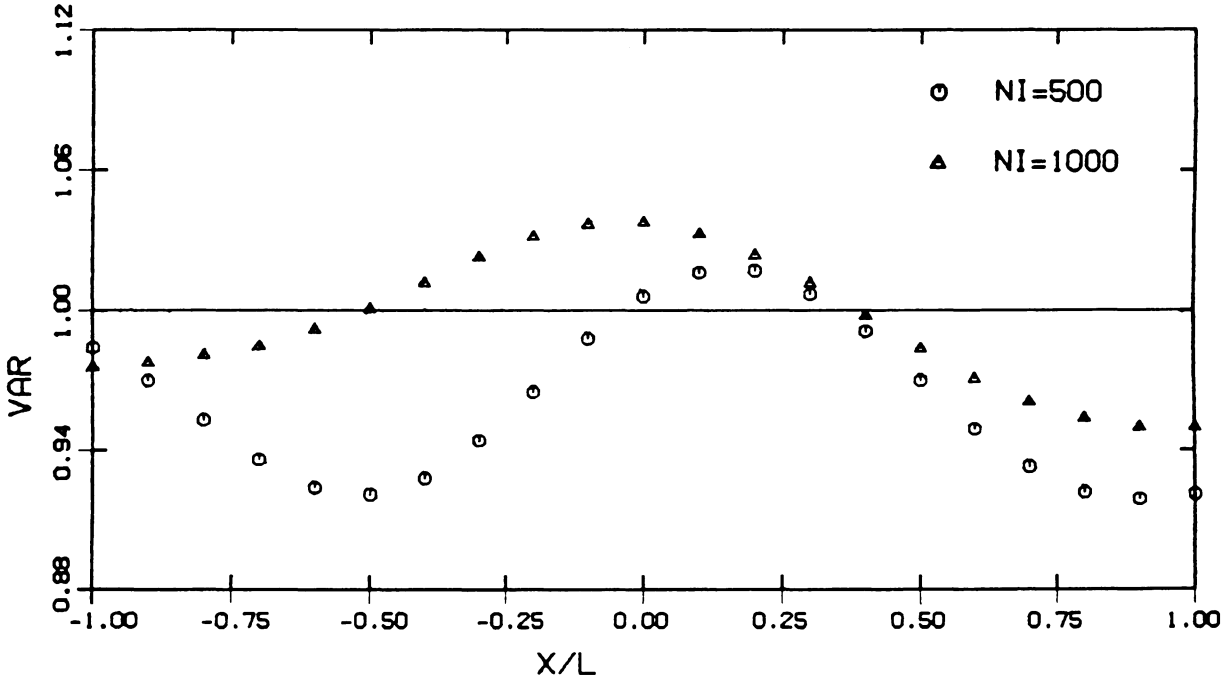

Figure 3.6 Variance of phase vs receiver location: $\phi_0^2 = 1.0$. The receiver separation is 0.1, and the number of receivers are 21.

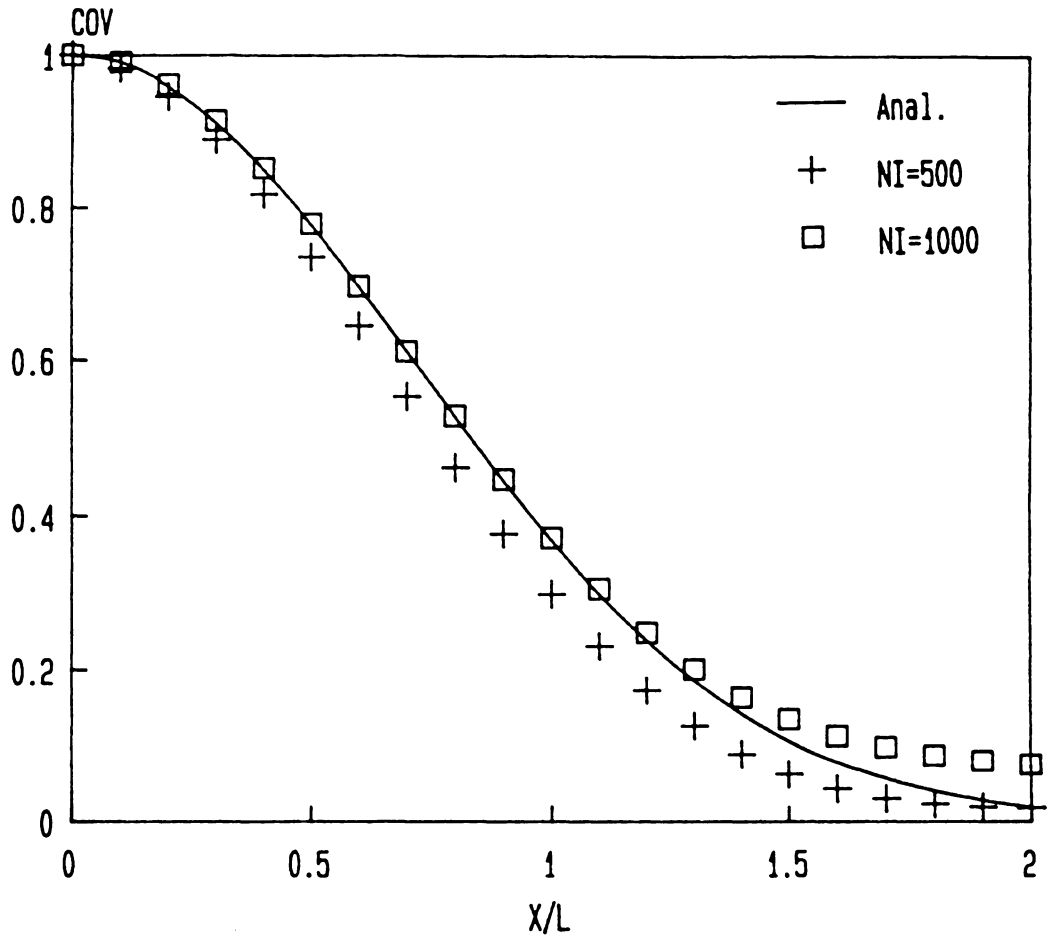

Figure 3.7 Normalized covariance of phase vs receiver separation: $\phi_0 = 1.0$.

Simulation results for $\phi_0^2 = 1.0$ with $\overline{W} = 5.0$ and $\overline{D} = 200$ are shown in Figs. 3.6 and 3.7, where the data are obtained for $\overline{W}_s = 2.0$ with 21 sample points which are separated by 0.1. We note that for $N_l = 1000$, the simulation result for the normalized covariance of $\phi(\bar{x})$ (normalized with respect to the sample variance at $\bar{x} = -1.0$) is in good agreement with the desired one, $e^{-\bar{x}^2}$, and the sample variances $\hat{\phi}_0^2$ at 21 sample points are well within the range, $1.0 \pm S_\varepsilon(\hat{\phi}_0^2)$, where $S_\varepsilon(\hat{\phi}_0^2) = \sqrt{2/N_l} = 0.045$ (More accurately, $\hat{\phi}_0^2 \pm S_\varepsilon(\hat{\phi}_0^2)$ include the desired variance $\phi_0^2 = 1.0$).

There are several other parameters related to implementation of the wave-kinetic numerical method and the Huygens-Fresnel diffraction formula. First, for the wave-kinetic numerical method [cf. Eqs. (3.48), (3.61), and (3.71)], the ray spacing $\overline{\Delta x}$ must be small enough so that errors involved in the discretization and the linearization for the wave-kinetic numerical method [cf. Secs. 2.3.3 and 3.2.1] become negligible. We note that to implement the higher-order approximation given by (3.71), where we first compute the spectrum of irradiance $\tilde{I}(\Omega)$, we need an inverse FFT [cf. Eq. (3.61)] to compute irradiance $I_L(\bar{x})$. [For the Liouville approximation, we use the direct summation formula (3.48). We may use the spectral representation (3.62), in which case an inverse FFT is also needed.] We denote the sampling interval in the spatial frequency domain by Δf, which is related to $\Delta\Omega$ by $\Delta f = \Delta\Omega/2\pi$. Discussions regarding the choice of Δf will be given in the next section.

Next, to implement the Huygens-Fresnel diffraction integral [cf. Eq. (3.83)], we need two Fourier transform operations. The sampling interval for a FFT will also be denoted by $\overline{\Delta x}$, which is related to Δf by $\overline{\Delta x} = 1/N_{FFT}\Delta f$, where N_{FFT} is the number of sampling points. The interval in the spatial angular frequency domain, Δq, in (3.79) and (3.83) is related to Δf by $\Delta q = 2\pi\Delta f$. [Note that in the wave-kinetic numerical method, the ray spacing $\overline{\Delta x}$ is not directly related to Δf.] For the Huygens-Fresnel formula, $\overline{\Delta x}$ must satisfy the Nyquist criterion, i. e., $\overline{\Delta x} \leq 1/2\, f_{max,u}$, where $f_{max,u}$ is such

that $|u_0(q)| \simeq 0$ for $|q| \gtrsim 2\pi f_{max,u}$. It turns out from single-realization calculations [cf. Sec. 3.6.2] that $\overline{\Delta x}$ for the wave-kinetic numerical method can be chosen to be approximately one half of that for the Huygens-Fresnel formula. This may be explained as follows. In the wave-kinetic numerical method, we compute the spectrum of irradiance $\tilde{I}(\Omega)$ [or $I(\bar{x})$ in case of the Liouville approximation], whereas in the Huygens-Fresnel diffraction integral formulation we compute $\tilde{u}(\Omega)$ [$U(q)$ in the previous notation]. Since $\tilde{I}(\Omega)$ is the autocorrelation of $\tilde{u}(\Omega)$, the BW of $\tilde{I}(\Omega)$ is twice as wide as $\tilde{u}(\Omega)$ [$U(q)$ in the previous notation for H-F], and thus the corresponding factor for $\overline{\Delta x}$ seems to follow.

Finally, we wish to mention a linear interpolation scheme briefly. In numerical simulation, much computing time is spent in calculating the random phase $\phi(\bar{x})$ or the random angle $\Delta(\bar{x})$ $(= \phi'(\bar{x})/\bar{k})$. Thus, if we first compute and store discrete data ϕ_k and Δ_k with a certain interval $\overline{\Delta p}$ for each realization, and then compute intermediate values, whenever necessary, by a linear interpolation, then we may reduce computing time by making $\overline{\Delta p}$ as large as possible. Numerical calculations indicate that for the Huygens-Fresnel formula [cf. Eqs. (3.83) and (3.85)], we do not need the linear interpolation scheme, since we need to compute only discrete phases, $\phi_n = \phi(\bar{x} = n\,\overline{\Delta x})$, in this case, and for $\overline{\Delta p}$ larger than $\overline{\Delta x}$, the linear interpolation introduces significant errors. On the other hand, for the wave-kinetic numerical method (especially for the higher-order approximation given by (3.70) or (3.71)), we have to compute discrete spectral values $\tilde{I}(n\overline{\Delta x} \pm \frac{2\pi}{\gamma} m\Delta f)$, $(n,\ m = 0,\ \pm 1, \ldots)$, which in turn requires the data $\phi_{nm} = \phi(n\overline{\Delta x} \pm \frac{2\pi}{\gamma} m\Delta f)$ and $\Delta_n = \Delta(n\,\overline{\Delta x})$. [For the Liouville approximation given by (3.48) or (3.62), we need to compute only Δ_n.] Thus, we will use a linear interpolation scheme for the higher-order approximation. It turns out that the interpolation interval $\overline{\Delta p}$ can be made as large as $\overline{\Delta x}$ for the Huygens-Fresnel formula. [Thus, the interpolation scheme will also be useful for the Liouville approximation,

since $(\overline{\Delta x})_{HF} \simeq 2\,(\overline{\Delta x})_{WK}$.] Numerical calculations show that this works very well and reduces computation time considerably.

In our current research, we are not interested in the optimization of the simulation algorithms, i. e., choosing the values of the input parameters in such a way that computing time is minimized for moderate accuracy. We are rather interested in the accuracy of the simulation schemes discussed before. Since we do not want any unexpected errors due to a marginal choice of the values of the input parameters, we will allow enough of a margin for those parameters, and thus the values of the input parameters used for numerical calculations in the following sections will be somewhat different from those discussed in this section.

3.6.2 Single-Realization Calculations

In this section, the implementations of the wave-kinetic numerical method and the Huygens-Fresnel formula with specifically chosen values of the input parameters are discussed, and the results for single realizations from both methods are compared to each other. In this and the subsequent section, we will use the following abbreviations for convenience. We denote the wave-kinetic numerical method with the Liouville approximation by W-K(LV). The wave-kinetic numerical method with higher-order correction to the Liouville approximation (which we called the higher-order approximation before) will be denoted simply by W-K. The angular-spectral representation of the Huygens-Fresnel diffraction formula will be abbreviated by H-F. We noticed before that W-K is equivalent to H-F, within the validity of the thin-screen approximation [cf. Sec. 3.2].

The phase-screen parameters for numerical calculations in this and the subsequent section are: $\gamma = 13.856$, $1.0 \leq \phi_0 \leq 10.0$. We first discuss a criterion for choosing the value of the parameter Δf for a FFT (for W-K, we need an inverse FFT to compute

$I(\bar{x})$ and for H-F we need a forward and an inverse FFT to compute $u(\bar{x})$). In single-realization calculations, we have computed $I(\bar{x})$ for $|\bar{x}| \leq \bar{W}_{eff}/2$, where $\bar{W}_{eff}$ ($> \bar{W}$) is large enough so that all the scattering effects from a finite screen with width $\bar{W}$ are included within the region, i. e., for $|\bar{x}| > \bar{W}_{eff}/2$, $I(\bar{x}) = 1.0$, which is the irradiance from the input plane wave with a unit amplitude. Numerical results [cf. Figs. 3.9 and 3.10] indicate that for $\gamma = 13.856$ and $\phi_0 \leq 10.0$, $\bar{W}_{eff} \lesssim 8.0$. Thus, to avoid the *aliasing* effects, which may be introduced by an inverse FFT operation, we need $\Delta f \lesssim 1/\bar{W}_{eff}$. Assuming that $\bar{W}_{eff} \simeq 10.0$ (for $\bar{W} \leq 7.0$ and the values of γ and ϕ_0 given above), we choose $\Delta f \simeq 0.1$ in our numerical calculations.

Throughout this section, we choose $\gamma = 13.865$, $\bar{W} = 5.0$, and $\bar{D} = 1000.0$. The values for $\overline{\Delta x}$ used to implement W-K and H-F are $(\overline{\Delta x})_{WK} = 0.04$ and $(\overline{\Delta x})_{HF} = 0.08$. For W-K(LV), we set $\overline{\Delta x} = 0.005$, which is considerably smaller than $(\overline{\Delta x})_{WK}$, since we are interested only in the errors inherent in the Liouville approximation and we wish to avoid errors due to discretization. The interpolation interval $\overline{\Delta p}$ is chosen to be 0.08. For both W-K and H-F, we choose $N_{FFT} = 128$ and $\Delta f = 0.09766[= 1/(0.08\times128)]$. The number of sampling points for a FFT is chosen in such a way that $N_{FFT} \simeq \bar{W}_{eff}/\overline{\Delta x}$. Similarly, for a given $\overline{\Delta x}$ and $\bar{W}_{eff}$, the number of rays (i. e., the number of the Gaussian beamlets) is given by $N_r \simeq \bar{W}_{eff}/\overline{\Delta x}$ for the wave-kinetic numerical method. Notice that the entire spectral content of $\tilde{I}(f)$ $[= \tilde{I}(\Omega = 2\pi f)]$ is contained within $f \lesssim f_{max,I} = N_{FFT}\times\Delta f/2 = 6.25$, which is shown in Fig. 3.8. It follows that for a given Δf, N_{FFT} for W-K is large enough. We also note that $(\overline{\Delta x})_{HF} = 0.08$ is small enough for H-F, since $1/2\, f_{max,u} \simeq 1/f_{max,I} \gtrsim 0.16$.

The irradiance data $I(\bar{x})$ for $|\bar{x}| \leq 4.0$ from single realizations are plotted in Figs. 3.9 and 3.10. The results from W-K(LV) and H-F are presented in Fig. 3.9, which indicates that W-K(LV) is accurate for $\phi_0 = 1.0$ [$\zeta = 0.144$], but introduces some errors for $\phi_0 = 2.0$ [$\zeta = 0.289$]. More detailed numerical calculations for a single Gaussian eddy

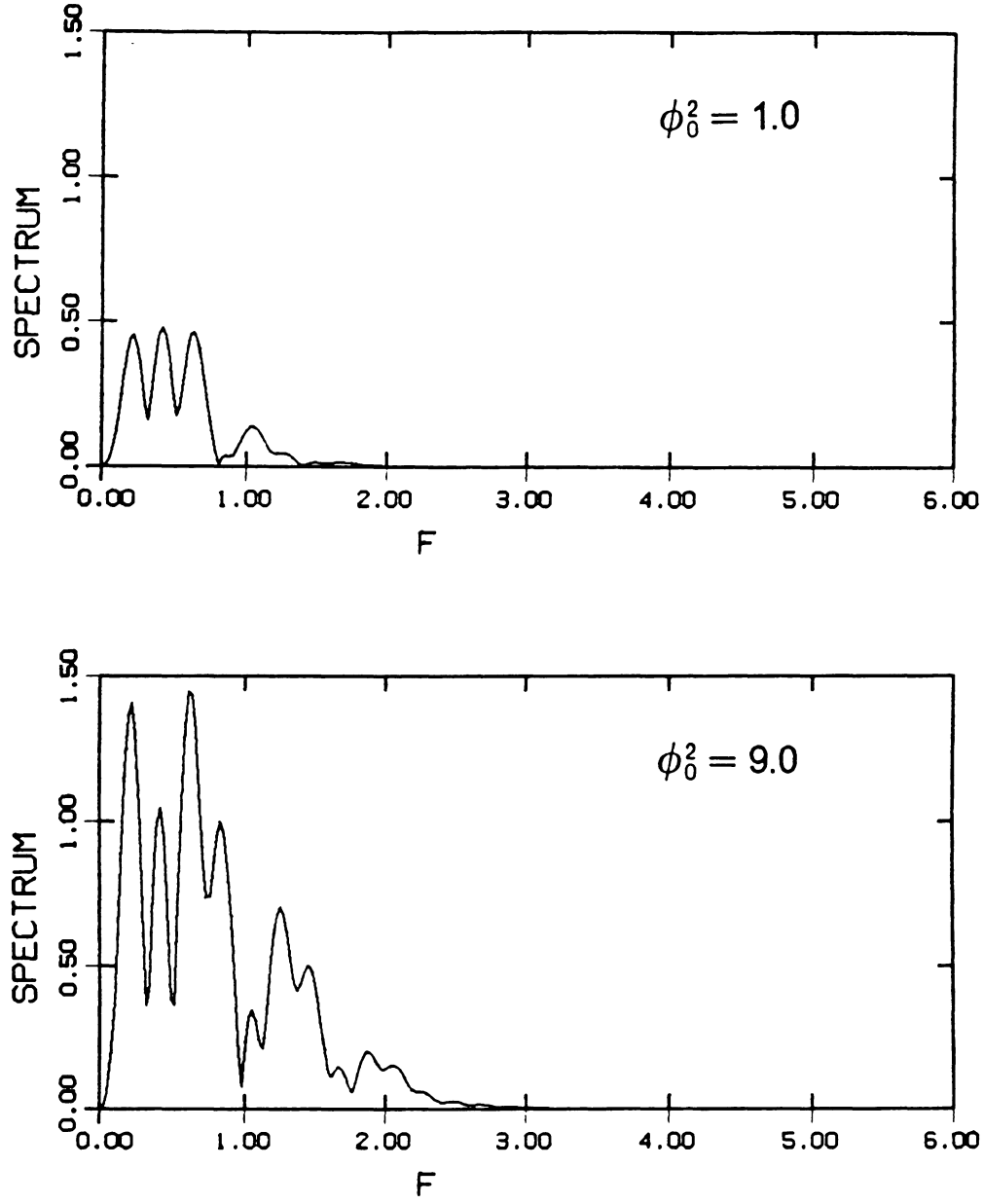

Figure 3.8 Spectrum of irradiance for a specific realization: W-K ($f = \Omega/2\pi$).

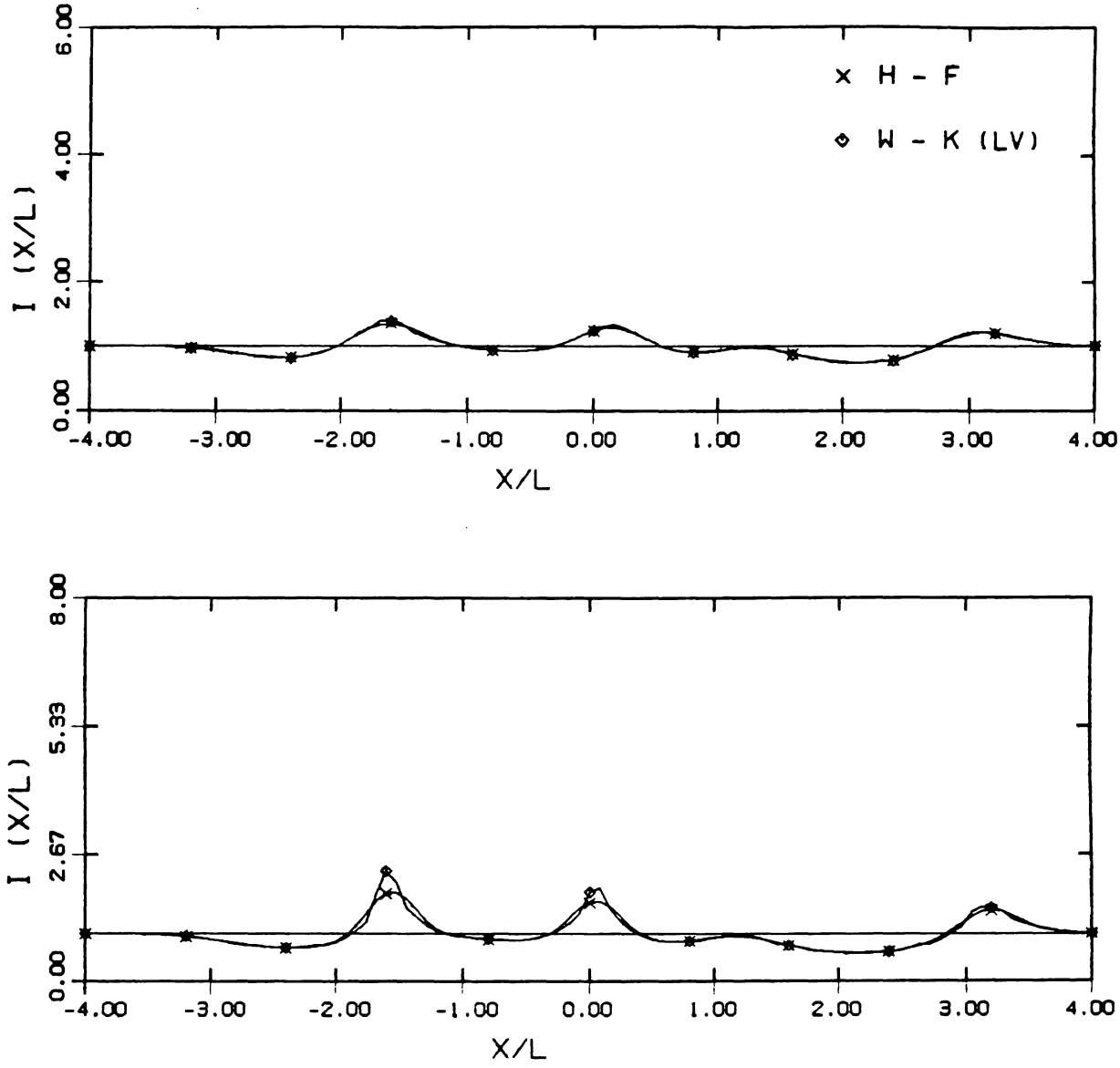

Figure 3.9 Instantaneous realization of irradiance at $z = L$ ($\gamma = 13.856$) : $\phi_0 = 1.0$ ($\zeta = 0.144$) (top), $\phi_0 = 2.0$ ($\zeta = 0.289$) (bottom); W-K(LV) and H-F.

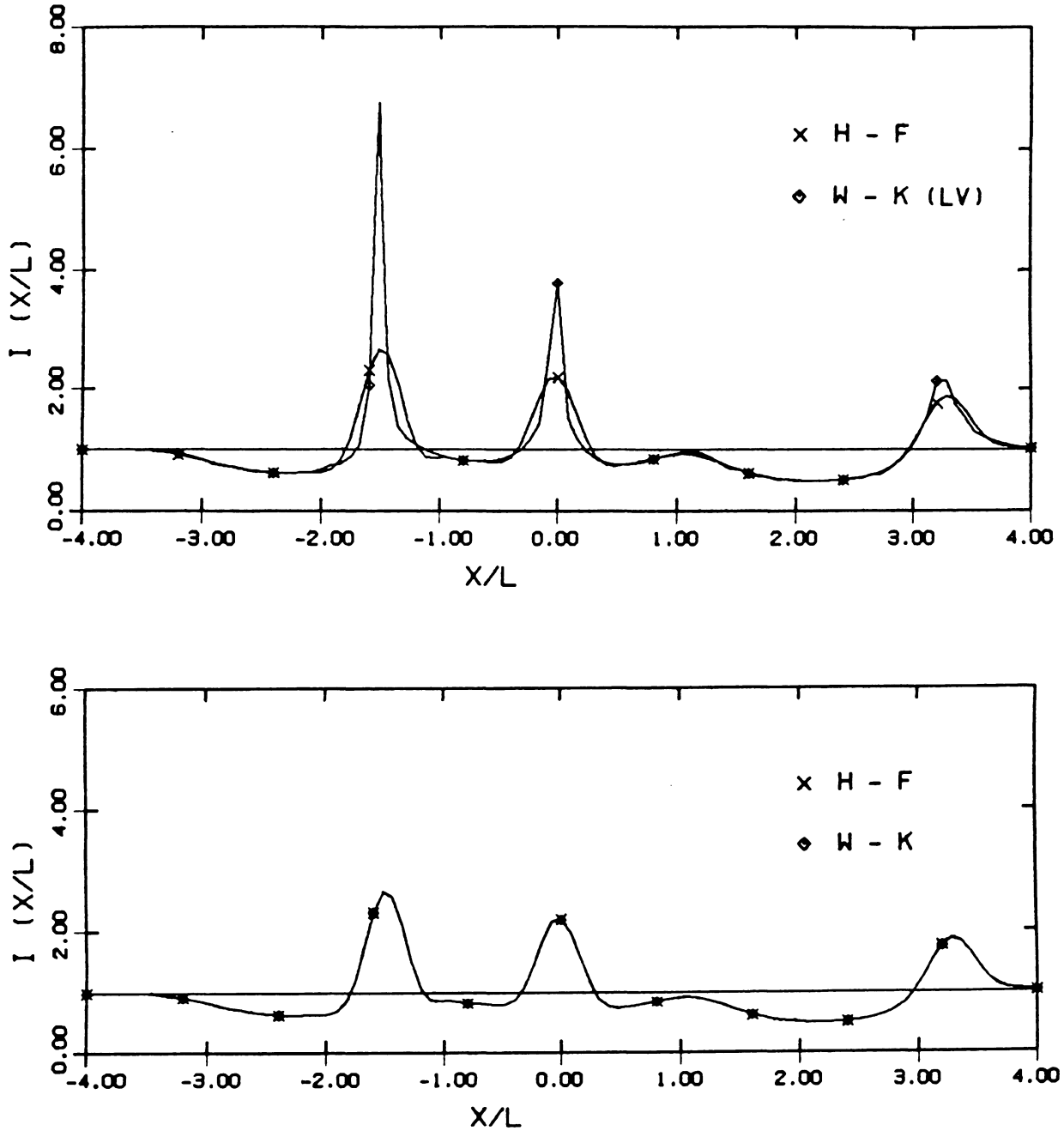

Figure 3.10 Instantaneous realization of irradiance at $z = L$ ($\gamma = 13.856$) : $\phi_0 = 3.0$ ($\zeta = 0.433$) ; W-K(LV), W-K and H-F.

indicate that W-K(LV) is valid for $\zeta \lesssim 0.2$. If we include all the higher-order terms (W-K), then the results become accurate, which is shown in Fig. 3.10. It is interesting to note that for $\zeta \gtrsim 0.2$, the Liouville approximation introduces extra peaks in the place where irradiance peaks appear. This seems to be due to ray crossings which occur in those places. Thus, we can say that the Liouville approximation is good for smaller ζ for which the ray crossings do not occur.

Finally, we note that computing times for W-K and H-F are comparable. In the array processor FPS 164 (manufactured by Floating Point System, Inc.), the CPU time for the data in Fig. 3.10 from W-K and H-F are 5.50 *secs.* and 4.66 *secs.*, respectively.

3.6.3 Computation of Statistics from Many Realizations

In this section, the statistical quantities σ_I^2 and $c_I(\bar{x})$ for one-dimensional Gaussian phase screens are computed by numerical simulation. For wave propagation calculations, W-K(LV) and W-K are used. The simulation results are compared with those obtained from numerical integration of the corresponding analytical expressions, (3.112) and (3.113). The values for the phase-screen parameters are $\gamma = 13.856$ and $\phi_0^2 = 1.0,\ 12.0$ ($\zeta = 0.144,\ 0.5$). For the parameters $\overline{W}$ and $\overline{D}$, we choose $\overline{W} = 5.0$, $\overline{D} = 1000.0$ for $\phi_0^2 = 1.0$; $\overline{W} = 7.0$, $\overline{D} = 4000.0$ for $\phi_0^2 = 12.0$.

First, we wish to discuss the results from W-K(LV). To implement this, we let $\overline{\Delta x} = 0.005$. The corresponding number of rays are $N_r = \overline{W}_{eff}/\overline{\Delta x}$, where we let $\overline{W}_{eff} = 10.0$ [cf. Sec. 3.6.2]. We put 11 receivers separated by $0.1\,\ell$ so that $\overline{W}_s = 1.0$ in this case.

Irradiance fluctuations for $\phi_0^2 = 1.0$ at the receiver at $\bar{x} = -0.5$ are plotted in Fig. 3.11, which shows that there are some unusually large samples. (Note that for irradiance, we do not have smaller outliers since irradiance is always positive and its average

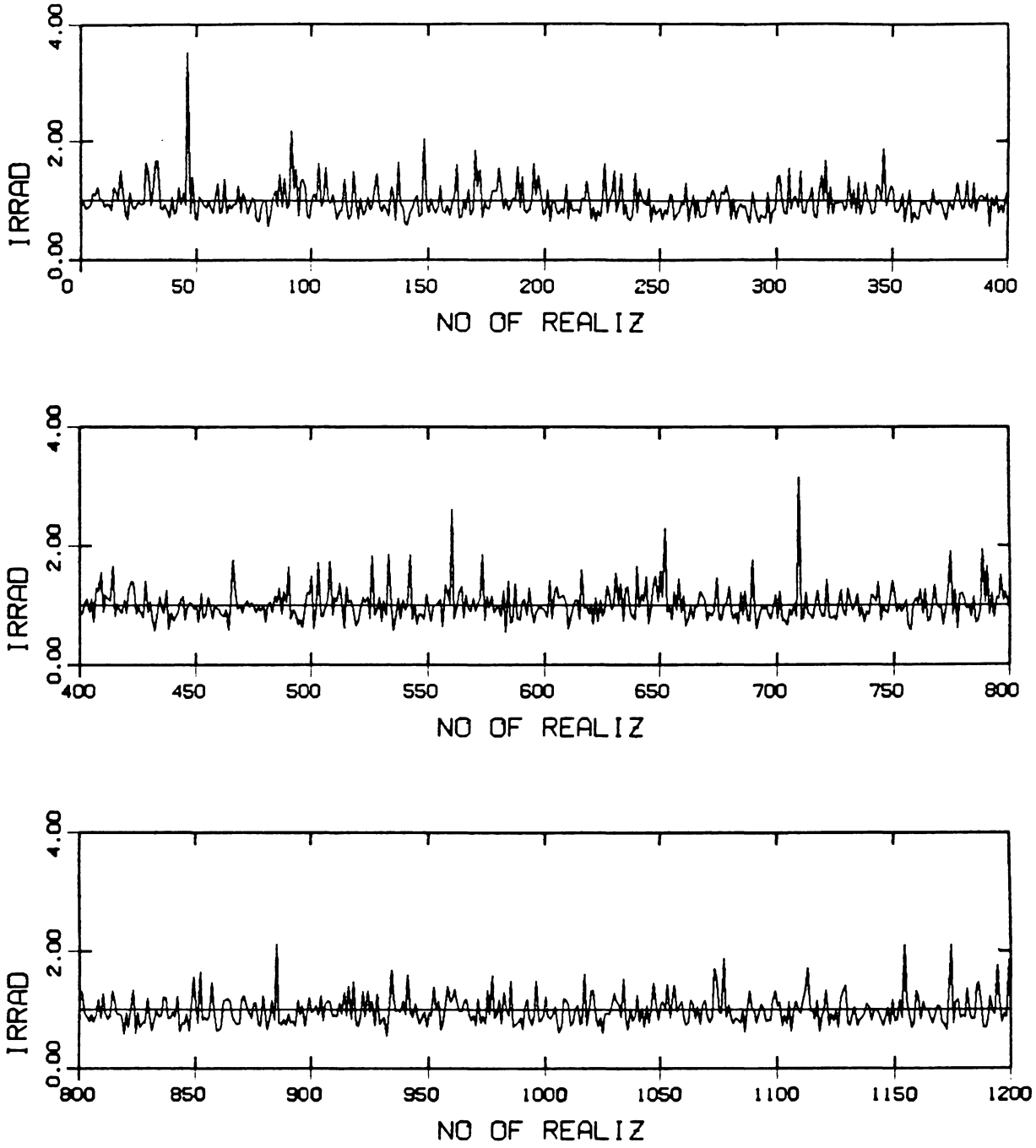

Figure 3.11 Irradiance fluctuation at the receiver at $\bar{x} = -0.5$: $\gamma = 13.856$, $\phi_0^2 = 1.0$ ($\zeta = 0.144$); W-K(LV).

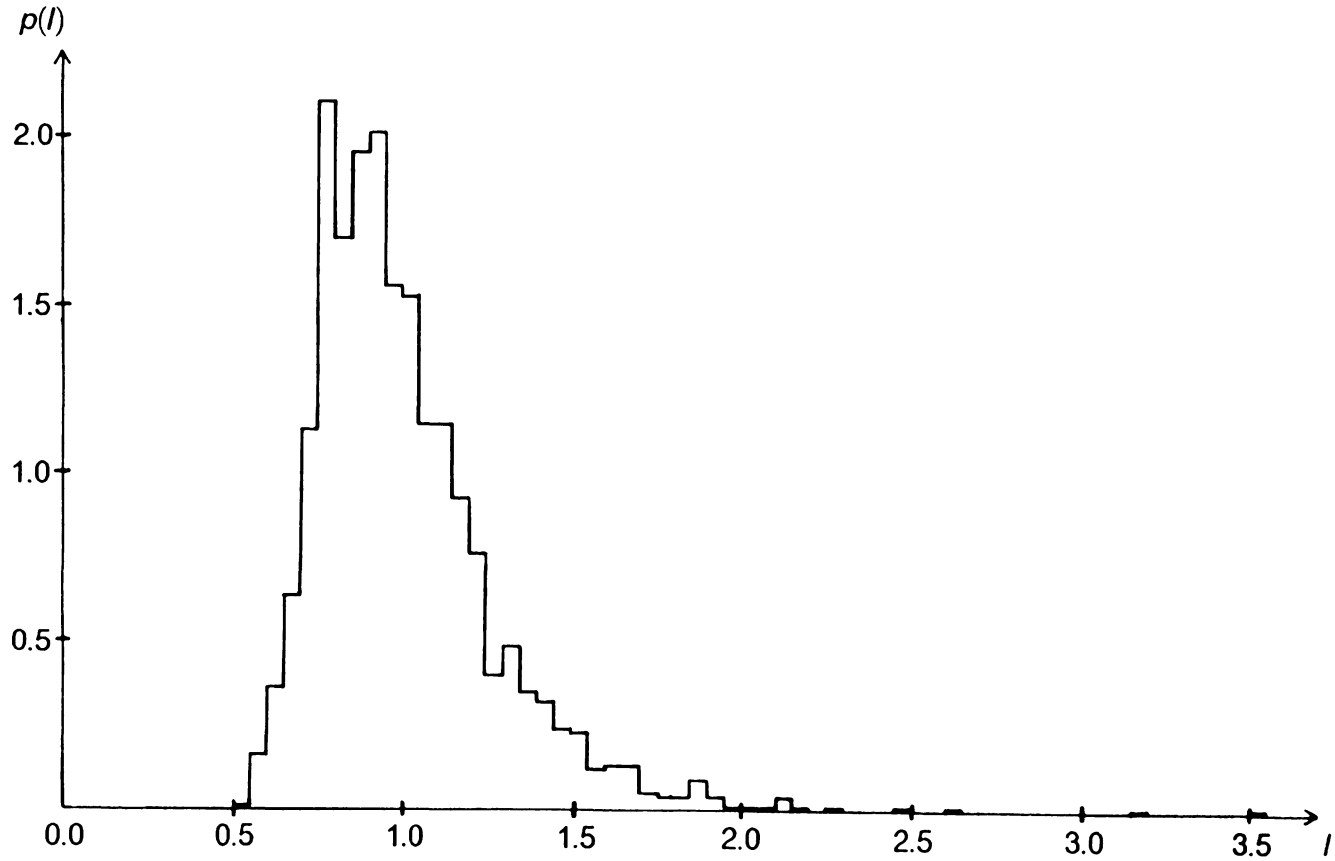

Figure 3.12 Distribution of irradiance samples at the receiver at $\bar{x} = -0.5$: $\gamma = 13.856$, $\phi_0^2 = 1.0$ ($\zeta = 0.144$); W-K(LV).

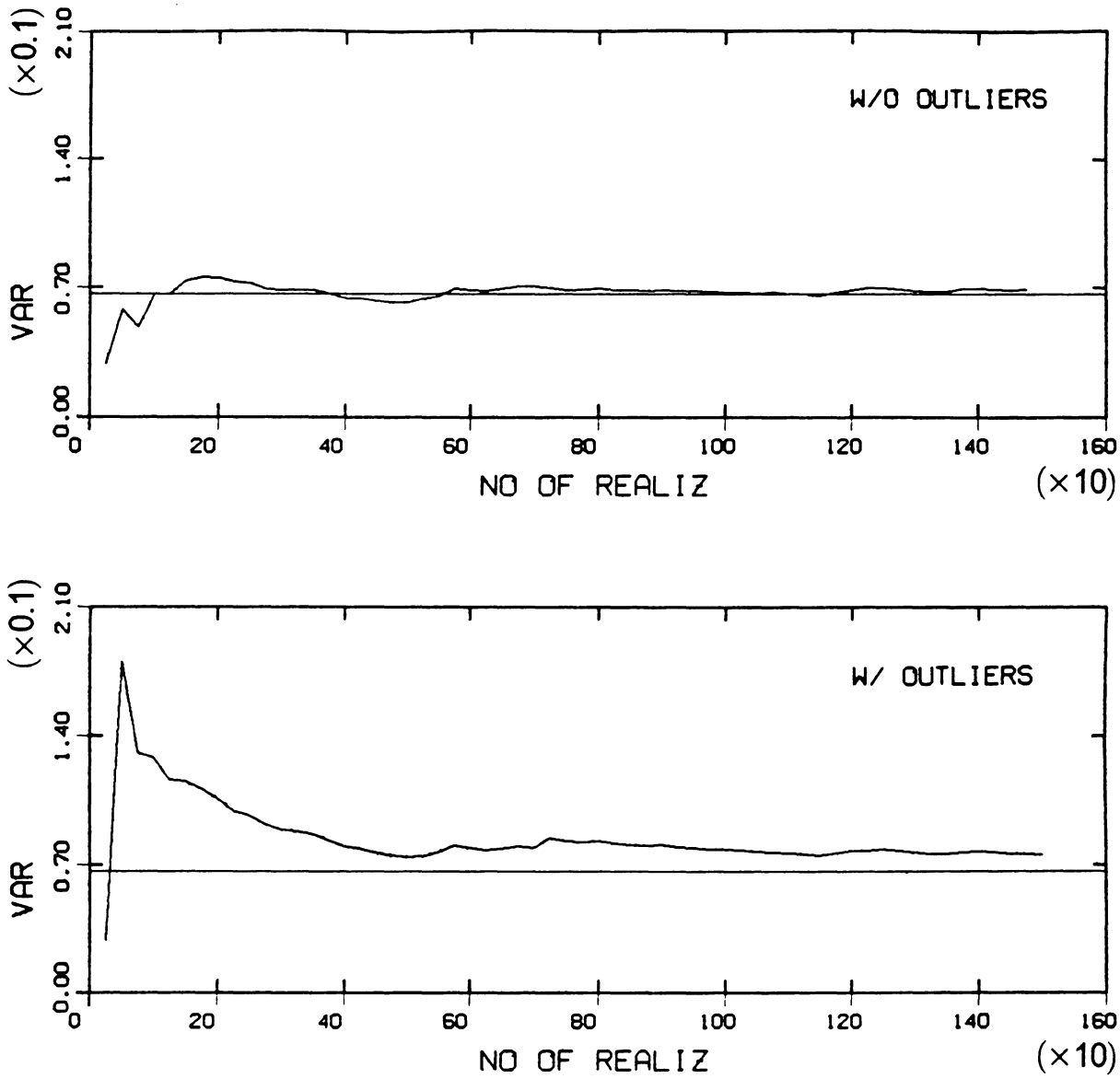

Figure 3.13 Effects of outliers on variance. Sample data are taken from the receiver at $\bar{x} = -0.5$: $\gamma = 13.856$, $\phi_0^2 = 1.0$ ($\zeta = 0.144$); W-K(LV).

is 1.0 in our case.) To see this more clearly, we computed $p(I)$ (i. e., histogram from the data with an interval $\Delta I = 0.005$). This is plotted in Fig. 3.12. The outliers are usually classified into two groups: *mild* outliers and *extreme* outliers. For small N_I, or even for large N_I [$\sim O(1000)$], the effects of a few extreme outliers are significant, especially for small scintillation index σ_I^2. It appears that we have to remove the outliers, to obtain a good convergence of the estimators as N_I increases. The effects of the outliers on variance are shown in Fig. 3.13.

For this problem ($\phi_0^2 = 1.0$), we have $\sigma_I^2 = 0.066$ from the analytical calculation [cf. Eq. (3.112) or Fig. 3.2]. Thus, we define outliers as $I \geq I_{out}$, with

$$I_{out} = < I > + 7\, \sigma_I = 2.8 \ ,$$

and we neglect the data for a specific realization, if any of the irradiance data from 11 receivers is larger than 2.8. We note here that this procedure for removing outliers creates some difficulties in the general case for which σ_I^2 is unknown. More systematic approaches used in statistics, especially in the area of EDA (Exploratory Data Analysis), are recommended in that case. In EDA, the outliers are usually defined as samples larger than $Q_3 + 3\hat{s}$ or smaller than $Q_1 - 3\hat{s}$, where Q_1 and Q_3 are lower and upper quartiles, and $\hat{s}$ is a sample standard deviation. In this way, we may define and remove outliers from stored irradiance data, even when σ_I^2 is unknown.

The simulation results for $\phi_0^2 = 1.0$ [with the outliers (≥ 2.8) removed] are shown in Fig. 3.14, together with the result computed from the analytical expressions (3.112) and (3.113). We observe that $c_I(\bar{x})$ from numerical simulation and analytical calculation are in good agreement. We notice also that the scintillation index from simulation, $\hat{\sigma}_I^2 = 0.068$ is fairly close to $\sigma_I^2 = 0.066$. Since the number of realizations N_I is 1500 in this case, from (3.93) the standard error for $\hat{\sigma}_I^2$ is given by $S_\varepsilon(\hat{\sigma}_I^2) = \sigma_I^2 \sqrt{2/N_I} = 0.0024$. Thus, we observe that $\hat{\sigma}_I^2$ is within the range, $\sigma_I^2 \pm S_\varepsilon(\hat{\sigma}_I^2)$.

For the data in Fig. 3.14, we chose a rather large $\overline{W}$, i. e., $\overline{W} = 5.0$, as mentioned before. The rule of thumb given by (3.119) [or (3.118)] says that for $\overline{W}_s = 1.0$ and $\zeta = 0.144$, we need $\overline{W} \gtrsim 2.0$. The results for $\overline{W} = 2.0$ (all the other parameters are the same and $N_f = 1950$) are plotted in Fig. 3.15, which confirms the rule of thumb for edge effects.

Next, the simulation results for $\phi_0^2 = 12.0$ from W-K(LV) are shown in Fig. 3.16. Since $\sigma_I^2 = 0.962$ in this case, outliers larger than 8.0 ($= < I > + 7\,\sigma_I$) have been removed. The number of realizations is 900. As expected, since W-K(LV) is not valid for $\zeta = 0.5$, the normalized covariance and the scintillation index from simulation are quite different from those calculated from the analytical expressions.

Up to now, we have discussed the results from W-K(LV). We will now discuss the results from W-K for the same phase screens (i. e., $\gamma = 13.856$ and $\phi_0^2 = 1.0,\ 12.0$). As discussed in Sec. 3.6.2, we choose $\overline{\Delta x} = 0.04$ and $\overline{\Delta p} = 0.08$. Also, we let $\Delta f = 0.09766$ ($= 1/0.08\times128$) for $\phi_0^2 = 1.0$ and $\Delta f = 0.08224$ ($= 1/0.095\times128$) for $\phi_0^2 = 12.0$. The number of sampling points for the inverse FFT, N_{FFT}, is 128. The values for $\overline{W}$ and $\overline{D}$ are the same as before. We note that for the values of Δf given above, the receiver separations ($= 1/N_{FFT}\Delta f$) are 0.08 and 0.095 for $\phi_0^2 = 1.0$ and 12.0, respectively.

Irradiance fluctuations for $\phi_0^2 = 12.0$ at two receivers separated by 0.095 (ℓ) are plotted in Fig. 3.17, and their magnified versions are shown in Fig. 3.18. We observe some correlations between the data from the two receivers. Outliers also appear in the irradiance data from W-K. Simulation results obtained without removing any outliers [cf. Figs. 3.19 and 3.20], however, indicate that the effects of the outliers are insignificant. It turns out that outliers in this case are mild (i. e., the outliers are not excessively larger than I_{out}). On the other hand, the outliers in case of W-K(LV) are extreme ($\gg I_{out}$). We can explain this as follows. For each realization, eddy centers

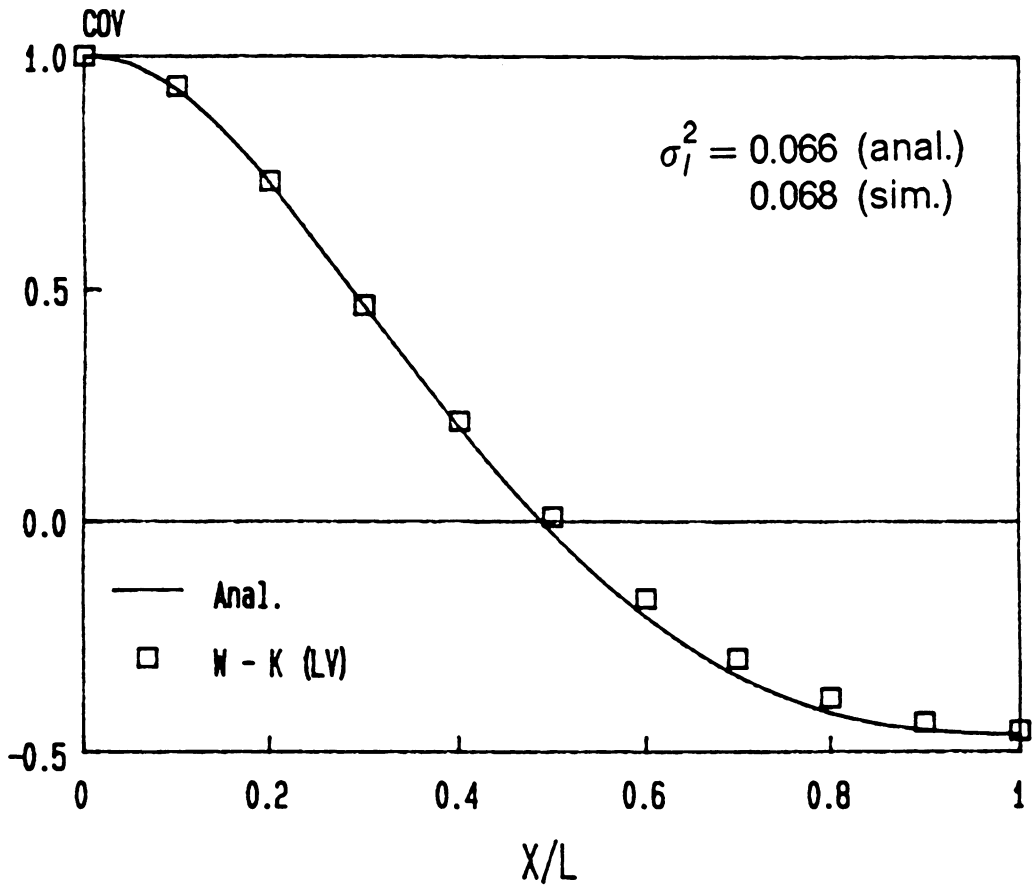

Figure 3.14 Normalized covariance of irradiance vs receiver separation: $\gamma = 13.856$, $\phi_0^2 = 1.0$ ($\zeta = 0.144$); W-K(LV).

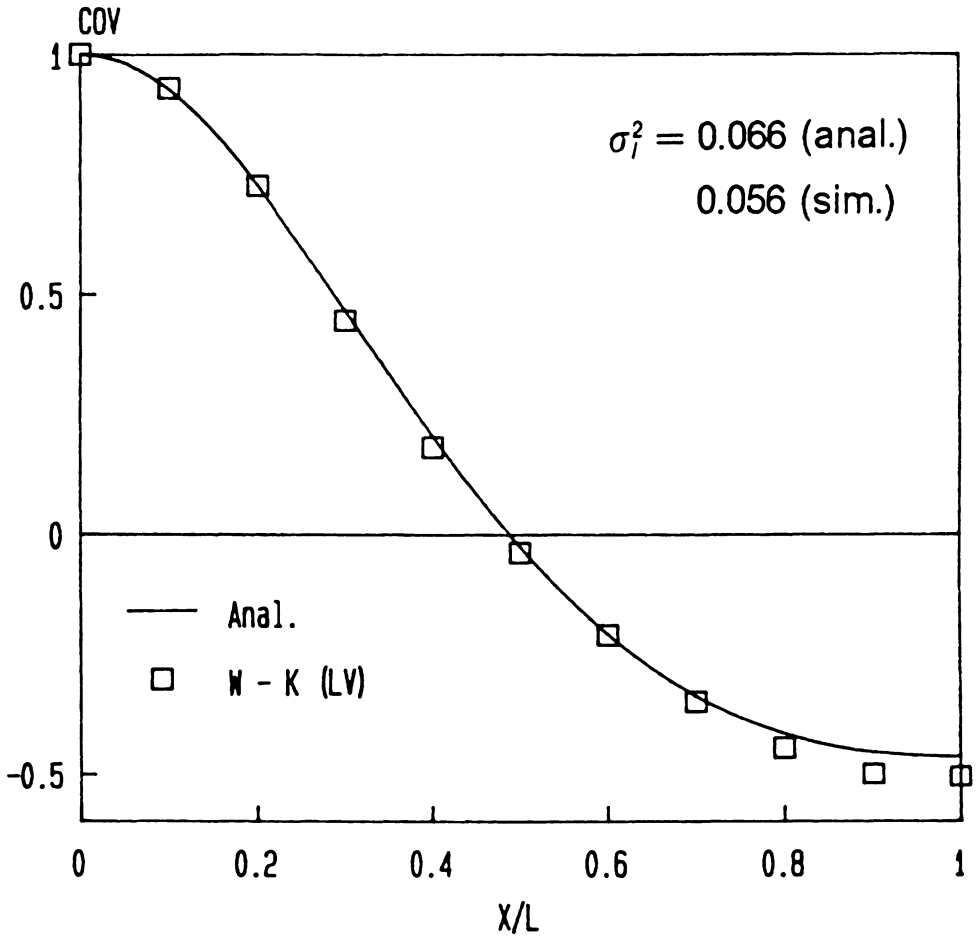

Figure 3.15 Normalized covariance of irradiance vs receiver separation: $\gamma = 13.856$, $\phi_0^2 = 1.0$ ($\zeta = 0.144$); W-K(LV). The screen width is 2.0 (not 5.0).

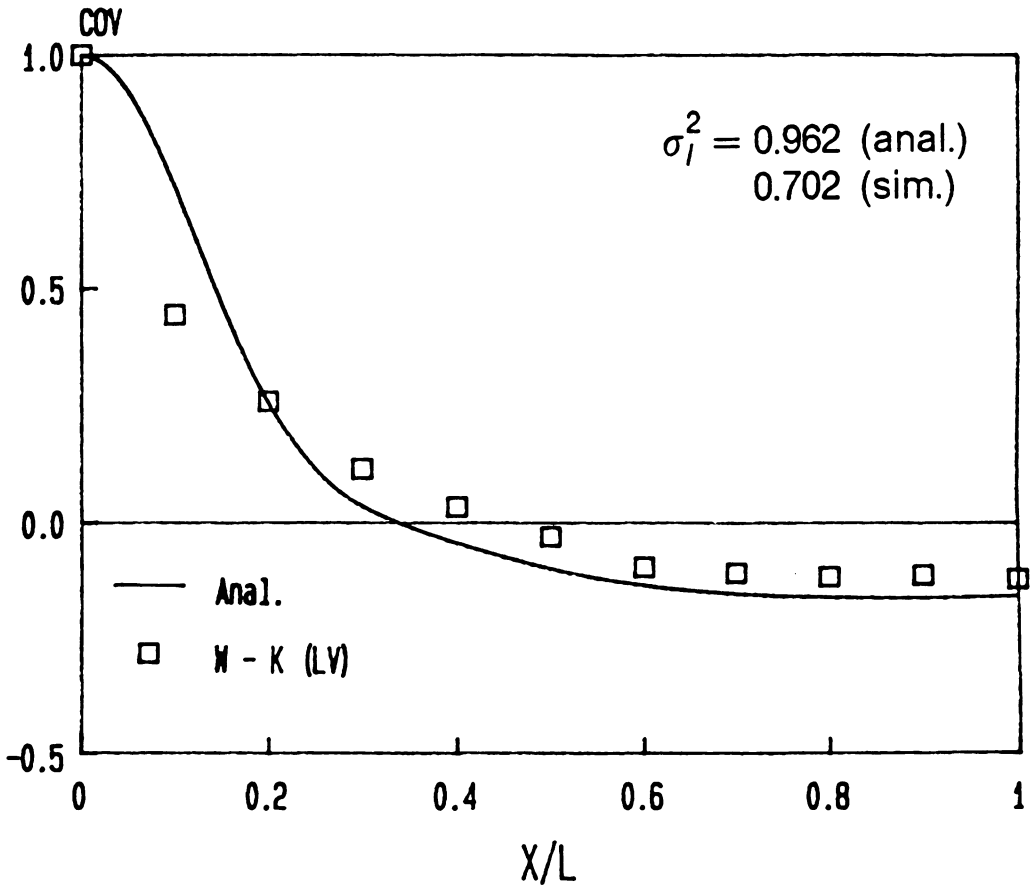

Figure 3.16 Normalized covariance of irradiance vs receiver separation: $\gamma = 13.856$, $\phi_0^2 = 12.0$ ($\zeta = 0.5$); W-K(LV).

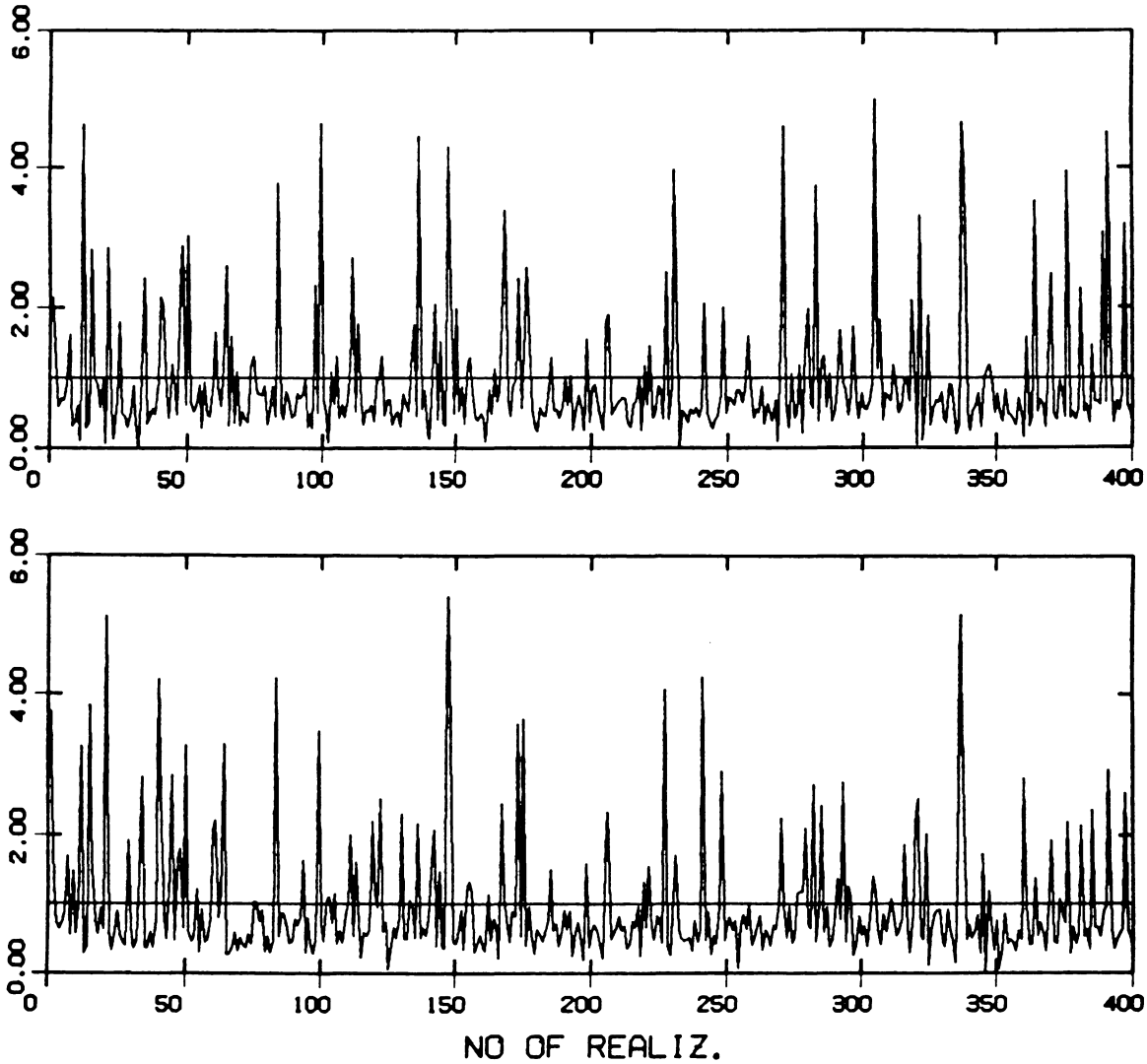

Figure 3.17 Irradiance fluctuations at 2 receivers separated by $0.095\,\ell$: $\gamma = 13.856$, $\phi_0^2 = 12.0$ ($\zeta = 0.5$); W-K.

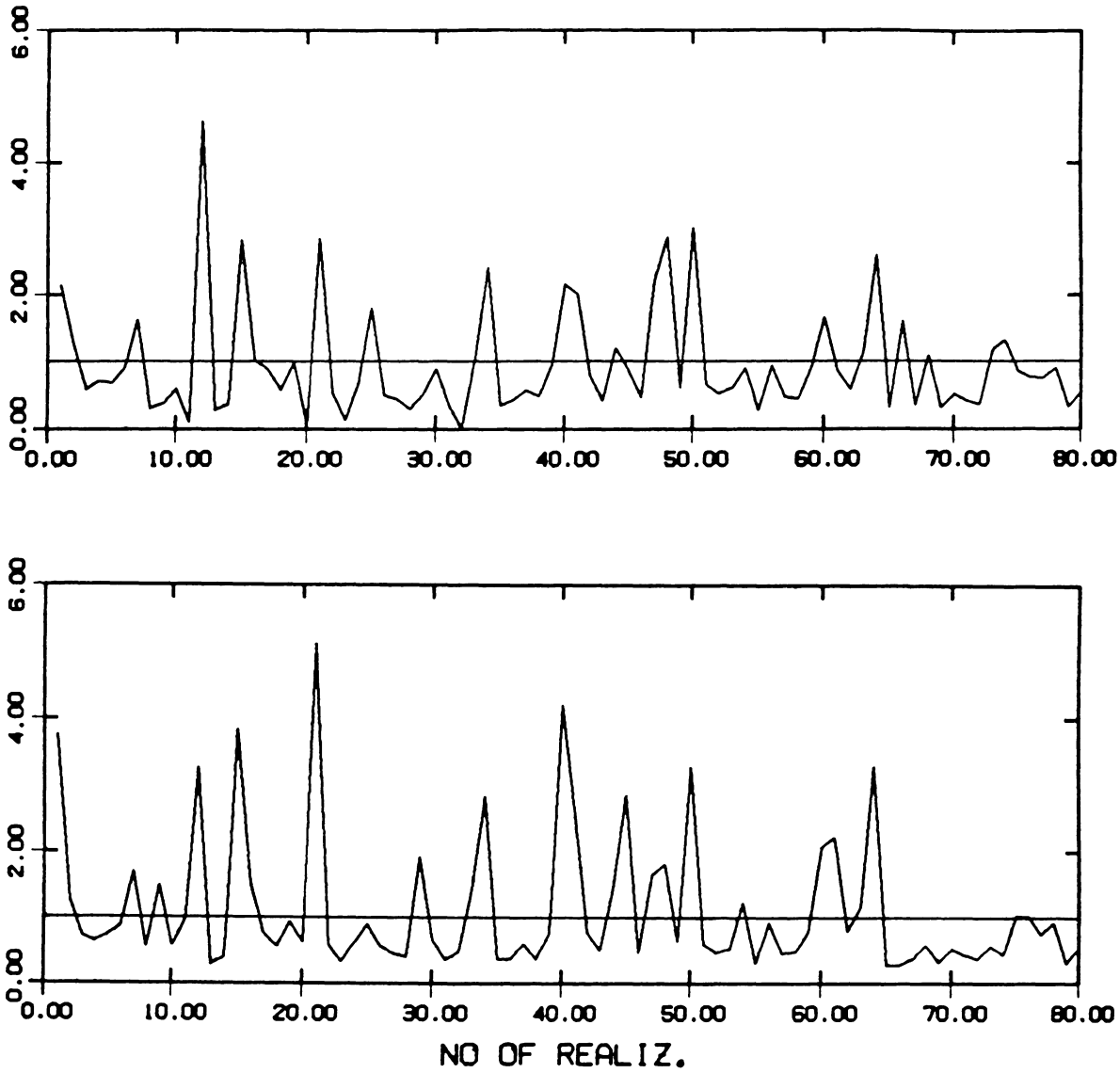

Figure 3.18 Detailed view of Figure 3.17.

(including random signs, ± 1, for the eddies) are distributed in a different fashion. For any specific realization, eddy centers can be unusually grouped (possibly with unusual distribution of random signs), which is common in numerical simulation, which utilizes a random number generator. In the region, where the unusual local grouping occurs, effective local ϕ_0^2 (or ζ) would be very large compared to an average value, and thus outliers appear. It follows that even for a phase screen with small $\zeta(\lesssim 0.2)$, effective local values of ζ can be larger than 0.2, and thus, in those regions, W-K(LV) introduces extra spikes [cf. Figs. 3.9 and 3.10], which results in extreme outliers.

The simulation results for $\phi_0^2 = 1.0$ and 12.0 (without removing outliers) are shown in Fig. 3.19 and Fig. 3.20, respectively. The number of realizations are 1500 for $\phi_0^2 = 1.0$ and 2495 for $\phi_0^2 = 12.0$. The results for $c_I(\bar{x})$ from numerical simulation and analytical calculation are in good agreement. We note that $\hat{c}_I(\bar{x})$ has larger errors around $\bar{x} = 0$ as we mentioned in Sec. 3.4. The scintillation index for $\phi_0^2 = 1.0$ from both methods are fairly close to each other, i. e., $\hat{\sigma}_I^2 = 0.067$ lies well within $\sigma_I^2 \pm S_\varepsilon(\hat{\sigma}_I^2)$, where $\sigma_I^2 = 0.066$ and $S_\varepsilon(\hat{\sigma}_I^2) = 0.0024$. For $\phi_0^2 = 12.0$, $\hat{\sigma}_I^2 = 0.840$ is quite different from $\sigma_I^2 = 0.962$. Our experience shows that for strong phase fluctuations it is not easy to obtain accurate results for σ_I^2 by numerical simulation, even though the normalized covariance of irradiance $c_I(\bar{x})$ comes out correctly. The standard error for $N_I = 2495$ and $\sigma_I^2 = 0.962$ is 0.027. It follows that $\hat{\sigma}_I^2 \simeq \sigma_I^2 - 4.5\, S_\varepsilon(\hat{\sigma}_I^2)$. [Notice that if we remove the mild outliers mentioned above, then $\hat{\sigma}_I^2$ becomes slightly smaller than this, and $\hat{c}_I(\bar{x})$ remains almost the same.] It appears that it is more difficult to simulate σ_I^2 than $c_I(\bar{x})$, in general.

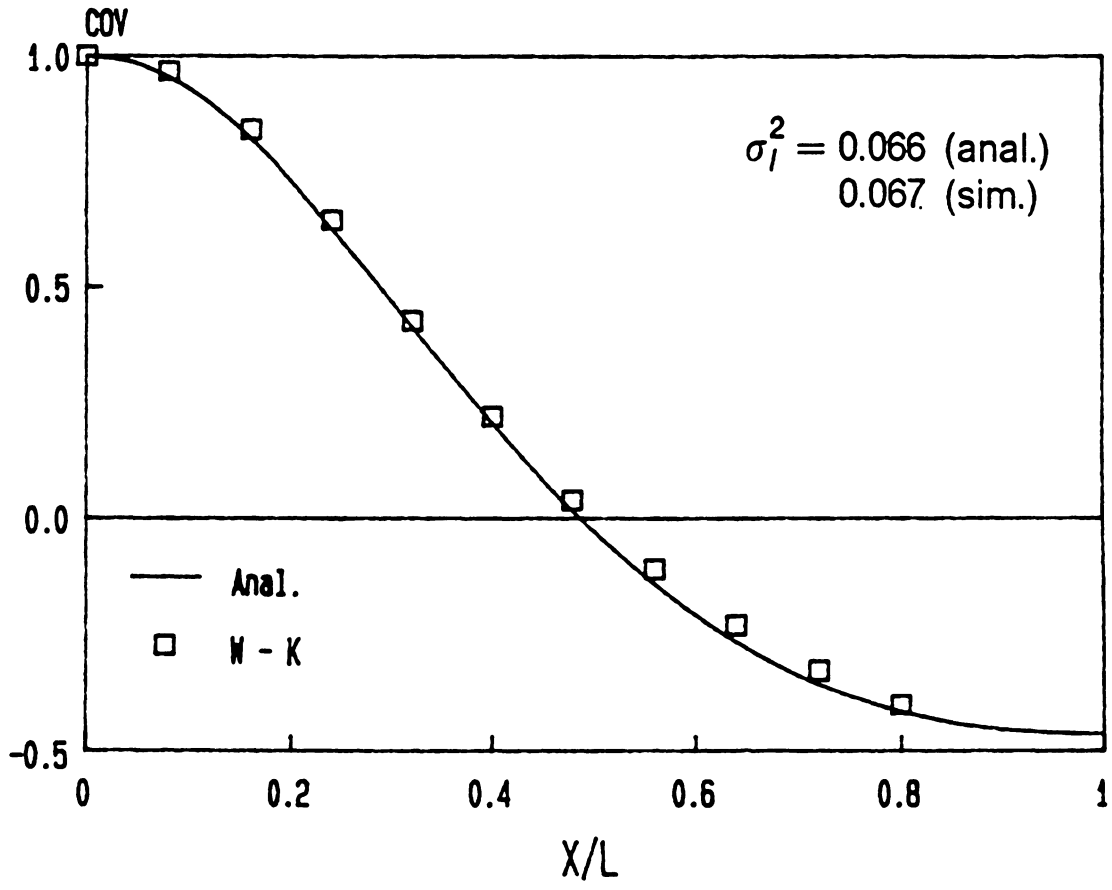

Figure 3.19 Normalized covariance of irradiance vs receiver separation: $\gamma = 13.856$, $\phi_0^2 = 1.0$ ($\zeta = 0.144$); W-K.

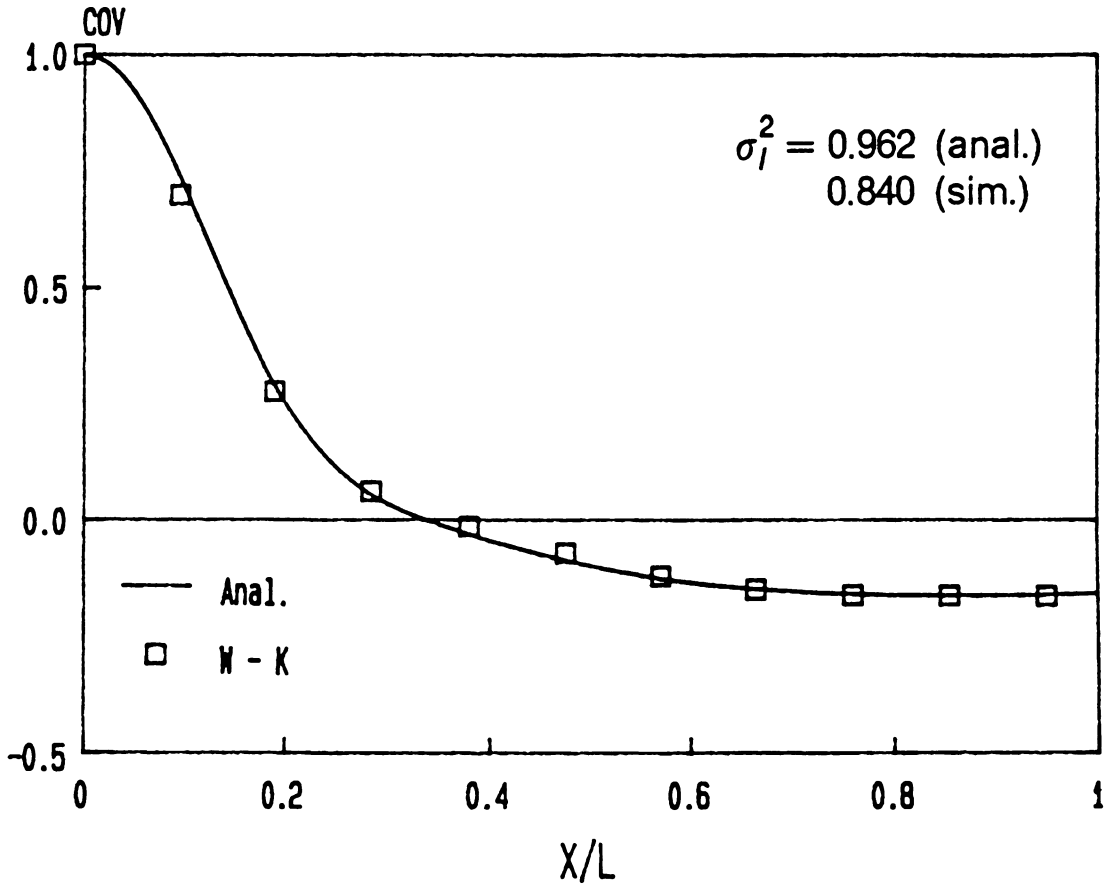

Figure 3.20 Normalized covariance of irradiance vs receiver separation: $\gamma = 13.856$, $\phi_0^2 = 12.0$ ($\zeta = 0.5$); W-K.

Appendix A3.1 The Third-Order Approximation in the Phase Difference

If we take the first two terms in the Taylor series expansion of the phase difference, $\phi(\bar{x}_0 + \frac{\bar{s}}{2}) - \phi(\bar{x}_0 - \frac{\bar{s}}{2})$, given by (3.50), then

$$\phi(\bar{x}_0 + \frac{\bar{s}}{2}) - \phi(\bar{x}_0 - \frac{\bar{s}}{2}) = \bar{k}\left[\Delta(\bar{x}_0)\bar{s} + \frac{1}{24}\Delta''(\bar{x}_0)\,\bar{s}^2\right] . \tag{A3.1}$$

Substituting this in (3.49) and following the same procedure as in the first-order approximation, we obtain

$$\begin{aligned}\bar{F}_L(\bar{x},\ \theta) = \frac{1}{2\pi}\frac{1}{\sqrt{2\pi}}\sum_n \int_{-\infty}^{\infty} d\bar{s}\ e^{-i\bar{k}\bar{s}[\delta\theta - \Delta_n'(\overline{\delta x} - \bar{L}\,\delta\theta)]}\, e^{i\frac{\bar{k}}{24}\Delta_n''\bar{s}^3} \\ \times e^{-(\overline{\delta x} - \bar{L}\,\delta\theta)^2/2\overline{\Delta x}^2} ,\end{aligned} \tag{A3.2}$$

where we let $\Delta(\bar{x}_0) \simeq \Delta_n + \Delta_n'(\bar{x}_0 - \bar{x}_{n0})$ and $\Delta''(\bar{x}_0) \simeq \Delta_n''$ for each beamlet. It follows that the irradiance $I_L(\bar{x})$ is given by

$$\begin{aligned}I_L(\bar{x}) = \frac{\gamma}{2\pi}\frac{1}{\sqrt{2\pi}}\sum_n \int_{-\infty}^{\infty} d\bar{s}\, e^{i\frac{\bar{k}}{24}\Delta_n''\bar{s}^3}\int_{-\infty}^{\infty} d\xi\ \left[e^{-i\gamma\bar{s}\xi}\right] \\ \times \left[e^{i\bar{k}\bar{s}\Delta_n'(\overline{\delta x} - \xi)}\, e^{-(\overline{\delta x} - \xi)^2/2\overline{\Delta x}^2}\right] .\end{aligned} \tag{A3.3}$$

Since the inner integral is in the form of the convolution integral, after replacing the terms in the brackets by their Fourier transforms and performing integration of the resulting expression with respect to the variable $\bar{s}$, we obtain

$$I_L(\bar{x}) = \int_{-\infty}^{\infty} d\Omega\ e^{i\Omega\bar{x}}\,\tilde{I}_L(\Omega) , \tag{A3.4}$$

where

$$\tilde{I}_L(\Omega) = \frac{\overline{\Delta x}}{2\pi} \sum_n \left[e^{-i\bar{x}_n\Omega}\, e^{-\overline{\Delta x}^2 C_n^2 \Omega^2/2} \right] \left[e^{-i\left(\frac{\bar{k}\Delta_n''}{24\bar{\gamma}^3} \right)\Omega^3} \right] . \qquad (A3.5)$$

In the above equation, all the parameters are the same as in Sec. 3.2.1.

Appendix A3.2 Two-Scale Expansion

From (2.45), we have (using the bar notations):

$$\left\{ \frac{\partial}{\partial \bar{z}} - \frac{i}{\bar{k}} \frac{\partial^2}{\partial \bar{x} \partial \bar{s}} - i\bar{k} \left[\delta n(\bar{x} + \frac{\bar{s}}{2}) - \delta n(\bar{x} - \frac{\bar{s}}{2}) \right] \right\} \hat{\Gamma}_2(\bar{x},\ \bar{s};\ \bar{z}) = 0 , \qquad (A3.6)$$

where

$$\hat{\Gamma}_2(\bar{x},\ \bar{s};\ \bar{z}) = u(\bar{x} + \frac{\bar{s}}{2},\ \bar{z}) u^*(\bar{x} - \frac{\bar{s}}{2},\ \bar{z}) . \qquad (A3.7)$$

Including the first two terms in the series expansion of $\delta n(\bar{x} + \frac{\bar{s}}{2}) - \delta n(\bar{x} - \frac{\bar{s}}{2})$, we obtain

$$\left[\frac{\partial}{\partial \bar{z}} - i \frac{\partial^2}{\partial \bar{x} \partial \hat{s}} - i\hat{s} \frac{\partial}{\partial \bar{x}} \delta n(\bar{x}) - \frac{i}{24} (\varepsilon \hat{s})^3 \frac{\partial^3}{\partial \bar{x}^3} \delta n(\bar{x}) \right] \tilde{\Gamma}_2(\bar{x},\ \hat{s};\ \bar{z}) = 0 , \qquad (A3.8)$$

where $\varepsilon = \bar{k}^{-2/3} = (k\ell)^{-2/3}$, $\hat{s} = \bar{k}\bar{s}$, and $\tilde{\Gamma}_2(\bar{x},\ \hat{s} = \bar{k}\bar{s};\ \bar{z}) = \hat{\Gamma}_2(\bar{x},\ \bar{s};\ \bar{z})$. Here, we notice that there are two scales, $\hat{s}$ and $\varepsilon\hat{s}$. Thus, we rewrite (A3.6) as

$$\left\{ \frac{\partial}{\partial \bar{z}} - i \frac{\partial^2}{\partial \bar{x} \partial \hat{s}} - i\varepsilon^{-3/2} \left[\delta n(\bar{x} + \frac{\varepsilon^{3/2}}{2} \bar{s}) - \delta n(\bar{x} - \frac{\varepsilon^{3/2}}{2} \bar{s}) \right] \right\} \tilde{\Gamma}_2(\bar{x},\ \hat{s};\ \bar{z}) = 0, \qquad (A3.9)$$

and solve the equation for $\tilde{\Gamma}_2$ [with the initial condition $\tilde{\Gamma}_2(\bar{x},\ \hat{s};\ 0) = \tilde{\Gamma}_{20}(\bar{x},\ \hat{s}) = \hat{\Gamma}_{20}(\bar{x},\ \bar{s} = \hat{s}/\bar{k})$], using a perturbation-series expansion with two scales $\hat{s}_0 = \hat{s}$ and

$\hat{s}_1 = \varepsilon\hat{s}$. After somewhat lengthy manipulations [See, for example, Ref. 121], the ε^0 terms in the perturbation-series expansion yield:

$$(\mathscr{L}_q + \mathscr{L}_c)\,\hat{F}(\bar{x}_0,\ \kappa_1,\ \theta_0,\ \hat{s}_1;\ \bar{z}) = 0\ , \tag{A3.10}$$

where

$$\mathscr{L}_q = \frac{\partial}{\partial \bar{z}} + \theta_0\,\frac{\partial}{\partial \bar{x}_0} + \delta n^{(1)}(\bar{x}_0)\,\frac{\partial}{\partial \theta_0}\ , \tag{A3.11}$$

$$\mathscr{L}_c = \kappa_1\,\frac{\partial}{\partial \hat{s}_1} + \delta n^{(2)}(\bar{x}_0)\,\hat{s}_1\,\frac{\partial}{\partial \theta_1} - \frac{i}{24}\,\delta n^{(3)}(\bar{x}_0)\,\hat{s}_1^3\ , \tag{A3.12}$$

and $\hat{F}$ is related to $\hat{\Gamma}_2(\bar{x},\ \bar{s};\ \bar{z}) = \tilde{\Gamma}_2(\bar{x},\ \hat{s} = \bar{k}\bar{s};\ \bar{z})$ by

$$\begin{aligned}\hat{\Gamma}_2(\bar{x},\ \bar{s};\ \bar{z}) = \frac{1}{2\pi}\int_{-\infty}^{\infty} d\kappa_0\, e^{i\kappa_0\bar{x}}\int_{-\infty}^{\infty} d\bar{x}_0\, e^{-i\bar{x}_0\kappa_0}\int_{-\infty}^{\infty} d\theta_0\, e^{i\bar{k}\theta_0\bar{s}} \\ \times\,\hat{F}(\bar{x}_0,\ \kappa_1 = \varepsilon\kappa_0,\ \theta_0,\ \hat{s}_1 = \varepsilon\bar{k}\bar{s};\ \bar{z}) = 0\ .\end{aligned} \tag{A3.13}$$

In (A3.11) and (A3.12), $\delta n^{(m)}(\bar{x}_0) = \dfrac{\partial^m}{\partial \bar{x}_0^m}\,\delta n(\bar{x}_0)$. Note that in this section, $\bar{x}_0$ and θ_0 represent $\bar{x}_0(\bar{z})$ and $\theta_0(\bar{z})$, not $\bar{x}(0)$ and $\theta(0)$ as defined in Sec. 3.2. From (A3.13), we can see that if $\hat{F}$ is not a function of κ_1 and $\hat{s}_1$, then it becomes the same as the WDF defined as (3.19). If we neglect the correction term, $\mathscr{L}_c$, then the resulting kinetic equation is the same as that from the Liouville approximation. We denote the solution for the equation by $F_q(\bar{x}_0,\ \theta_0;\ \bar{z})$. Since $\hat{F}$ is not a function of κ_1 and $\hat{s}_1$ at $z = 0$, the initial condition is given by $\hat{F}(\bar{x}_0,\ \kappa_1,\ \theta_0,\ \hat{s}_1;\ 0) = F_q(\bar{x}_0,\ \theta_0;\ 0)$. From (A3.11), the trajectory equations for $\bar{x}_0$ and θ_0 are given by

$$\frac{d\bar{x}_0}{d\bar{z}} = \theta_0\ ,\qquad \frac{d\theta_0}{d\bar{z}} = \frac{\partial}{\partial \bar{x}_0}\,\delta n(\bar{x}_0)\ , \tag{A3.14}$$

which are the classical G.O. trajectory equations. It follows that F_q can be calculated as before [cf. Eq. (3.41)]. Now, we let $\hat{F} = H F_q$. It can be shown that $\hat{F}$ defined in this way is the solution of (A3.10), provided that H satisfies the equation,

$$(\mathscr{L}_q + \mathscr{L}_c) H = 0 \ , \tag{A3.15}$$

with the initial condition $H(\bar{x}_0, \kappa_1, \theta_0, \hat{s}_1; 0) = H_0 = 1$. Using the expressions for $\mathscr{L}_q$ and $\mathscr{L}_c$, we can show that H can be obtained from the equation,

$$\frac{d}{d\bar{z}} (\ln H) = \frac{i}{24} \hat{s}_1^3 \, \delta n^{(3)}(\bar{x}_0) \ , \quad (H_0 = 1) \ . \tag{A3.16}$$

The characteristic equations for κ_1 and $\hat{s}_1$ are

$$\frac{d\hat{s}_1}{d\bar{z}} = \kappa_1 \ , \quad \frac{d\kappa_1}{d\bar{z}} = \hat{s}_1 \, \delta n^{(2)}(\bar{x}_0) \ , \tag{A3.17}$$

where $\bar{x}_0$, in turn, satisfies (A3.14).

It is difficult to solve the characteristic equations for $\hat{s}_1(\bar{z})$ and $\kappa_1(\bar{z})$ in the forward direction. To compute the irradiance, we need $\hat{\Gamma}_2(\bar{x}, \bar{s} = 0; \bar{z})$, i. e. ,

$$\begin{aligned} I(\bar{x}; \bar{z}) &= \hat{\Gamma}_2(\bar{x}, \bar{s} = 0; \bar{z}) \\ &= \frac{1}{2\pi} \int_{-\infty}^{\infty} d\kappa_0 \, e^{i\kappa_0 \bar{x}} \int_{-\infty}^{\infty} d\bar{x}_0 \, e^{-i\bar{x}_0 \kappa_0} \int_{-\infty}^{\infty} d\theta_0 \, \hat{F}_I(\bar{x}_0, \kappa_0, \theta_0; \bar{z}) \ , \end{aligned} \tag{A3.18}$$

where $\hat{F}_I(\bar{x}_0, \kappa_0, \theta_0; \bar{z}) = \hat{F}(\bar{x}_0, \kappa_1 = \varepsilon\kappa_0, \theta_0, \hat{s}_1 = 0; \bar{z})$. Thus, we can compute H by tracing $\hat{s}_1$ and κ_1 backwards with the conditions, $\hat{s}_1(\bar{z} = \bar{L}) = 0$ and $\kappa_1(\bar{z} = \bar{L}) = \varepsilon\kappa_0$. Let us introduce a new variable $\zeta = \bar{L} - \bar{z}$. We replace $\bar{z}$ in $\bar{x}_0$, θ_0, $\hat{s}_1$, κ_1, H by $\bar{L} - \zeta$, divide the resulting expressions for $\hat{s}_1$ and κ_1 by $\varepsilon\kappa_0$, and denote the results by $\tilde{x}_0$, $\tilde{\theta}_0$, $\tilde{s}_1$, $\tilde{\kappa}_1$, and $\tilde{H}$, respectively. We also introduce

$$\beta = [3i/(\varepsilon\kappa_0)^3] \ \ln[\tilde{H}(0)/\tilde{H}(\zeta)] \ . \tag{A3.19}$$

It follows then that characteristic equations given by (A3.14), (A3.16), and (A3.17) becomes:

$$\begin{aligned}
&\frac{d\tilde{x}_0}{d\zeta} = -\tilde{\theta}_0 \ , \quad \frac{d\tilde{\theta}_0}{d\zeta} = -\frac{\partial}{\partial \tilde{x}_0}\,\delta n(\tilde{x}_0) \ ; \\
&\frac{d\tilde{s}_1}{d\zeta} = -\tilde{\kappa}_1 \ , \quad \frac{d\tilde{\kappa}_1}{d\zeta} = -\tilde{s}_1\,\delta n^{(2)}(\tilde{x}_0) \ ; \\
&\frac{d\beta}{d\zeta} = -\frac{1}{8}\,\tilde{s}_1^3\,\delta n^{(3)}(\tilde{x}_0) \ ,
\end{aligned} \tag{A3.20}$$

where the corresponding initial conditions are $\tilde{x}_0(0) = \bar{X}_0$, $\tilde{\theta}_0(0) = \Theta_0$, $\tilde{s}_1(0) = 0$, and $\beta(\zeta = 0) = 0$. Note that $\bar{X}_0 = \bar{x}_0(\bar{z} = \bar{L})$, $\Theta_0 = \theta_0(\bar{z} = \bar{L})$. Since $\tilde{x}_0$ is only a function of $\bar{X}_0$ and Θ_0, i. e., $\tilde{x}_0 = \tilde{x}_0(\bar{X}_0,\ \Theta_0;\ \zeta)$, so are $\tilde{s}_1$ and β. Let $\beta(\bar{X}_0,\ \Theta_0;\ \zeta = \bar{L}) = \beta_s(\bar{X}_0,\ \Theta_0)$. Using the fact that $\tilde{H}(\zeta = 0) = H(\bar{z} = \bar{L})$ and $\tilde{H}(\zeta = \bar{L}) = H_0 = 1$, from (A3.19) we obtain:

$$H(\bar{z} = \bar{L}) = e^{-(\frac{i}{3})(\varepsilon\kappa_0)^3\beta_s(\bar{x}_0,\ \theta_0)} \ , \tag{A3.21}$$

from which $\hat{F} = H\,F_q$ (and thus $\hat{F}_l$) can be calculated. Substituting the resulting expressions for $\hat{F}_l$ in (A3.18), one can show that

$$\begin{aligned}
I_L(\bar{x}) &= \hat{\Gamma}_2(\bar{x},\ \bar{s} = 0;\ \bar{z} = \bar{L}) \\
&= \frac{1}{2\pi}\int_{-\infty}^{\infty} d\Theta_0 \int_{-\infty}^{\infty} d\bar{X}_0\ \frac{1}{\varepsilon\,\beta_s^{1/3}}\,Ai\left(\frac{\bar{X}_0 - \bar{x}}{\varepsilon\,\beta_s^{1/3}}\right) F_q(\bar{X}_0,\ \Theta_0) \ ,
\end{aligned} \tag{A3.22}$$

where $Ai(\bar{x})$ is the Airy function defined as

$$(3a)^{-1/3}\,Ai[(3a)^{-1/3}\,x] = \frac{1}{2\pi}\int_{-\infty}^{\infty} dt\ e^{i(at^3 + xt)} \ . \tag{A3.23}$$

For a one-dimensional Gaussian phase screen, we can calculate β_s without any difficulty, using the impulse approximation. After straight-forward but tedious calculations, we obtain

$$\beta_s(\bar{X}_0,\ \Theta_0) \simeq (\bar{k}/2\gamma)^3\, \Delta''(\bar{X}_0 - \bar{L}\Theta_0)\ . \tag{A3.24}$$

The expression for $F_q(\bar{X}_0,\ \Theta_0)$ are given by (3.41), with $\bar{x}$ and θ being replaced by $\bar{X}_0$ and Θ_0. Substituting the expressions for β_s and F_q in (A3.22) and assuming that each beamlet is sharply peaked around $(\bar{x}_n,\ \theta_n)$ [cf. Eq. (3.41)], we obtain

$$I_L(\bar{x}) = \frac{1}{\sqrt{2\pi}} \sum_n \int_{-\infty}^{\infty} d\bar{x}_0 \left[\frac{1}{\beta_n}\, Ai\left(\frac{\bar{X}_0 - \bar{x}}{\beta_n} \right) \right] \left[\frac{1}{C_n}\, e^{-(\bar{x}_0 - \bar{x}_n)^2/2\overline{\Delta x^2}\&Cn2} \right], \tag{A3.25}$$

where $\beta_n = \varepsilon\, \beta_s^{1/3}(\bar{X}_0 = \bar{x}_n,\ \Theta_0 = \theta_n)$, and $\bar{x}_n$ and C_n are the same as in Sec. 3.2.2 [cf. Eqs. (3.46) and (3.47)]. Using $\bar{x}_{n0} = n\,\Delta x = \bar{x}_n - \bar{L}\theta_n$, $(\theta_n = \Delta_n)$ [cf. Eq. (3.55)], we can show that

$$\beta_n = (\bar{k}\ \Delta_n'')^{1/3}/2\gamma\ . \tag{A3.26}$$

Note that (A3.25) is the convolution integral. The Fourier transform [defined as (3.59)] of $(a\pi)Ai(-ax)$ is given by $\frac{1}{2}\, e^{-i\Omega^3\Omega^3/3}$. Replacing the terms in the square brackets by their Fourier transforms, we obtain

$$I_L(\bar{x}) = \int_{-\infty}^{\infty} d\Omega\ e^{i\Omega\bar{x}}\, \tilde{I}_L(\Omega)\ , \tag{A3.27}$$

where

$$\tilde{I}_L(\Omega) = \frac{\overline{\Delta x}}{2\pi} \sum_n \left[e^{-i\bar{x}_n\Omega}\, e^{-\overline{\Delta x^2} C_n^2 \Omega^2/2} \right] \left[e^{-i\beta_n^3\Omega^3/3} \right]\ , \tag{A3.28}$$

which is reproduced as (3.63) in the text. It is interesting to compare the complexity involved in the above derivation with that in Appendix A3.1, which is much simpler.

Appendix A3.3 Edge Diffraction

For a screen with width W, we have from (2.76) and (2.78) (with the bar notations):

$$u(\bar{x},\ \bar{L}) = \sqrt{\frac{\bar{k}}{2\pi i\bar{L}}} \int_{-\bar{W}/2}^{\bar{W}/2} d\bar{x}'\ e^{i\bar{k}(\bar{x}-\bar{x}')^2/2\bar{L}}\, u_0(\bar{x}')\ , \tag{A3.29}$$

where $u_0(\bar{x}')$ can be represented as the inverse Fourier transform,

$$u_0(\bar{x}') = \int_{-\infty}^{\infty} dq\ e^{iq\bar{x}'}\, U_0(q)\ . \tag{A3.30}$$

Substituting (A3.30) in (A3.29), we obtain

$$u(\bar{x},\ \bar{L}) = \sqrt{\frac{\bar{k}}{2\pi i\bar{L}}} \int_{-\infty}^{\infty} dq\, U_0(q) \int_{-\bar{W}/2}^{\bar{W}/2} d\bar{x}'\ e^{iq\bar{x}'}\, e^{i\bar{k}(\bar{x}-\bar{x}')^2/2\bar{L}}\ . \tag{A3.31}$$

Let us change the integration variable: $t = \bar{x}' - \bar{x}$. After a simple manipulation, this becomes

$$u(\bar{x},\ \bar{L}) = \int_{-\infty}^{\infty} dq\ e^{iq\bar{x}'}\, e^{i\bar{L}q^2/2\bar{k}}\, U_0(q)\, G(\bar{x},\ \bar{L},\ q)\ , \tag{A3.32}$$

where

$$G(\bar{x},\ \bar{L},\ q) = \sqrt{\frac{\bar{k}}{2\pi i\bar{L}}} \int_{-\bar{W}/2-\bar{x}}^{\bar{W}/2-\bar{x}} dt\ e^{i\frac{\bar{k}}{2}\bar{L}\left(t+\frac{\bar{L}}{\bar{k}}q\right)^2}\ . \tag{A3.33}$$

Define the Fresnel integral as

$$g_F(\bar{x}) = \int_0^{\bar{x}} d\xi \; e^{i\pi \xi^2/2} \; . \tag{A3.34}$$

Let $\xi = \sqrt{\frac{\bar{k}}{\pi \bar{L}}} \left(t + \frac{\bar{L}}{\bar{k}} q \right)$. It follows then that G can be represented as

$$\begin{aligned} G(\bar{x}, \bar{L}, q) = \frac{1}{\sqrt{2i}} \Bigg\{ & g_F \left[\sqrt{\frac{\bar{k}}{\pi \bar{L}}} \left(\frac{\bar{W}}{2} - \bar{x} + \frac{\bar{L}}{\bar{k}} q \right) \right] \\ & + g_F \left[\sqrt{\frac{\bar{k}}{\pi \bar{L}}} \left(\frac{\bar{W}}{2} + \bar{x} - \frac{\bar{L}}{\bar{k}} q \right) \right] \Bigg\} \; , \end{aligned} \tag{A3.35}$$

which is reproduced as (3.121) in the text.

4. Two-Dimensional Gaussian Extended Medium

In this chapter, the simulation schemes discussed in Chap. 2 are applied to a two-dimensional Gaussian extended medium. The input is assumed to be a plane wave with unit amplitude. The covariance of irradiance, for which no analytical expression is available in this case, is computed by numerical simulation. The simplified model is used for realization of an extended medium, and for wave propagation calculations the wave-kinetic numerical method and the Huygens-Fresnel diffraction formula are used. The results from both methods are compared to each other. As in the previous chapter, we will use the bar notations, whenever convenient.

4.1 Simulation Model

Let us now consider a plane wave propagating in a two-dimensional extended medium with a Gaussian correlation function given by (3.1). The geometry for this problem is sketched in Fig. 4.1, where L represents observation distance. As in the one-dimensional phase-screen problem in Chap. 3, the fluctuating part of the refractive-index fluctuation, $\delta n(x, z)$, can be modeled as a sum of weighted two-dimensional Gaussian eddies, the centers of which are uniformly distributed over the rectangular region of thickness L and width W. For convenience, we reproduce (3.2) here:

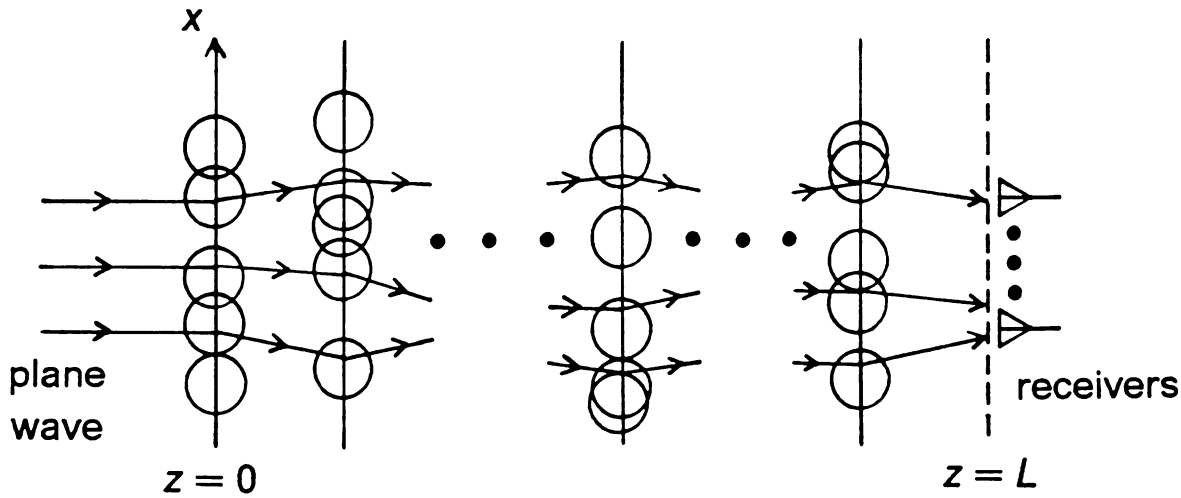

Figure 4.1 Geometry for numerical simulation of two-dimensional Gaussian extended medium.

$$\delta n(x,\ z) = \eta_0 \sum_{m=1}^{N_E} q_m\, e^{-2\,[(x-x_m^c)^2 + (z-z_m^c)^2]/\ell^2}\ , \tag{4.1}$$

where $\eta_0 = <\delta n^2>^{1/2}$, $q_m = \pm 1$, and $(x_m^c,\ z_m^c)$ represent eddy centers. The number density of Gaussian eddies per unit area is given by (3.3), i. e., $N_s = 4/\pi\ell^2$, and the total number of eddies N_E is the same as in (3.4), except that now we have to replace D in (3.4) by L:

$$N_E = N_x N_z\ , \qquad N_x = \frac{2}{\sqrt{\pi}}\frac{W}{\ell}\ , \quad N_z = \frac{2}{\sqrt{\pi}}\frac{L}{\ell}\ . \tag{4.2}$$

In the simplified model as shown in Fig. 2.2 or 4.1, the medium is divided into thin slabs, and all the eddies in each slab are projected into a single transverse line. We denote the number of layers and the thickness of each layer, respectively, by N and Z so that

$$Z = L/N\ . \tag{4.3}$$

It follows then that the general model described by (4.1) becomes [cf. Fig. (3.11)]:

$$\begin{aligned}\delta n(x,\ z) &= \eta_0 \sum_{l=1}^{N}\sum_{m=1}^{N_{LE}} q_{ml}\, e^{-2\,[(x-x_{ml}^c)^2 + (z-z_{ml}^c)^2]/\ell^2} \\ &\equiv \sum_{l=1}^{N} \delta n_l(x,\ z)\ ,\end{aligned} \tag{4.4}$$

where N_{LE} is the number of eddies for each layer, i. e.,

$$N_{LE} = N_E/N\ , \tag{4.5}$$

and $(x_{ml}^c,\ z_{ml}^c)$ represent eddy centers for the l-th layer with

$$z_{ml}^{c} = Z\,(l-1)\ , \quad (l = 1,\ 2,\ \ldots,\ N)\ . \tag{4.6}$$

With the impulse approximation, which is equivalent to the thin-screen approximation for each layer as discussed in Sec. 3.1 [cf. Eq. (3.12) and discussions following the equation], equation (4.4) may be simplified further as:

$$\delta n(x,\ z) \simeq \sqrt{\frac{\pi}{2}}\,\eta_0 \ell \sum_{l=1}^{N} \sum_{m=1}^{N_{LE}} q_{ml}\, e^{-2\,(x - x_{ml}^{c})^2/\ell^2}\, \delta(z - z_{ml}^{c})\ . \tag{4.7}$$

We assume that $|\delta n| \ll 1$ and Z is small enough (or N is large enough for a given L), so that the thin-screen approximation holds for each layer. As in the phase-screen problem, the phase fluctuation from each layer becomes an important quantity. We denote the phase fluctuation introduced by the l-th layer by $\phi_l(x)$, which is related to $\delta n_l(x,\ z)$ by

$$\phi_l(x) = k \int_{z_{ml}^{c} - Z/2}^{z_{ml}^{c} + Z/2} dz\ \ \delta n_l(x,\ z)\ . \tag{4.8}$$

From (4.8) and (4.4) [or (4.7)], we find [cf. Eqs. (3.6)-(3.8)]:

$$\phi_l(x) \simeq \phi_{0E} \sum_{m=1}^{N_{LE}} q_{ml}\, e^{-2(x - x_{ml}^{c})^2/\ell^2}\ , \tag{4.9}$$

where

$$\phi_{0E} = \sqrt{\frac{\pi}{2}}\, k \ell \eta_0\ . \tag{4.10}$$

We note that to describe an extended-medium problem completely we need three parameters [cf. Eq. (2.7)]. (In the parabolic approximation regime, we need only two

parameters as in the phase-screen problem, i. e., an electric field $u(\bar{x}, \bar{L})$ or moments of the field Γ_{nm} can be determined completely by two parameters [cf. Eqs. (2.8) or (1.1)], which will be discussed in detail later in this section. In our numerical simulation, however, we need three parameters since we have to realize an extended-medium.) A convenient choice of the parameters would be η_0, $\bar{k}$ and $\bar{L}$. To be consistent with the phase-screen problem in Chap. 3, however, we will use the parameters $\bar{k}$, ϕ_0 and γ (or ζ) to describe an extended-medium problem. [Notice that for the phase-screen problem the parameters ϕ_0 and γ (or ζ) have been used.] Using the bar notations, we define γ and ζ as before [cf. Eq. (3.17)]:

$$\gamma = \bar{k}/\bar{L} \ , \quad \zeta = 2\phi_0/\gamma \ . \tag{4.11}$$

For convenience, we also introduce a parameter γ_L such that

$$\gamma_L = \bar{k}/\bar{Z} = \gamma N \ . \tag{4.12}$$

For physical implications of the parameters γ (or γ_L) and ζ, similar arguments as in the previous chapter [cf. discussions following equation (3.17)] will hold. The parameter ϕ_0 represents the (total) r.m.s. phase fluctuation at $\bar{z} = \bar{L}$.

Now for ϕ_0, we note that the following. For an extended-medium problem, in general, it is not easy to find an expression for $\phi(x)$ (and thus an expression for ϕ_0) for a given $\delta n(x, z)$, where $\phi(x)$ represents the phase fluctuation at $z = L$. One may therefore say that ϕ_0 is not a proper parameter in this case. In this thesis, however, we are interested in the random focusing region as mentioned in Sec. 3.1. Since random focusing effects occur at $\zeta \sim 1$ and $\gamma \gg 1$, we choose $\gamma = 13.856$ and $0 < \zeta \lesssim 1.0$ in our numerical simulation. It follows that we are in the G.O. region ($\gamma \gg 1$) and $\phi(x)$ is given by [cf. Eqs. (3.6) and (3.7)]:

$$\phi(x) \simeq k \int_0^L dz \ \delta n(x, z) \ . \tag{4.13}$$

From this equation and (4.1), we find [cf. Eqs. (3.5), (3.9) and (3.10)]:

$$\phi_0^2 = \phi_{0E}^2 N_z = \sqrt{\pi} \ \bar{k}^2 \bar{L} \eta_0^2 \ . \tag{4.14}$$

The corresponding angle $\theta(x)$ is related to $\phi(x)$ by (3.13), and the relationship between ϑ_0 and ϕ_0 is given by (3.16). [If the equation (4.13) does not hold, then it would be better to use a different set of parameters, for example, η_0, $\bar{k}$ and $\bar{L}$.]

As in the phase-screen problem, we let $\bar{k} = 1.0472 \times 10^7$ ($\lambda = 0.6 \, \mu m$) and $\ell = 10^{-2} \, m$ throughout this chapter, so that the small-angle approximation (or the parabolic wave equation) can be applied. As mentioned before, to determine an electric field $u(\bar{x}, \bar{L})$ or moments of the field Γ_{nm} we need only two parameters in the parabolic approximation regime (but for numerical simulation three parameters are required even in this case). Just for reference, possible choices of the two parameters will be discussed briefly. In the moment equation (1.1), Q_{nm} is given by

$$\begin{aligned} Q_{nm} = & \sum_{i=1}^{n} \sum_{j=1}^{n} A(\vec{\rho}_i - \vec{\rho}_j) - \sum_{i=1}^{n} \sum_{j=1}^{m} [A(\vec{\rho}_i - \vec{\rho}_j') + A(\vec{\rho}_j - \vec{\rho}_i')] \\ & + \sum_{i=1}^{m} \sum_{j=1}^{m} A(\vec{\rho}_i' - \vec{\rho}_j') \ , \end{aligned} \tag{4.15}$$

with

$$A(\vec{\rho}) = \int_{-\infty}^{\infty} dz \ B_n(\vec{\rho}, z) \ . \tag{4.16}$$

For a two-dimensional extended medium, we have to replace $\vec{\rho}$, $\vec{\rho}_i$, $\vec{\rho}_j'$, Δ_i, and Δ_j' in (1.1), (4.15), and (4.16) by x, x_i, x_j', $\partial^2/\partial x_i^2$, and $\partial^2/\partial x_j'^2$, respectively, and $B_n(x, z)$ is given by (3.1). One can therefore see from (1.1) that the parameters $\hat{\gamma}$ and $\hat{\zeta}$ such that [see, for example, Ref. 50]:

$$\hat{\gamma} = \bar{L}/\bar{k}\ (= 1/\gamma)\ , \quad \hat{\zeta} = \sqrt{\pi}\ \eta_0^2 \bar{k}^3\ (= \phi_0^2/\hat{\gamma})\ , \tag{4.17}$$

would suffice to determine Γ_{nm} completely. [Or equivalently, any two of the parameters γ, ζ and ϕ_0 will do.] If one is interested in a field itself, $u(\bar{x}, \bar{L})$, then one may choose $\bar{k}/\bar{L}$ and $\eta_0\bar{k}^2$, instead of $\hat{\gamma}$ and $\hat{\zeta}$ [cf. Eq. (2.8)].

4.2 Wave-Kinetic Numerical Method

In our numerical simulation, we approximate an extended medium by N layers of eddies, as discussed in the previous section. In this section, the irradiance at $\bar{z} = \bar{L}$ for a given realization of the extended medium will be computed, using the wave-kinetic numerical method. For convenience, we introduce different variables for transverse coordinate $\bar{x}(\bar{z})$, angle $\theta(\bar{z})$, and the WDF $\bar{F}(\bar{x}, \theta; \bar{z})$, for each layer. The transverse coordinate for the l-th layer, $\bar{x}[\bar{z} = (l-1)\bar{Z}]$, will be denoted by $\bar{x}_{l-1}$, which is shown in Fig. 4.2.

The variable θ_{l-1} represents the angle just before passing through the l-th layer, and θ_l represents the angle right after passing through the l-th layer. (Note that the impulse approximation will be used in wave propagation calculations.) The corresponding variables for the n-th ray center will be denoted by $\bar{x}_{n,l-1}$, $\theta_{n,l-1}$, and θ_{nl}, respectively. For the WDF's just in front of and behind the l-th layer, the notations $\bar{F}_{l-1}(\bar{x}_{l-1}, \theta_{l-1})$ and $\bar{F}^+_{l-1}(\bar{x}_{l-1}, \theta_l)$ will be used, respectively. In the observation plane, $\bar{z} = N\bar{Z} = \bar{L}$, we denote $\bar{x}_N$, θ_N, $\bar{x}_{nN}$, θ_{nN}, and $\bar{F}_N(\bar{x}_N, \bar{s}_N)$ simply by $\bar{x}$, θ, $\bar{x}_n$, θ_n, and $\bar{F}_L(x, \theta)$, to be consistent with the notations used in the previous chapter.

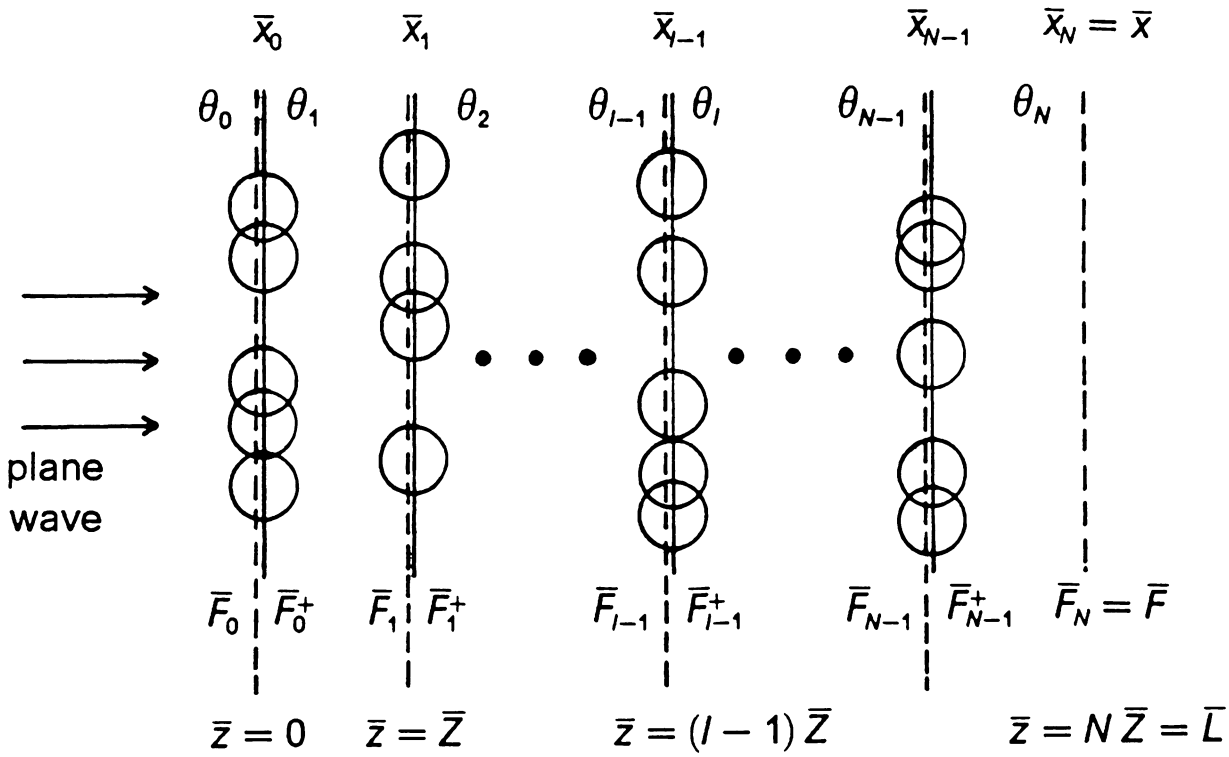

Figure 4.2 Simulation model which shows relevant variables for wave-kinetic numerical method.

The input WDF is given by [cf. Eq. (3.21)]:

$$\bar{F}_0(\bar{x}_0, \theta_0) = \frac{\bar{W}_0}{\sqrt{2\pi}} e^{-2\bar{x}_0^2/\bar{W}_0^2} e^{-\bar{k}^2\bar{W}_0^2\theta_0^2/2} , \tag{4.18}$$

where we let $\bar{W}_0 \to \infty$ for a plane wave. To compute the output WDF $\bar{F}_L(\bar{x}, \theta)$ and thus the irradiance $I_L(\bar{x})$, we will first use the Liouville approximation. Next, the idea of the higher-order approximations in the phase-screen problem will be extended to this extended-medium problem, to obtain a more accurate expression for $I_L(\bar{x})$.

4.2.1 Liouville Approximation

Let us first introduce new variables for difference coordinates in two-dimensional phase space: $\overline{\delta x}_l = \bar{x}_l - \bar{x}_{nl}$, $\delta\theta_l = \theta_l - \theta_{nl}$. As before, we denote a discretization interval and the number of rays by $\overline{\Delta x}$ and N_r, respectively. With these notations, the discretized input WDF can be represented as [cf. Eqs. (3.22) and (3.23)]:

$$\bar{F}_0(\bar{x}_0, \theta_0) = \sum_{n=1}^{N_r} \Lambda_n e^{-\overline{\delta x}_0^2/2\overline{\Delta x}^2} e^{-\bar{k}^2\bar{W}_0^2\,\delta\theta_0^2/2} , \tag{4.19}$$

where $\overline{\delta x}_0 = \bar{x}_0 - \bar{x}_{n0}$ with $\bar{x}_{n0} = n\overline{\Delta x}$, $\delta\theta_0 = \theta_0 - \theta_{n0}$ with $\theta_{n0} = 0$ in this case, and

$$\Lambda_n = \frac{\bar{W}_0}{2\pi} e^{-2(n\overline{\Delta x})^2/\bar{W}_0^2} . \tag{4.20}$$

For calculation of ray trajectories, we utilize the impulse approximation for each layer, as in the single-layer problem (i. e., the phase-screen problem). It follows that the l-th layer introduces an angle impulse $\Delta_l(\bar{x}) = \frac{1}{\bar{k}} \frac{d\phi_l(\bar{x})}{d\bar{x}}$, and thus the angle impulse for the n-th ray center becomes $\Delta_{nl} = \Delta_l(\bar{x} = \bar{x}_{n,l-1})$ [cf. Eqs. (3.29)-(3.32)]. Using the expression (4.9) for $\phi_l(\bar{x})$, we find

$$\Delta_{nl} = -2\sqrt{2\pi}\,\eta_0 \sum_{m=1}^{N_{LE}} q_{ml}\,\bar{d}_{nm,l}\,e^{-2\,\bar{d}^2_{nm,l}} \ , \quad (\bar{d}_{nm,l} = \bar{x}_{n,l-1} - \bar{x}^c_{ml}) \ . \tag{4.21}$$

Here we have assumed that the thickness of each slab, $\bar{Z}$, is large enough, i. e., $\bar{Z} \gg 1$. [Note that $\bar{Z}$ is also assumed to be sufficiently small, in order that the simplified model and the thin-screen approximation for each slab may be valid. For a specific value of $\bar{Z}$ used in numerical simulation, see Sec. 4.4.]. From the results of Sec. 3.2.1 [cf. Eqs. (3.39) and (3.40)], the coordinate transformation for the l-th layer is then given by

$$\begin{bmatrix} \overline{\delta x}_{l-1} \\ \delta\theta_{l-1} \end{bmatrix} = T_{nl} \begin{bmatrix} \overline{\delta x}_l \\ \delta\theta_l \end{bmatrix} \ , \tag{4.22}$$

where

$$T_{nl} \equiv \begin{bmatrix} a_l & b_l \\ c_l & d_l \end{bmatrix} = \begin{bmatrix} 1 & -\bar{Z} \\ -\Delta_{nl}' & 1 + \bar{Z}\,\Delta_{nl}' \end{bmatrix} \ , \tag{4.23}$$

with

$$\begin{aligned} \Delta_{nl}' &= \frac{1}{\bar{k}} \ \frac{d\Delta_l(\bar{x})}{d\bar{x}} \Big|_{\bar{x} = \bar{x}_{n,l-1}} \\ &= -2\sqrt{2\pi}\,\eta_0 \sum_{m=1}^{N_{LE}} q_{ml}\,(1 - 4\,\bar{d}^2_{nm,l})\,e^{-2\,\bar{d}^2_{nm,l}} \ . \end{aligned} \tag{4.24}$$

Since angle impulses and (transverse) ray bendings are added up for each layer, $\bar{x}_{nl}$ and θ_{nl} in the above equation [cf. $\overline{\delta x}_l = \bar{x}_l - \bar{x}_{nl}$, $\delta\theta_l = \theta_l - \theta_{nl}$] are given by

$$\begin{aligned} \bar{x}_{nl} &= \bar{x}_{n0} + \bar{Z} \sum_{p=1}^{l} \theta_{np} \\ \theta_{nl} &= \theta_{n0} + \sum_{p=1}^{l} \Delta_{np} \ , \end{aligned} \tag{4.25}$$

where $\bar{x}_{n0} = n\overline{\Delta x}$ and $\theta_{n0} = 0$ in our case.

Let us now introduce transformation matrices $\tilde{T}_{nl}$, $(l = 1, 2, \ldots, N)$, such that

$$\begin{aligned}\tilde{T}_{nl} &\equiv \begin{bmatrix} A_l & B_l \\ C_l & D_l \end{bmatrix} \\ &= T_{nl}\, T_{n,l+1} \cdots T_{nN} \ .\end{aligned} \tag{4.26}$$

It follows then that initial coordinates transform into final coordinates by

$$\begin{bmatrix} \overline{\delta x_0} \\ \delta\theta_0 \end{bmatrix} = \tilde{T}_{n1} \begin{bmatrix} \overline{\delta x} \\ \delta\theta \end{bmatrix} , \tag{4.27}$$

where the simplified notations (i. e., $\bar{x} = \bar{x}_N$, $\theta = \theta_N$, $\bar{x}_n = \bar{x}_{nN}$ and $\theta_n = \theta_{nN}$) are used, and $\overline{\delta x} = \bar{x} - \bar{x}_n$, $\delta\theta = \theta - \theta_n$. We note that $|\tilde{T}_{nl}| = A_l D_l - B_l C_l = 1$ for all l, since energy is conserved in the Liouville approximation, i. e., $|T_{nl}| = 1$ [cf. Eq. (4.23)]. Substituting (4.27) into (4.19), we obtain

$$F_L(\bar{x}, \theta) = \sum_{n=1}^{N_r} \Lambda_n \, e^{-[\hat{\alpha}_x \overline{\delta x}^2 - 2\hat{\alpha}_{x\theta} \overline{\delta x}\, \delta\theta + \hat{\alpha}_\theta \delta\theta^2]} , \tag{4.28}$$

where

$$\begin{aligned}\hat{\alpha}_x &= \alpha_x A_1^2 + \alpha_\theta C_1^2 \\ \hat{\alpha}_{x\theta} &= -(\alpha_x A_1 B_1 + \alpha_\theta C_1 D_1) \\ \hat{\alpha}_\theta &= \alpha_x B_1^2 + \alpha_\theta D_1^2 \ ,\end{aligned} \tag{4.29}$$

with $\alpha_x = 1/2\overline{\Delta x^2}$, $\alpha_\theta = \bar{k}^2 \overline{W_0^2}/2$.

The irradiance at $\bar{z} = \bar{L}$ can be calculated by the wavenumber integration of $F_L(\bar{x}, \theta)$ [cf. Eq. (3.20)]. Using the fact that $|\tilde{T}_{n1}| = A_1 D_1 - B_1 C_1 = 1$, after straight-forward calculations we obtain

$$I_L(\bar{x}) = \frac{1}{\sqrt{2\pi}} \sum_{n=1}^{N_r} \frac{1}{|S_n|} e^{-2(n\overline{\Delta x})^2/\overline{W}_0^2} e^{-(\bar{x}-\bar{x}_n)^2/2S_n^2\overline{\Delta x}^2} , \tag{4.30}$$

where

$$S_n^2 = \left(\frac{\bar{L}}{\bar{k}\overline{W}_0\overline{\Delta x}} \right)^2 + C_n^2 , \tag{4.31}$$

with

$$C_n = D_1 . \tag{4.32}$$

In the above equation, the n-th ray center at $\bar{z} = \bar{L}$ is given by

$$\bar{x}_n = \bar{x}_{n0} + \bar{Z} \sum_{l=1}^{N} \theta_{nl} , \quad (\bar{x}_{n0} = n\overline{\Delta x}) . \tag{4.33}$$

As in the phase-screen problem, we let $\overline{W}_0 \to \infty$ for a plane wave, and thus S_n in (4.30) may be replaced by C_n. It follows that the final expression for $I_L(\bar{x})$ from the Liouville approximation (or the first-order approximation) becomes

$$I_L(\bar{x}) = \frac{1}{\sqrt{2\pi}} \sum_{n=1}^{N_r} \frac{1}{|C_n|} e^{-(\bar{x}-\bar{x}_n)^2/2C_n^2\overline{\Delta x}^2} . \tag{4.34}$$

Compare this with the corresponding expression (3.48) for a phase-screen problem. Only the expressions for C_n and $\bar{x}_n$ are different [cf. Eqs. (4.32), (4.33), (3.46), and (3.47)]. For a single layer ($N = 1$) with $\bar{Z}$ replaced by $\bar{L}$, $\tilde{T}_{n1}$ in (4.26) becomes T_n in (3.39), and C_n and $\bar{x}_n$ given above reduce to those for a phase-screen problem.

For later comparison with the results from higher-order approximations, we wish to find an expression for the spectrum of irradiance $\tilde{I}_L(\Omega)$ [cf. Eqs. (3.61) and (3.62)]. Introducing a Fourier transform as before, i. e.,

$$I_L(\bar{x}) = \int_{-\infty}^{\infty} d\Omega \; e^{i\bar{x}\Omega} \tilde{I}_L(\Omega) \; , \tag{4.35}$$

we find

$$\tilde{I}_L(\Omega) = \frac{\overline{\Delta x}}{2\pi} \sum_{n}^{N_r} e^{-i\bar{x}_n\Omega} e^{-\overline{\Delta x}^2 c_n^2 \Omega^2/2} \; . \tag{4.36}$$

Notice the formal similarity between this and (3.62).

4.2.2 Higher-Order Approximations

In this section, we will extend the idea in Sec. 3.2.2 to an extended-medium problem [cf. Fig. 4.2]. Let us denote the electric fields at $\bar{z} = \bar{z}_l^-$ and $\bar{z}_l^+$, where $\bar{z}_l = (l-1)\overline{Z}$, by $u_{l-1}(\bar{x}_{l-1})$ and $u_l(\bar{x}_{l-1})$, respectively. It follows then from the impulse approximation that

$$u_l(\bar{x}_{l-1}) = u_{l-1}(\bar{x}_{l-1}) \, e^{i\phi_l(\bar{x}_{l-1})} \; , \tag{4.37}$$

where $\phi_l(\bar{x})$ is given by (4.9) with $(x - x_{ml}^c)/\ell$ being replaced by $\bar{x} - \bar{x}_{ml}^c$. From the definition of the WDF (3.19), the WDF at $\bar{z} = \bar{z}_l^+$ is given by

$$\overline{F}_{l-1}^{+}(\bar{x}_{l-1}, \; \theta_l) = \frac{1}{2\pi} \int_{-\infty}^{\infty} d\bar{s} \; e^{-i\bar{k}\theta_l\bar{s}} \left[e^{i\,\delta\phi_l(\bar{x}_{l-1},\; \bar{s})} \hat{\Gamma}_2(\bar{x}_{l-1}, \; \bar{s}; \bar{z}_l^{\,-}) \right] \; , \tag{4.38}$$

where

$$\delta\phi_l(\bar{x}_{l-1}, \; \bar{s}) = \phi(\bar{x}_{l-1} + \bar{s}/2) - \phi(\bar{x}_{l-1} - \bar{s}/2) \; , \tag{4.39}$$

and

$$\hat{\Gamma}_2(\bar{x}_{l-1},\ \bar{s};\ \bar{z}_l^{-}) = u_{l-1}(\bar{x}_{l-1} + \bar{s}/2)u^{*}_{l-1}(\bar{x}_{l-1} - \bar{s}/2)\ . \tag{4.40}$$

Using the relationship between $\hat{\Gamma}_2(\bar{x}_{l-1},\ \bar{s};\ \bar{z}_l^{-})$ and the WDF at $\bar{z} = \bar{z}_l^{-}$,

$$\hat{\Gamma}_2(\bar{x}_{l-1},\ \bar{s};\ \bar{z}_l^{-}) = \bar{k}\int_{-\infty}^{\infty} d\theta_{l-1}\ e^{i\bar{k}\theta_{l-1}\bar{s}}\ \bar{F}_{l-1}(\bar{x}_{l-1},\ \theta_{l-1})\ , \tag{4.41}$$

we obtain

$$\begin{aligned}\bar{F}^{+}_{l-1}(\bar{x}_{l-1},\ \theta_l) = \frac{\bar{k}}{2\pi}\int_{-\infty}^{\infty} d\bar{s}\ e^{-i\bar{k}\theta_l\bar{s}}\ e^{i\,\delta\phi_l(\bar{x}_{l-1},\ \bar{s})} \\ \times\left[\int_{-\infty}^{\infty} d\theta_{l-1}\ e^{i\bar{k}\theta_{l-1}\bar{s}}\ \bar{F}_{l-1}(\bar{x}_{l-1},\ \theta_{l-1})\right]\ .\end{aligned} \tag{4.42}$$

The phase difference $\delta\phi_l$ in the above equation can be expanded in the Taylor series [cf. Eqs. (3.65) and (3.66)]:

$$\delta\phi_l(\bar{x}_{l-1},\ \bar{s}) = \bar{k}\ \Delta_l(\bar{x}_{l-1})\ \bar{s} + h_l(\bar{x}_{l-1},\ \bar{s})\ , \tag{4.43}$$

with

$$h_l(\bar{x}_{l-1},\ \bar{s}) = 2\bar{k}\sum_{m=1}^{\infty}\frac{\Delta_l^{(2m)}(\bar{x}_{l-1})}{(2m+1)!}\left(\frac{\bar{s}}{2}\right)^{2m+1}\ , \tag{4.44}$$

where $\Delta_l(\bar{x}) = \dfrac{1}{\bar{k}}\dfrac{d\phi_l(\bar{x})}{d\bar{x}}$ [cf. Eq. (4.21)] and $\Delta_l^{(2m)}(\bar{x}) = \dfrac{d^{2m}\Delta_l}{d\bar{x}^{2m}}$.

Now for the first layer, we have

$$\bar{F}^{+}_0(\bar{x}_0,\ \theta_1) = \frac{1}{2\pi}\int_{-\infty}^{\infty} d\bar{s}_0\ e^{-i\bar{k}\theta_1\bar{s}_0}\ e^{i\,\delta\phi_1(\bar{x}_0,\ \bar{s}_0)}\ , \tag{4.45}$$

which is obtained by substituting $u_0(\bar{x}_0) = 1$ in (4.36). Application of the discretization scheme [cf. Eq. (3.52)] to the above equation leads to

$$\bar{F}_0^+(\bar{x}_0,\ \theta_1) = \frac{1}{2\pi} \sum_n \int_{-\infty}^{\infty} d\bar{s}_0\ e^{-i\bar{k}\theta_1 \bar{s}_0}\, e^{i\,\delta\phi_1(\bar{x}_0,\ \bar{s}_0)}\, G(\bar{x}_0 - \bar{x}_{n0})\ , \tag{4.46}$$

where $\bar{x}_{n0} = n\overline{\Delta x}$, and

$$G(\bar{x}) = \frac{1}{\sqrt{2\pi}}\ e^{-\bar{x}^2/2\overline{\Delta x}^2}\ . \tag{4.47}$$

Using the series expansion of $\delta\phi_1$, which is given by (4.43), we obtain

$$\bar{F}_0^+(\bar{x}_0,\ \theta_1) = \frac{1}{2\pi} \sum_n \int_{-\infty}^{\infty} d\bar{s}_0\ e^{ih_1(\bar{x}_0,\ \bar{s}_0)}\, e^{-i\bar{k}\bar{s}_0[\theta_1 - \Delta_1(\bar{x}_0)]}\, G(\bar{x}_0 - \bar{x}_{n0})\ . \tag{4.48}$$

Since $G(\bar{x}_0 - \bar{x}_{n0})$ is sharply peaked around $\bar{x}_0 = \bar{x}_{n0}$ (i. e., $|\bar{x}_0 - \bar{x}_{n0}| \simeq \overline{\Delta x}$, and $\overline{\Delta x}$ can be made arbitrarily small so that $\overline{\Delta x} \ll 1$), we may let

$$\begin{aligned} &\Delta_1(\bar{x}_0) \simeq \Delta_{n1} + \Delta_{n1}'(\bar{x}_0 - \bar{x}_{n0}) \\ &h_1(\bar{x}_0,\ \bar{s}_0) \simeq h_{n1}(\bar{s}_0) + h_{n1}'(\bar{s}_0)\,(\bar{x}_0 - \bar{x}_{n0})\ , \end{aligned} \tag{4.49}$$

where $\Delta_{n1} = \Delta_1(\bar{x}_{n0})$ and $\Delta_{n1}' = \dfrac{\partial}{\partial \bar{x}_0} \Delta_1(\bar{x}_0)\big|_{\bar{x}_0 = \bar{x}_{n0}}$ [cf. Eqs. (4.21) and (4.24)]; $h_{n1}(\bar{s}_0) = h_1(\bar{x}_{n0},\ \bar{s}_0)$ and $h_{n1}'(\bar{s}_0) = \dfrac{\partial}{\partial \bar{x}_0} h_1(\bar{x}_0,\ \bar{s}_0)\big|_{\bar{x}_0 = \bar{x}_{n0}}$. Note that for a single-layer problem we have let $\Delta(\bar{x}_0) \simeq \Delta_n + \Delta_n'(\bar{x}_0 - \bar{x}_{n0})$ and $h(\bar{x}_0,\ \bar{s}) \simeq h_n(\bar{s})$ [cf. Eqs. (3.54) and (3.67)], which is accurate enough for a sufficiently small $\overline{\Delta x}$. For a multiple-layer problem, however, even the more accurate approximations given above introduce some errors, since small errors from each layer are accumulated. In addition, for the layers other than the first one (i. e., for the layers such that $2 \le l \le N$), we need another kind of approximation to obtain a closed-form solution. This also introduce errors. Details

will be discussed later in this section. Substituting (4.49) in (4.48) and using the notations, $\overline{\delta x_0} = \bar{x}_0 - \bar{x}_{n0}$ and $\delta\theta_1 = \theta_1 - \theta_{n1}$ with $\theta_{n1} = \Delta_{n1}$, we obtain

$$\bar{F}_0^+(\bar{x}_0,\ \theta_1) \simeq \frac{1}{2\pi} \sum_n \int_{-\infty}^{\infty} d\bar{s}_0\ e^{i h_{n1}(\bar{s}_0)}\, e^{i h_{n1}'(\bar{s}_0)\,\overline{\delta x_0}}\, e^{-i\bar{k}\bar{s}_0(\delta\theta_1 - \Delta_{n1}'\,\overline{\delta x_0})}\, G(\overline{\delta x_0}) \ . \tag{4.50}$$

For free-space propagation (of distance $\bar{Z}$), we have [cf. Eq. (3.55)]:

$$\begin{bmatrix} \overline{\delta x_{l-1}} \\ \delta\theta_{l-1} \end{bmatrix} = \begin{bmatrix} 1 & -\bar{Z} \\ 0 & 1 \end{bmatrix} \begin{bmatrix} \overline{\delta x_l} \\ \delta\theta_l \end{bmatrix} , \quad (l = 1,\ 2,\ \ldots,\ N) \ . \tag{4.51}$$

Substitution of (4.51) in (4.50) gives rise to the WDF at $\bar{z} = \bar{Z}^-$:

$$\begin{aligned} \bar{F}_1(\bar{x}_1,\ \theta_1) &\equiv \sum_n \bar{F}_{n1}(\bar{x}_1,\ \theta_1) \\ &\simeq \frac{1}{2\pi} \sum_n \int_{-\infty}^{\infty} d\bar{s}_0\ e^{i h_{n1}(\bar{s}_0)}\, e^{i h_{n1}'(\bar{s}_0)\,(\overline{\delta x_1} - \bar{Z}\,\delta\theta_1)} \\ &\quad \times e^{-i\bar{k}\bar{s}_0[\delta\theta_1 - \Delta_{n1}'\,(\overline{\delta x_1} - \bar{Z}\,\delta\theta_1)]}\, G(\overline{\delta x_1} - \bar{Z}\,\delta\theta_1) \ , \end{aligned} \tag{4.52}$$

where $\bar{x}_{n1}$ and θ_{n1} (which are included in $\overline{\delta x_1}$ and $\delta\theta_1$) are given by (4.25).

Next for the second layer, we have from (4.42), (4.43) and (4.52):

$$\begin{aligned} \bar{F}_1^+(\bar{x}_1,\ \theta_2) = \frac{\bar{k}}{2\pi} \sum_n \int_{-\infty}^{\infty} d\bar{s}_1\ & e^{i h_2(\bar{x}_1,\ \bar{s}_1)}\, e^{-i\bar{k}\bar{s}_1[\theta_2 - \Delta_2(\bar{x}_1)]} \\ \times \left[\int_{-\infty}^{\infty} d\theta_1\ e^{i\bar{k}\theta_1\bar{s}_1}\, \bar{F}_{n1}(\bar{x}_1,\ \theta_1) \right] , \end{aligned} \tag{4.53}$$

where $\bar{F}_1^+(\bar{x}_1,\ \theta_2)$ is the WDF at $\bar{z} = \bar{Z}^+$. The Gaussian function G is given by

$$G(\overline{\delta x_1} - \bar{Z}\,\delta\theta_1) = \frac{1}{\sqrt{2\pi}}\, e^{-(\bar{x}_1 - \bar{x}_{n1} - \bar{Z}\,\delta\theta_1)^2 / 2\overline{\Delta x}^2} \ , \tag{4.54}$$

which is now sharply peaked around $\bar{x}_1 = \bar{x}_{n1} + \bar{Z}\,\delta\theta_1$, i. e., $|\bar{x}_1 - \bar{x}_{n1} - \bar{Z}\,\delta\theta_1| \simeq \overline{\Delta x} \ll 1$. It follows that to use the same level of approximation as in (4.49) we have to let

$$\begin{aligned} \Delta_2(\bar{x}_1) &\simeq \Delta_2(\bar{x}_{n1} + \bar{Z}\,\delta\theta_1) + \Delta_2'(\bar{x}_{n1} + \bar{Z}\,\delta\theta_1)\,(\bar{x}_1 - \bar{x}_{n1} - \bar{Z}\,\delta\theta_1) \\ h_2(\bar{x}_1,\ \bar{s}_1) &\simeq h_2(\bar{x}_{n1} + \bar{Z}\,\delta\theta_1,\ \bar{s}_1) + h_2'(\bar{x}_{n1} + \bar{Z}\,\delta\theta_1,\ \bar{s}_1)\,(\bar{x}_1 - \bar{x}_{n1} - \bar{Z}\,\delta\theta_1)\ , \end{aligned} \tag{4.55}$$

which is valid if $\overline{\Delta x} \ll 1$. This approximation, however, does not allow a closed form expression for $I_L(\bar{x})$. In order to obtain one, we need further approximations. Note that

$$\begin{aligned} \Delta_2(\bar{x}_1) &\simeq \sum_{p=0}^{\infty} \frac{\Delta_{n2}^{(p)}}{p!}(\bar{Z}\,\delta\theta_1)^p + (\overline{\delta x}_1 - \bar{Z}\,\delta\theta_1)\sum_{p=0}^{\infty}\frac{\Delta_{n2}^{(p+1)}}{p!}(\bar{Z}\,\delta\theta_1)^p \\ &= [\Delta_{n2} - \frac{1}{2}\Delta_{n2}''(\bar{Z}\delta\theta_1)^2 - \cdots] + [\Delta_{n2}' + \Delta_{n2}''(\bar{Z}\delta\theta_1) + \cdots]\overline{\delta x}_1\ , \end{aligned} \tag{4.56}$$

where $\Delta_{n2}^{(p)} = \dfrac{d^p\Delta_2(\bar{x}_1)}{d\bar{x}_1^p}\Big|_{\bar{x}_1=\bar{x}_{n1}}$. A similar approximation holds for $h_2(\bar{x}_1,\ \bar{s}_1)$. Since $\Delta_{n2}^{(p)}$ and $h_{n2}^{(p)}(\bar{s}_1) = \dfrac{\partial^p h_2(\bar{x}_1,\ \bar{s}_1)}{\partial\bar{x}_1^p}\Big|_{\bar{x}_1=\bar{x}_{n1}}$ have the same order of magnitude for all p, assuming that $|\bar{Z}\,\delta\theta_1| \sim \bar{Z}\vartheta_0 \ll 1$ (where ϑ_0 is the r.m.s. angle fluctuation at $\bar{z} = \bar{L}$) we may simplify (4.55) further:

$$\begin{aligned} \Delta_2(\bar{x}_1) &\simeq \Delta_{n2} + \Delta_{n2}'\,(\bar{x}_1 - \bar{x}_{n1}) \\ h_2(\bar{x}_1,\ \bar{s}_1) &\simeq h_{n2}(\bar{s}_1) + h_{n2}'(\bar{s}_1)\,(\bar{x}_1 - \bar{x}_{n1})\ . \end{aligned} \tag{4.57}$$

Notice that for the N-th layer (i. e., at $\bar{z} = \bar{z}_N$, where $\bar{z}_N = (N-1)\bar{Z}$), the exponent of the Gaussian function G becomes $(\overline{\delta x}_{N-1} + \bar{Z}\sum_{l=1}^{N-1}\delta\theta_l)^2/2\overline{\Delta x^2}$ [cf. Eq. (A4.3)] and $|\bar{Z}\sum_{l=1}^{N-1}\delta\theta_l| \sim (N-1)\,\bar{Z}\vartheta_0 \simeq \bar{L}\vartheta_0$. Thus, to apply the above approximation to all the remaining $(N-2)$ layers, $\bar{L}\vartheta_0 \sim \zeta$ must be small enough even for a sufficiently small $\overline{\Delta x}$. Incorporating the approximation (4.57) in (4.53), we obtain

$$\bar{F}_1^+(\bar{x}_1,\ \theta_2) \simeq \frac{\bar{k}}{2\pi} \sum_n \int_{-\infty}^{\infty} d\bar{s}_1\ e^{i h_{n2}(\bar{s}_1)}\, e^{i h_{n2}'(\bar{s}_1)\,\overline{\delta x}_1}\, e^{-i\bar{k}\bar{s}_1(\delta\theta_2 - \Delta_{n2}'\,\overline{\delta x}_1)} \times \int_{-\infty}^{\infty} d\theta_1\ e^{i\bar{k}\bar{s}_1\delta\theta_1}\, \bar{F}_{n1}(\bar{x}_1,\ \theta_1)\ , \tag{4.58}$$

where we used the fact that [cf. Eq. (4.25)]:

$$\delta\theta_l - \delta\theta_{l-1} = \theta_l - \theta_{l-1} - \Delta_{nl}\ . \tag{4.59}$$

After free-space propagation (of distance $\bar{Z}$) described by (4.51), the WDF at $\bar{z} = \bar{z}_3$ ($\bar{z}_3 = 2\bar{Z}$) becomes

$$\bar{F}_2(\bar{x}_2,\ \theta_2) = \bar{F}_1^+(\overline{\delta x}_1 = \overline{\delta x}_2 - \bar{Z}\ \delta\theta_2,\ \theta_2)\ . \tag{4.60}$$

See Appendix A4.1 for details.

We repeat the above procedure for the remaining $(N-2)$ layers to obtain $\bar{F}_L(\bar{x},\ \theta)$. In the final expression for $I_L(\bar{x})$, which results from the wavenumber $(\bar{k}\theta)$ integration of $\bar{F}_L(\bar{x},\ \theta)$, all θ_l integrals decouple and we obtain [cf. Appendix A4.1]:

$$\tilde{I}_L(\Omega) = \frac{\overline{\Delta x}}{2\pi} \sum_n \left\{ e^{-i\bar{x}_n\Omega}\, e^{-\overline{\Delta x}^2[\Omega + g_n(\Omega)]^2/2} \right\} \left\{ e^{-i\sum_{l=1}^{N} h_{nl}[\bar{s} = \alpha_l(\Omega)]} \right\}\ , \tag{4.62}$$

with

$$g_n(\Omega) = \sum_{l=1}^{N} \delta\phi_{nl}'[\bar{s} = \alpha_l(\Omega)]\ , \tag{4.63}$$

where the Fourier transform is defined as (4.35), and $\alpha_l(\Omega)$ satisfies the recursive relation,

$$\alpha_N = \Omega/\gamma_L$$
$$\alpha_l = \alpha_{l+1} + [\Omega + \sum_{p=l+1}^{N} \delta\phi_{np}'(\bar{s} = \alpha_p)] / \gamma_L \ , \quad (l = N-1,\ N-2, \ldots, 1) \ . \tag{4.64}$$

In the above equations,

$$\delta\phi_{nl}(\bar{s}) = \delta\phi_l(\bar{x}_{l-1} = \bar{x}_{n,l-1},\ \bar{s})$$
$$\delta\phi_{nl}'(\bar{s}) = \frac{\partial}{\partial \bar{x}_{l-1}} \delta\phi_l(\bar{x}_{l-1},\ \bar{s})\,|_{\bar{x}_{l-1} = \bar{x}_{n,l-1}} \tag{4.65}$$
$$h_{nl}(\bar{s}) = h_l(\bar{x}_{l-1} = \bar{x}_{n,l-1},\ \bar{s}) = \delta\phi_{nl}(\bar{s}) - \bar{k}\Delta_{nl}\bar{s} \ ,$$

and $\bar{x}_n$ is given by (4.33). [For $\delta\phi_l(\bar{x}_{l-1},\ \bar{s})$ and $h_l(\bar{x}_{l-1},\ \bar{s})$, see Eqs. (4.39), (4.43) and (4.44).] Representing h_{nl} in terms of $\delta\phi_{nl}$, we may rewrite (4.62) as:

$$\tilde{I}_L(\Omega) = \frac{\overline{\Delta x}}{2\pi} \sum_n e^{-i[\bar{x}_n\Omega - \gamma_L \sum_{l=1}^{N} (\bar{z}\delta_{nl})\alpha_l]} e^{-\overline{\Delta x}^2[\Omega + g_n(\Omega)]^2/2} e^{-i\sum_{l=1}^{N} \delta\phi_{nl}(\alpha_l)} \ , \tag{4.66}$$

which is more convenient for numerical calculation. The equation (4.62) [or (4.66)] is the least limited closed-form expression for $\tilde{I}_L(\Omega)$ we can find using the wave-kinetic numerical method. In what follows, we will denote the wave-kinetic numerical method with the approximation (4.57) [which leads to the above expressions for $\tilde{I}_l(\Omega)$, (4.62) or (4.66)] by W-K(III), and the wave-kinetic numerical method with the Liouville aproximation [cf. Eq. (4.34) or (4.36)] by W-K(LV). In the above derivation, we have assumed that $\bar{L}\vartheta_0 \sim \zeta$ is not large (and $\overline{\Delta x} \ll 1$.) Numerical calculations in Sec. 4.4.2 indicate that W-K(III) is valid for $\zeta \lesssim 1.2$, which seems to be sufficient for our purpose. (Note that we are interested in the random focusing region, $0.5 \lesssim \zeta \lesssim 1.0$, where wave statistics are not well understood.)

The irradiance spectrum $\tilde{I}_L(\Omega)$ from W-K(III) looks somewhat complicated, and is not easily expressed as the product of the expression (4.36) from W-K(LV) with a cor-

rection factor. However, further simplified expressions can be obtained. First, let us neglect h_{nl}' in $\delta\phi_{nl}'$, i. e., let $\delta\phi_{nl}'(\bar{s}) = \bar{k}\Delta_{nl}'\bar{s} + h_{nl}'(\bar{s}) \simeq \bar{k}\Delta_{nl}'\bar{s}$ [cf. Eq. (4.65)], and denote the resulting α_l by $\left(\frac{\Omega}{\gamma_L}\right)\hat{\alpha}_l$. Note that $\hat{\alpha}_l$ is now a constant, not a function of Ω [see below]. This simplification is equivalent to the approximation, say for the second layer [cf. Eq. (4.57)]:

$$\begin{aligned} &\Delta_2(\bar{x}_1) \simeq \Delta_{n2} + \Delta_{n2}'\,(\bar{x}_1 - \bar{x}_{n1}) \\ &h_2(\bar{x}_1,\ \bar{s}_1) \simeq h_{n2}(\bar{s}_1)\ , \end{aligned} \tag{4.67}$$

which is the same approximation as in the phase-screen problem [cf. Sec. 3.2.2]. Replacing $\delta\phi_{nl}'(\bar{s})$ in (4.63) and (4.64) by $\bar{k}\Delta_{nl}'\bar{s}$, after some manipulations we obtain [cf. Appendix A4.2]:

$$\tilde{I}_L(\Omega) = \frac{\overline{\Delta x}}{2\pi} \sum_n \left[e^{-i\bar{x}_n\Omega}\, e^{-\overline{\Delta x}^2 C_n^2 \Omega^2/2}\right] \left[e^{-i\sum_{l=1}^{N} h_{nl}(\hat{\alpha}_l\Omega/\gamma_L)}\right] , \tag{4.68}$$

where $\bar{x}_n$ and $C_n = D_1$ are the same as in the Liouville approximation [cf. Eqs. (4.32) and (4.33)], and

$$\begin{aligned} \hat{\alpha}_l &= B_l/(-\bar{Z}) \\ &= \hat{\alpha}_{l+1} + (1 + \bar{Z}\sum_{p=l+1}^{N} \Delta_{np}'\,\hat{\alpha}_p)\ , \quad (\hat{\alpha}_N = 1)\ . \end{aligned} \tag{4.69}$$

For numerical implementation, it is more convenient to use the recursive relations for D_l and $\hat{\alpha}_l$ [cf. Eq. (A4.34)] which allows the simultaneous calculation of $\hat{\alpha}_l$ and D_l (and thus $D_1 = C_n$):

$$\begin{aligned} &\hat{\alpha}_N = 1\ , \quad D_N = d_N = 1 + \bar{Z}\,\Delta_{nN}' \\ &\hat{\alpha}_l = \hat{\alpha}_{l+1} + D_{l+1} \\ &D_l = d_l\,\hat{\alpha}_l - \hat{\alpha}_{l+1}\ , \quad (d_l = 1 + \bar{Z}\,\Delta_{nl}')\ . \end{aligned} \tag{4.70}$$

Equation (4.68) may also be rewritten as

$$\tilde{I}_L(\Omega) = \frac{\overline{\Delta x}}{2\pi} \sum_n e^{-i\left[\bar{x}_n - \sum_{l=1}^{N} (\bar{Z}\Delta_{nl})\,\hat{\alpha}_l\right]\Omega} e^{-\overline{\Delta x}^2 C_n^2 \Omega^2/2} e^{-i\sum_{l=1}^{N} \delta\phi_{nl}(\hat{\alpha}_l \Omega/\gamma_L)} \quad . \tag{4.71}$$

The wave-kinetic numerical method with the approximation (4.67), which leads to the expression (4.68) [or (4.71)], will be simply called W-K(II). Note the similarity between (4.68) and (3.69). For a single layer, $\hat{\alpha}_1 = 1$ and (4.68) reduces to (3.69). Comparing (4.68) with (4.36) from W-K(LV), we now can see clearly the correction factor, i. e., the former is a sum of products of $\tilde{I}_L^{(0)}(\Omega) \equiv e^{-i\bar{x}_n\Omega} e^{-\overline{\Delta x}^2 C_n^2 \Omega^2/2}$ with correction factors $e^{-i\sum_{l=1}^{N} h_{nl}(\hat{\alpha}_l \Omega/\gamma_L)}$.

The correction factor (in fact the parameter $\hat{\alpha}_l$) in (4.68) can be simplied further. Neglecting Δ_{nl}' in the expression (4.69) for $\hat{\alpha}_l$, we may approximate $\hat{\alpha}_l$ as

$$\hat{\alpha}_l \simeq N + 1 - l \quad . \tag{4.72}$$

The wave-kinetic numerical method with this additional approximation will be called W-K(I). The resulting irradiance spectrum is given by

$$\tilde{I}_L(\Omega) \simeq \frac{\overline{\Delta x}}{2\pi} \sum_n \left[e^{-i\bar{x}_n\Omega} e^{-\overline{\Delta x}^2 C_n^2 \Omega^2/2}\right] \left\{e^{-i\sum_{l=1}^{N} h_{nl}[(N+1-l)\Omega/\gamma_L]}\right\} \quad , \tag{4.73}$$

or

$$\tilde{I}_L(\Omega) \simeq \frac{\overline{\Delta x}}{2\pi} \sum_n e^{-i\bar{x}_{n0}\Omega} e^{-\overline{\Delta x}^2 C_n^2 \Omega^2/2} e^{-i\sum_{l=1}^{N} \delta\phi_{nl}[(N+1-l)\Omega/\gamma_L]} \quad , \tag{4.74}$$

where we have used the fact that [cf. Eqs. (4.71) and (4.33)]:

$$\begin{aligned}\bar{x}_{n0} &= \bar{x}_n - \bar{Z}\sum_{l=1}^{N}\sum_{p=1}^{l}\Delta_{np} \\ &= \bar{x}_n - \bar{Z}\sum_{l=1}^{N}(N+1-l)\,\Delta_{np}\ .\end{aligned} \tag{4.75}$$

In equation (4.73), which is the simplest expression with a higher-order correction to W-K(LV), the term in the brace is the correction term. Notice that in the expression (4.73), Δ_{nl}' in $C_n = D_1$ (or D_l) is not neglected. It is just for formal comparison with the result from W-K(LV) [cf. Eq. (4.36)]. To be more consistent, we have to neglect Δ_{nl}' in C_n (or D_l) as well. In that case, $D_l = 1$ for all l, which can be seen easily from (A4.27), and thus $C_n = 1$. In view of numerical calculations, however, it does not make any difference since the Gaussian term, $e^{-\overline{\Delta x}^2 c_n^2 \Omega^2/2}$, can be neglected for a sufficiently small $\overline{\Delta x}$ [see below].

Up to now, we have discussed several different levels of approximations in the wave-kinetic numerical method, i. e., W-K(LV), W-K(I), W-K(II), and W-K(III). The corresponding expressions for irradiance or irradiance spectrum are given respectively by (4.36) [or (4.34)], (4.73) [or (4.74)], (4.68) [or (4.71)], and (4.62) [or (4.66)]. The validity of those approximations will be discussed in Sec. 4.4.2. In numerical calculations, we compute only the scattered part of the spectrum as in the phase-screen problem [cf. Eq. (3.71)], i. e.,

$$\begin{aligned}\tilde{I}_{Ls}(\Omega) &= F\{I_L(\bar{x}) - 1\} \\ &= \tilde{I}_L(\Omega) - \frac{\overline{\Delta x}}{2\pi}\sum_n e^{-i\bar{x}_{n0}\Omega}\, e^{-\overline{\Delta x}^2\Omega^2/2}\ ,\end{aligned} \tag{4.76}$$

where F represents the Fourier transform operation defined by (4.35). Finally, we note the following. Since $\Omega_{max} \sim \gamma$, $|C_n| \sim 1$, and $|\Omega + g_n(\Omega)| \sim |C_n\Omega| \lesssim \gamma$, the Gaussian terms, $e^{-\overline{\Delta x}^2\Omega^2/2}$, $e^{-\overline{\Delta x}^2 c_n^2\Omega^2/2}$ and $e^{-\overline{\Delta x}^2[\Omega + g_n(\Omega)]^2/2}$, in the various different ex-

pressions given above can be neglected for a sufficiently small $\overline{\Delta x}$ ($\ll 1/\gamma$), as in the phase-screen problem.

4.3 Huygens-Fresnel Diffraction Formula

Consider the simplified model for an extended medium, which represents an extended medium by N layers of Gaussian eddies as shown in Fig. 4.2. The idea for a single-layer problem in Sec. 3.3 can be easily extended to a multiple-layer problem. Let us denote the electric field at $\bar{z} = \bar{z}_l^-$ by $u_{l-1}(\bar{x})$, where $\bar{z}_l = (l-1)\bar{Z}$. It follows then that $u_l(\bar{x})$ represents the field behind the l-th layer, and $u_N(\bar{x})$ is the field in the observation plane, $\bar{z} = \bar{L}$. Applying the result from the single-layer problem to each layer repeatedly, we obtain

$$u_l(\bar{x}) = \int_{-\infty}^{\infty} dq \; e^{iq\bar{x}} \, e^{-iq^2/2\gamma_L} \, \hat{U}_{l-1}(q) \;, \quad (l = 1, 2, \ldots, N) \;, \tag{4.77}$$

with

$$\hat{U}_{l-1}(q) = \frac{1}{2\pi} \int_{-\infty}^{\infty} d\bar{x} \; e^{-iq\bar{x}} \left[u_{l-1}(\bar{x}) \, e^{i\phi_l(\bar{x})} \right] \;, \tag{4.78}$$

where $u_0(\bar{x}) = 1$, $\gamma_L = \bar{k}/\bar{Z} = k\ell^2/Z$, and $\phi_l(\bar{x})$ is given by (4.9). We may represent this symbolically as:

$$\begin{aligned} &u_0(\bar{x}) = 1 \\ &u_l(\bar{x}) = F_q^{-1}\left\{ e^{-iq^2/2\gamma_L} \; F_x\left[u_{l-1}(\bar{x}) \, e^{i\phi_l(\bar{x})} \right] \right\} \;, \quad (l = 1, 2, \ldots, N) \;, \end{aligned} \tag{4.79}$$

which indicates that two Fourier transform operations are required for each layer. From (3.83) and (3.82), we have

$$u_{nl} = \frac{1}{N} \sum_{m=1}^{N_{FFT}} e^{2\pi i (m-1)(n-1)/N_{FFT}} e^{-i(\Delta q)^2 M^2/2\gamma_L} \hat{U}_{m,l-1} \ , \tag{4.80}$$

with

$$\hat{U}_{m,l-1} = \sum_{k=1}^{N_{FFT}} e^{-2\pi i (m-1)(k-1)/N_{FFT}} u_{k,l-1} e^{i\phi_{kl}} \ , \tag{4.81}$$

where $u_{nl} = u_l(\bar{x} = \bar{x}_n)$, $\phi_{kl} = \phi_k(\bar{x} = \bar{x}_k)$, $\bar{x}_n = (n - 1 - N_{FFT}/2)\overline{\Delta x}$, and $\Delta q = 2\pi/N_{FFT}\overline{\Delta x}$. The expression for M is given by (3.84). Now, an existing algorithm can be applied directly to (4.80) and (4.81).

As we mentioned briefly in Chap. 1, the expression (4.79) is equivalent to the *split-step-Fourier* algorithm applied directly to the parabolic wave equation (2.8) (with the simplified model for δn) [90, 91]. The resulting expression from the *split-step-Fourier* algorithm is given by [cf. Appendix A4.3]:

$$F_x\{u(\bar{x},\ \bar{z} + \overline{\Delta z})\} = e^{-iq^2\overline{\Delta z}/2\bar{k}} \ F_x\left\{u(\bar{x},\ \bar{z})\, e^{i\bar{k}\,\delta n(\bar{x},\ \bar{z})\,\overline{\Delta z}}\right\} \ , \tag{4.82}$$

which is valid for $\overline{\Delta z} \ll 1$ due to the approximate integration involved in (A4.38), i. e.,

$$\begin{aligned} J &\equiv \bar{k} \int_{\bar{z}}^{\bar{z}+\overline{\Delta z}} d\bar{z}'\ \delta n(\bar{x},\ \bar{z}') \\ &\simeq \bar{k}\ \delta n(\bar{x},\ \bar{z})\,\overline{\Delta z} \ . \end{aligned} \tag{4.83}$$

In principle, this algorithm may be applied to the general model for $\delta n(\bar{x},\ \bar{z})$ [cf. Eq. (4.1)], but it would take excessively large amount of computing, since $\overline{\Delta z} \ll 1$ and the *two-dimensional* function $\delta n(\bar{x},\ \bar{z})$ has to be computed. On the other hand, in the

expression (4.79) the interval $\bar{Z}$ can be made relatively large (since we use the analytical expression for the integral J, i. e., $\phi_l(\bar{x})$ [cf. Eq. (4.8) or discussions given below]), and the random phase $\phi_l(\bar{x})$ is a *one-dimensional* function. [Numerical results in Sec. 4.4.3 indicate that $\bar{z} \simeq 80 \gg 1$ for the given values of the extended-medium parameters.] Now, if we use the simplified model for $\delta n(\bar{x}, \bar{z})$ [cf. Eq. (4.4) or (4.7)] in (4.83) or (A4.38) with the corresponding notational changes, i. e., $\overline{\Delta z} \to \bar{Z}$, $\bar{z}_l \to \bar{z}_l = (l-1)\bar{Z}$, and $\delta n(\bar{x}, \bar{z}') \to \delta n_l(\bar{x}, \bar{z}')$, then the integral J can be calculated analytically (i. e., $J = \phi_l(\bar{x})$ [cf. Eq. (4.9)]), and (4.82) becomes

$$F_x\{u(\bar{x}, \bar{z}_{l+1})\} = e^{-iq^2/2\gamma_L} \; F_x\left\{u(\bar{x}, \bar{z}_l)\, e^{i\phi_l(\bar{x})}\right\} , \tag{4.84}$$

which is the same as (4.79) where $u_l(\bar{x}) = u(\bar{x}, \bar{z}_{l+1})$.

4.4 Numerical Simulation

Some important input parameters for numerical simulation are discussed briefly in Sec. 4.4.1. The implementations of the wave-kinetic numerical method and the Huygens-Fresnel diffraction formula are studied by single-realization calculations, in Sec. 3.6.2. The validity of the various different levels of approximations involved in the wave-kinetic numerical method, i. e., W-K(LV), W-K(I), W-K(II), and W-K(III), is also discussed, by comparing the results for single realizations with those from the Huygens-Fresnel dffraction formula (which will be simply referred to as H-F in what follows). (Here we assume that results from H-F are accurate enough for a sufficiently small $\bar{Z}$ [cf. Sec. 3.6.2].) Finally in Sec. 3.6.3, we present simulation results for σ_l^2 and $c_l(\bar{x})$ from W-K(I) and H-F.

4.4.1 Important Input Parameters for Numerical Simulation

As in the phase-screen problem, let us denote the width of an extended medium and the region occupied by receivers, respectively, by $\overline{W}$ and $\overline{W}_s$. Similar edge effects occur in this case, and from the result in Sec. 3.6.1 we have the criterion for the margin of the screen width:

$$\overline{W} - \overline{W}_s \gtrsim 5\sqrt{2}\,\zeta \ . \tag{4.85}$$

In our numerical simulation, we put 11 receivers separated by approximately $0.1\,\ell$ so that $\overline{W}_s \simeq 1.0$, and $\overline{W}$ must be chosen by the above criterion. It follows that regarding an extended medium we have five important parameters: $\bar{k}$ (which is actually fixed as 1.0472×10^5), γ (or $\overline{L}$), ϕ_0, $\overline{W}$ and N_L [cf. Sec. 4.1]. (Note that the parameter ζ is determined by $\zeta = 2\phi_0/\gamma$, once ϕ_0 and γ are given.) The parameter N_L represents the number of layers, which is denoted simply by N in the preceding. For a given $\overline{L}$, N_L must be large enough so that the numerical results converge to certain values. For this, we perform a convergence test for given values of the parameters $\bar{k}$, γ, ϕ_0 (and $\overline{W}$).

For parameters related to the implementation of the methods for wave-propagation calculation, the same notations as in the phase-screen problem will be used, i. e., $\overline{\Delta x}$, Δf ($= \Delta q/2\pi$ or $\Delta\Omega/2\pi$), $\overline{\Delta p}$, N_r, N_{FFT} and N_l. The parameters N_r, N_{FFT} and N_l represent the number of rays (in the wave-kinetic numerical method), the number of sampling points for a FFT, and the number of realizations, respectively. The parameter Δf denotes the sampling interval in the spatial frequency domain for a FFT, and $\overline{\Delta x}$ stands for the ray spacing in the wave-kinetic numerical method, or the sampling interval for a FFT in the Huygens-Fresnel formula (i. e., $\overline{\Delta x} = 1/N_{FFT}\Delta f$) [cf. Sec. 3.6.1]. Finally, the parameter $\overline{\Delta p}$ represents the interval of discrete data points (ϕ_k or Δ_k) for the linear interpolation scheme used for the wave-kinetic numerical method [cf. Sec.

3.6.1]. The criteria for choosing the values of the parameters are discussed in detail in Secs. 3.6.1 and 3.6.2.

4.4.2 Single-Realization Calculations

In this section, we first discuss the implementation of the methods for wave-propagation calculation, briefly. Next, the results from the several different levels of approximations in the wave-kinetic numerical method are compared with those from H-F. The region of validity of W-K(LV), W-K(I), W-K(II) and W-K(III) is also discussed. The expressions used for numerical calculations are as follows: (4.34), (4.74), (4.71) and (4.66), respectively for W-K(LV), W-K(I), W-K(II) and W-K(III); (4.80) and (4.81) for H-F. [Notice that for W-K(I), (II) and (III) the corresponding expressions are actually used together with (4.76) as mentioned in Sec. (4.4.4).]

The values of the extended-medium parameters in this section are: $\bar{L} = 2560\,\pi$ (or $\gamma = 13.021$ with $\bar{k} = 1.0472\times10^5$), $1.0 \le \phi_0 \le 10.0$, $\overline{W} = 5.0$, and $N_L = 100$. To determine the value of N_L, we have performed a convergence test. For the given values of the extended-medium parameters, $N_L = 100$ seems to be large enough [cf. Fig. 4.3]. In single-realization calculations, we compute $I_L(\bar{x})$ for $|\bar{x}| \le \overline{W}_{eff}/2$ (where $\overline{W}_{eff} > \overline{W}$ is such that $I_{Ls}(\bar{x}) \equiv I_L(\bar{x}) - 1.0 = 0$ for $|\bar{x}| > \overline{W}_{eff}/2$) to see all the scattering effects from an extended medium with width $\overline{W}$, and thus we need $\Delta f \lesssim 1/\overline{W}_{eff}$ to avoid the *aliasing effects* for an inverse FFT, as in the phase-screen problem. Numerical results indicate that for the above values of the parameters, $\overline{W}_{eff} \lesssim 8.0$ [cf. Figs. 4.5 - 4.9]. Allowing for some margin, we let $\overline{W}_{eff} = 10.0$ (but the irradiance data $I_L(\bar{x})$ are plotted only for $|\bar{x}| \le 4.0$), and thus we choose $\Delta f \simeq 1.0$ in our numerical calculations.

The values of the parameters for wave-propagation calculations are the following. We choose $(\overline{\Delta x})_{WK} = 0.04$ and $(\overline{\Delta x})_{HF} = 0.08$ for W-K(I), (II), (III) and H-F, respectively. For W-K(LV), we set $\overline{\Delta x} = 0.005$. The reasons for choosing different values of $\overline{\Delta x}$ are

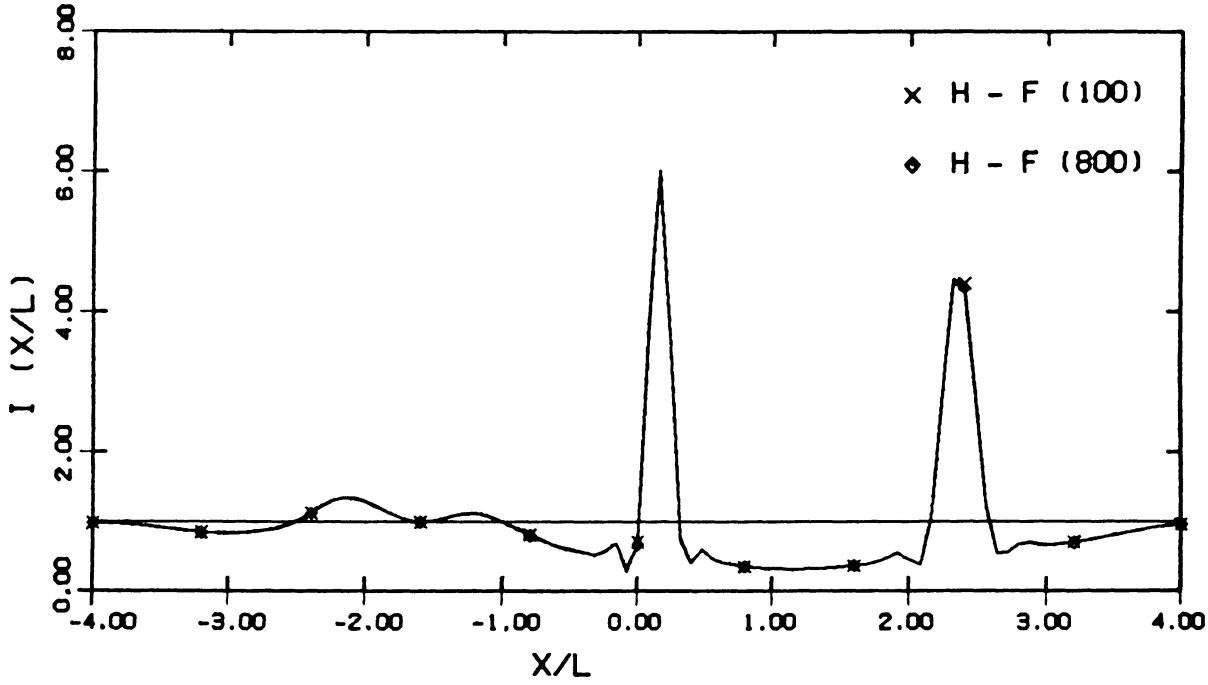

Figure 4.3 Convergence test for the layer thickness. Instantaneous irradiance profile: $\gamma = 13.0$, $\phi_0^2 = 5.0$ ($\zeta = 0.768$); H-F.

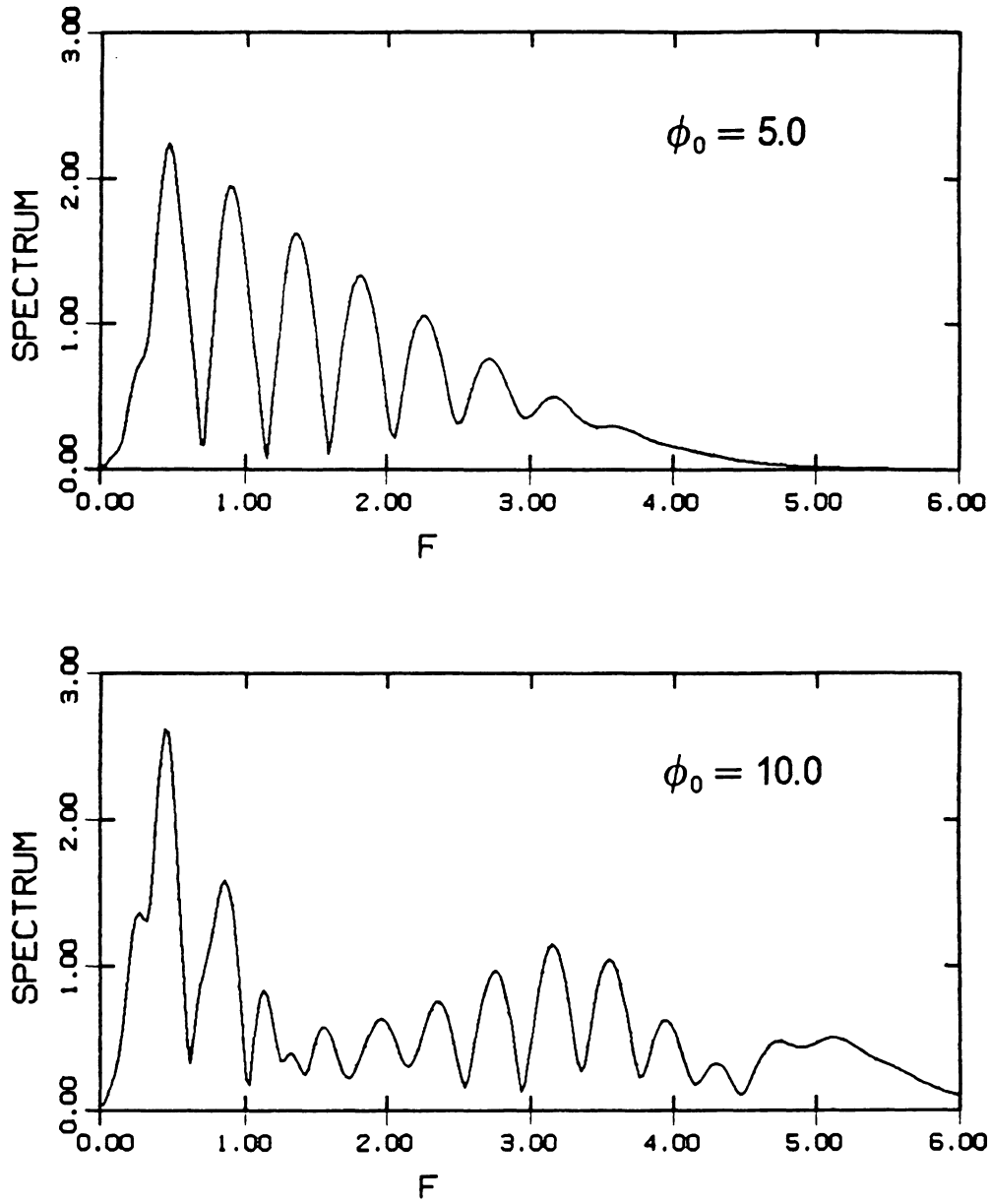

Figure 4.4 Spectrum of irradiance for a specific realization: H-F ($f = q/2\pi$).

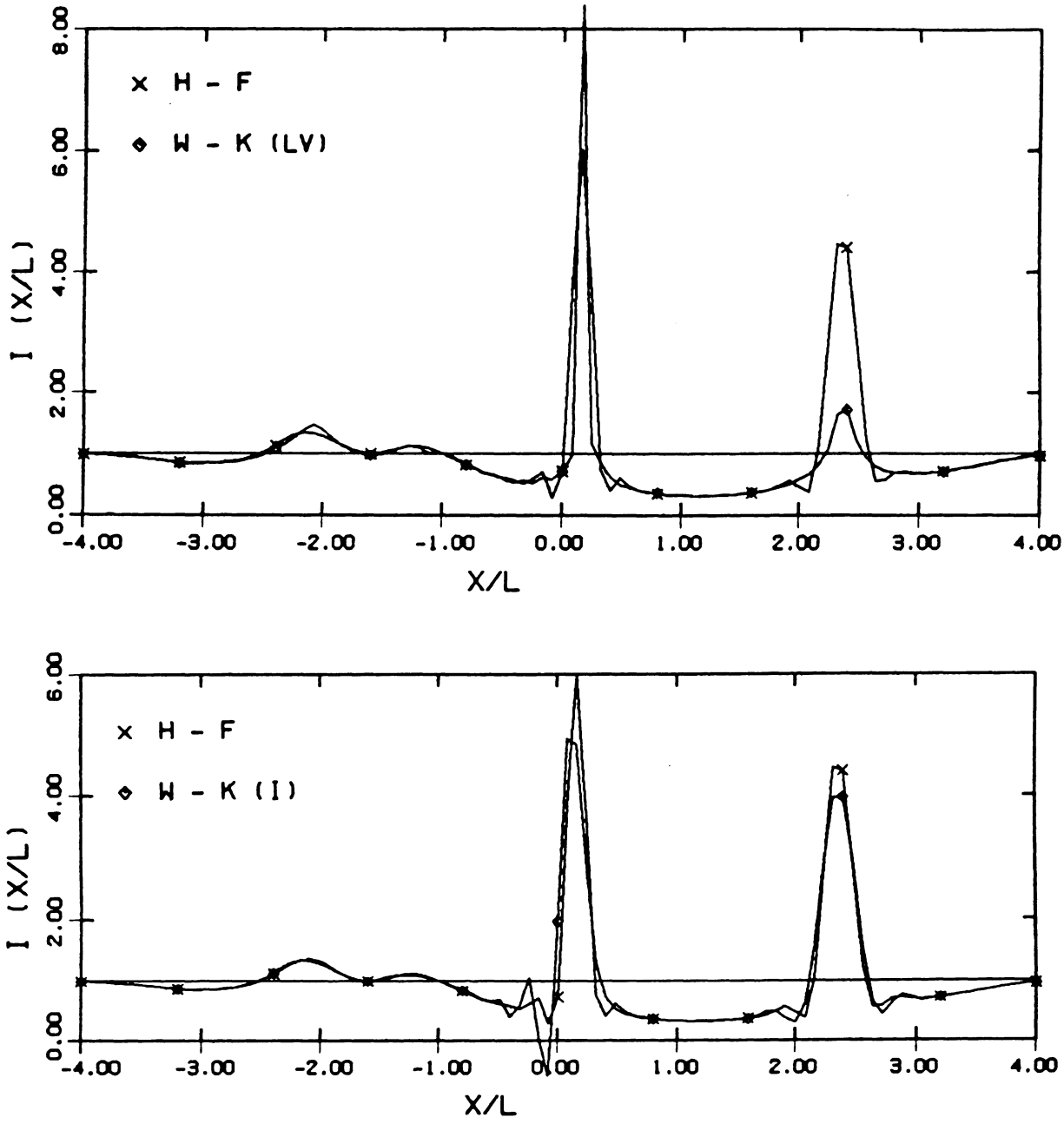

Figure 4.5 Instantaneous realization of irradiance at $z/\ell = 2560\,\pi$ ($\gamma = 13.0$) : $\phi_0 =$ 5.0 ($\zeta = 0.768$) ; W-K(LV), W-K(I), W-K(II), W-K(III) and H-F.

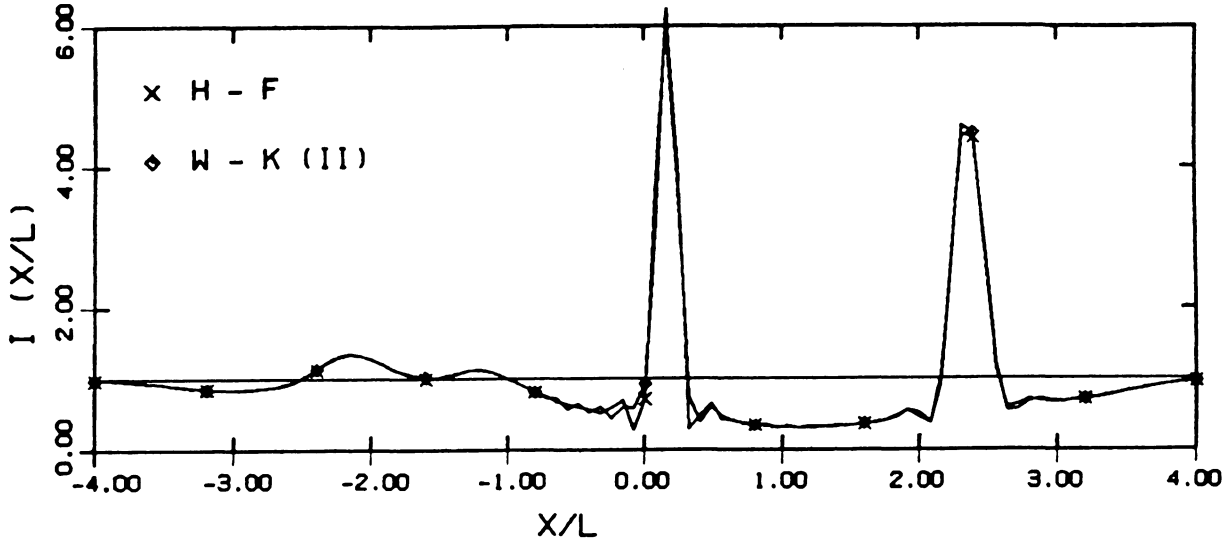
x H - F
◇ W - K (II)
I (X/L)
X/L
0.00
2.00
4.00
6.00
-4.00
-3.00
-2.00
-1.00
0.00
1.00
2.00
3.00
4.00

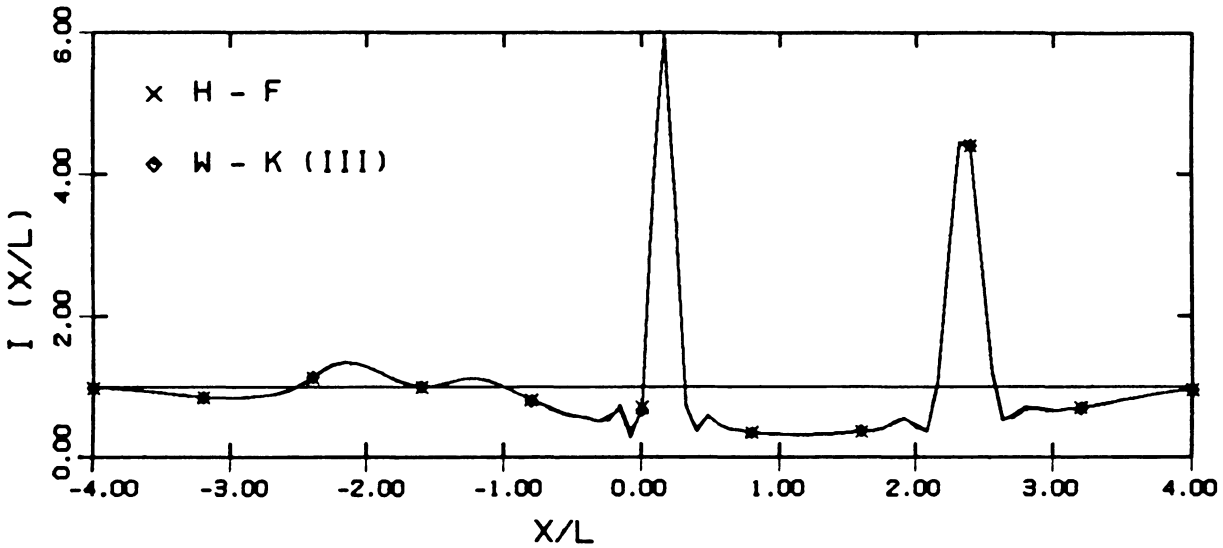
x H - F
◇ W - K (III)
I (X/L)
X/L
0.00
2.00
4.00
6.00
-4.00
-3.00
-2.00
-1.00
0.00
1.00
2.00
3.00
4.00

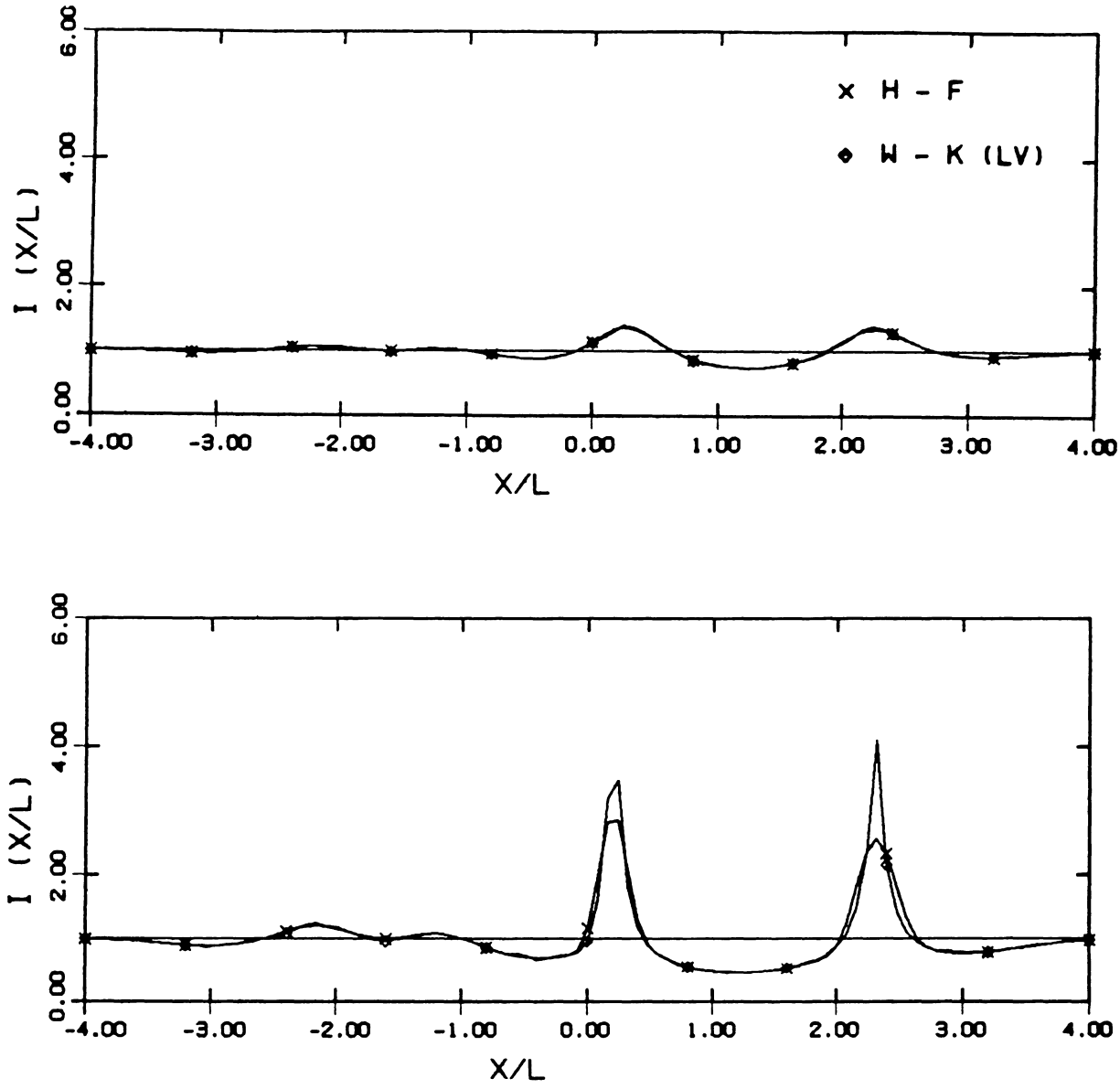

Figure 4.6 Instantaneous realization of irradiance at $z/\ell = 2560\,\pi$ ($\gamma = 13.0$) : $\phi_0 =$ 1.0 ($\zeta = 0.154$) (top), $\phi_0 = 2.0$ ($\zeta = 0.307$) (bottom); W-K(LV) and H-F.

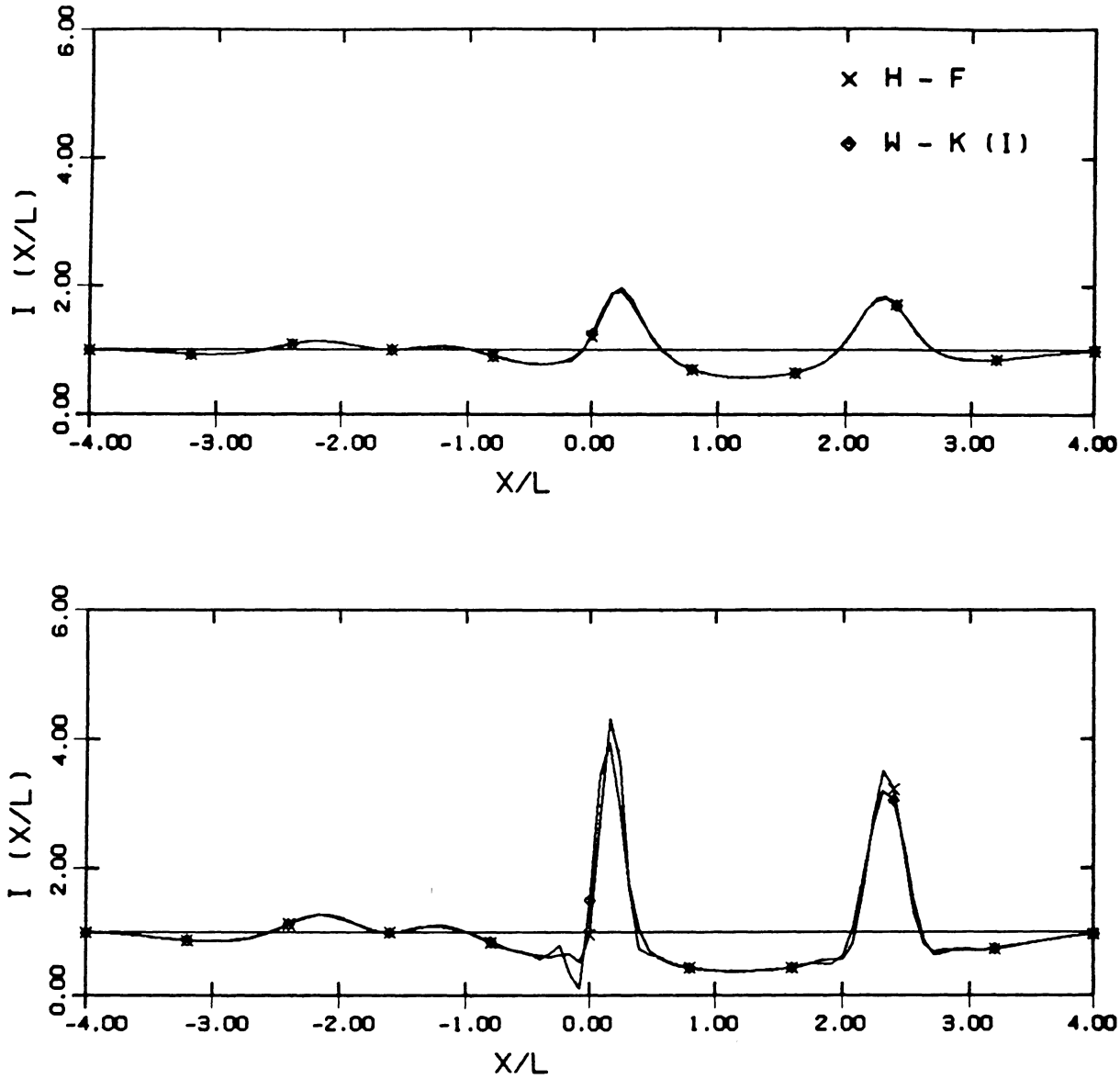

Figure 4.7 Instantaneous realization of irradiance at $z/\ell = 2560\,\pi$ ($\gamma = 13.0$) : $\phi_0 =$ 2.0 ($\zeta = 0.307$) (top), $\phi_0 = 4.0$ ($\zeta = 0.614$) (bottom); W-K(I) and H-F.

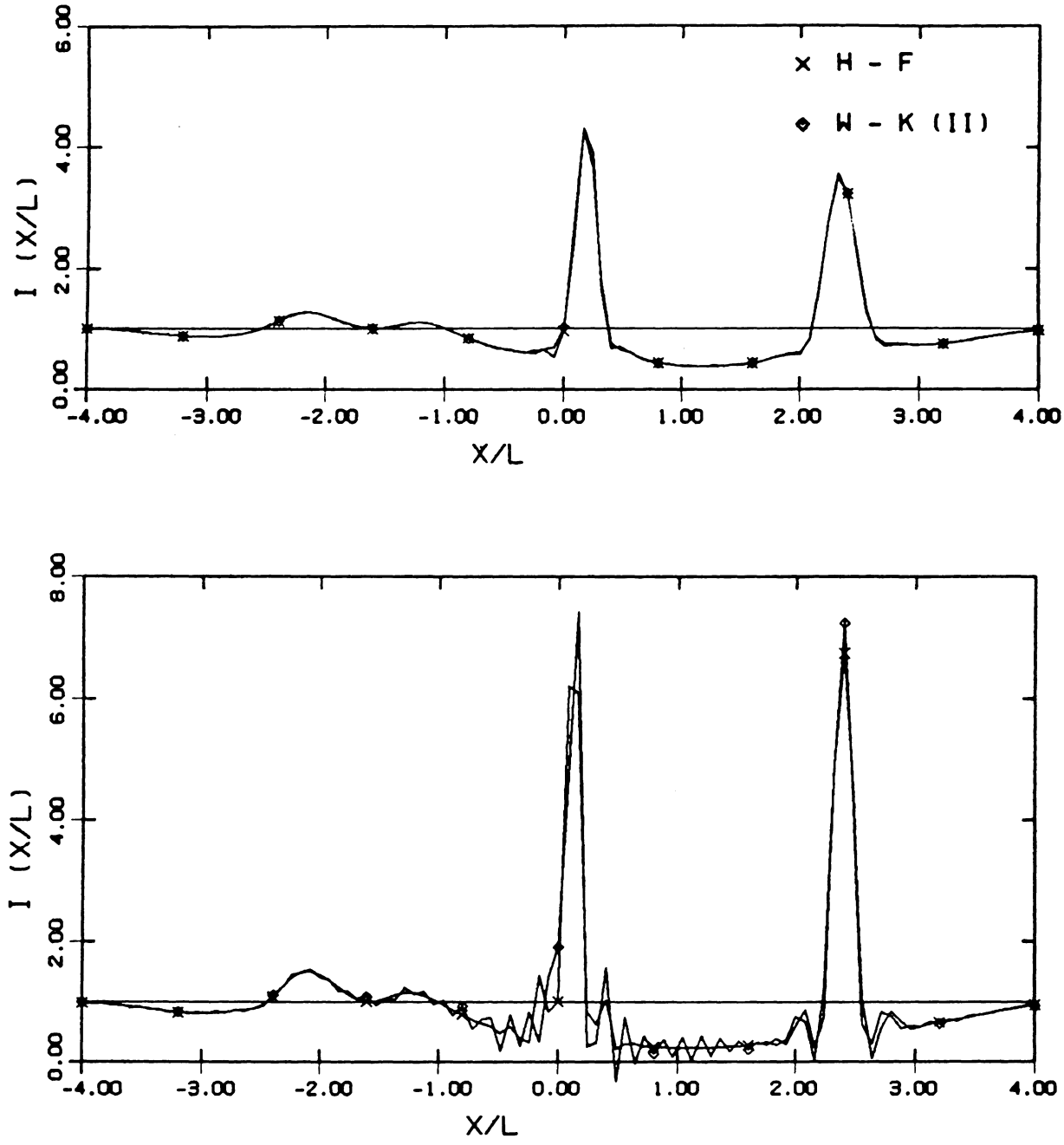

Figure 4.8 Instantaneous realization of irradiance at $z/\ell = 2560\,\pi$ ($\gamma = 13.0$) : $\phi_0 =$ 4.0 ($\zeta = 0.614$) (top), $\phi_0 = 7.0$ ($\zeta = 1.075$) (bottom); W-K(II) and H-F.

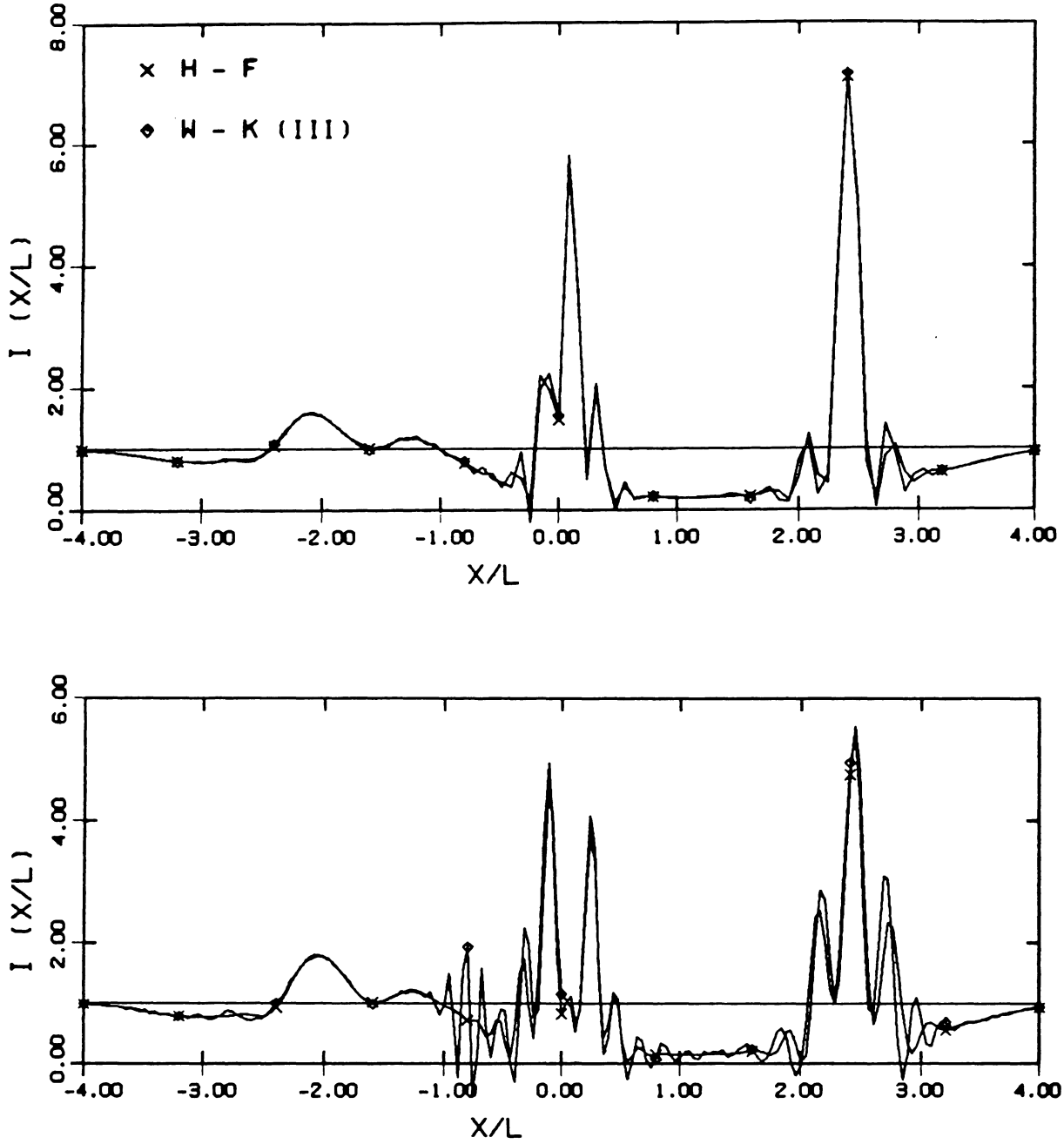

Figure 4.9 Instantaneous realization of irradiance at $z/\ell = 2560\,\pi$ ($\gamma = 13.0$) : $\phi_0 =$ 8.0 ($\zeta = 1.229$) (top), $\phi_0 = 10.0$ ($\zeta = 1.536$) (bottom); W-K(III) and H-F.

discussed in Secs. 3.6.1 and 3.6.2. The interpolation interval $\overline{\Delta p}$ is chosen as 0.08. For W-K(I), (II), (III) and H-F, we choose $N_{FFT} = 128$ and $\Delta f = 0.09766$ [$= 1/(0.08\times128)$], where N_{FFT} is chosen such that $N_{FFT} \simeq \overline{W}_{eff}/\overline{\Delta x}$ with $\overline{W}_{eff} = 10.0$. For the given $\overline{\Delta x}$ and $\overline{W}_{eff}$, the number of rays [for W-K(LV), W-K(I), (II), (III)] is determined by $N_r \simeq \overline{W}_{eff}/\overline{\Delta x}$. The irradiance spectra $\tilde{I}_L(f)$ for $\phi_0 = 5.0$ and 10.0 are plotted in Fig. 4.4. The entire spectral content of $\tilde{I}_L(f)$ is contained well within $f \lesssim f_{max,I} = N_{FFT}\times\Delta f/2 = 6.25$, which indicates that the N_{FFT} for W-K is large enough for the given Δf . It also indicates that $(\overline{\Delta x})_{HF} = 0.08$ is small enough for H-F, since $1/2f_{max,\,U} \simeq 1/f_{max,I} \gtrsim 0.16$.

The irradiance data for $\phi_0 = 5.0$ from W-K(LV), W-K(I), (II), (III), together with those from H-F, are plotted in Fig. 4.5, which shows the errors involved in the different levels of approximations in the wave-kinetic numerical method. We note that errors (i. e., extra peaks) occur in the place where irradiance peaks appear, as in the phase-screen problems. More detailed numerical calculations [cf. Fig. 4.6 - 4.9] indicate that W-K(LV), (I), (II) and (III) are valid for $\zeta \lesssim 0.2$, 0.5, 0.9, and 1.2, respectively. As we mentioned before [cf. Secs. 3.1 and 4.2.2], W-K(III) is sufficient for our purpose, since we are interested in the random focusing region ($0.5 \lesssim \zeta \lesssim 1.0$), where wave statistics are not well understood. Note that wave statistics in the two limiting cases, i. e., in the weak-fluctuation region ($\zeta \ll 1$, $\sigma_I^2 \ll 1$) and the saturation region ($\zeta \gg 1$, $\sigma_I^2 \simeq 1$) are reasonably well understood.

Finally, we wish to mention computing times, briefly. In the array processor FPS 164, the CPU times for the data in Figs. 4.5 - 4.9 from W-K(I), (II), (III), and H-F are 49.57, 59.05, 66.31, and 35.59 *secs*, respectively. Notice that for $N_{FFT} = 256$ (with $\Delta f = 0.09766$), the corresponding CPU times are 59.19, 69.68, 91.84, and 70.56, respectively. The data indicate that computing times are comparable.

4.4.3 Computation of Statistics from Many Realizations

In this section, the normalized variance of irradiance σ_I^2 and the normalized covariance of irradiance $c_I(\bar{x})$ (which are defined in Sec. 3.4) are computed by numerical simulation. For wave-propagation calculations, W-K(I) and H-F are used, and the simulation results are compared to each other. The values of the extended-medium parameters are $\gamma = 13.856$, $\phi_0^2 = 1.0,\ 5.0$ ($\zeta = 0.144,\ 0.323$), $\overline{W} = 5.0$, and $N_L = 100$. The values of the parameters for wave-propagation calculations are the same as in the previous section.

Irradiance fluctuations for $\phi_0^2 = 5.0$ at three receivers separated by 0.08 (ℓ) are plotted in Fig. 4.10, and their enlarged versions are shown in Fig. 4.11. Some correlations among the three data sets are observed. Let us define outliers as before, i. e., $I \geq I_{out} = < I > + 7\,\sigma_I$ with $< I > = 1.0$. Since σ_I^2 is unknown in this case, we may use $\hat{\sigma}_I^2$ obtained from numerical simulation. If we use $\hat{\sigma}_I^2$ from W-K(I), i. e., $\hat{\sigma}_I^2 = 0.128$ ($\hat{\sigma}_I \simeq 0.358$) [cf. Fig. 4.13], then $I_{out} = 3.5$. The irradiance data in Fig. 4.10 indicate that there appear outliers, but they are *mild* outliers (i. e., not excessively larger than I_{out}) [cf. discussions in Sec. 3.6.3].

The simulation results for $\phi_0^2 = 1.0$ and 5.0 (obtained without removing outliers) are shown in Fig. 4.12 and Fig. 4.13, respectively. The number of realizations are 1500 for both cases. The results from W-K(I) and H-F are in good agreement, which confirms the region of validity of W-K(I) ($\zeta \lesssim 0.5$). The scintillation index from W-K(I) and H-F are fairly close to each other: for $\phi_0^2 = 1.0$, $\hat{\sigma}_I^2 = 0.0213$ and 0.0215, respectively; for $\phi_0^2 = 5.0$, $\hat{\sigma}_I^2 = 0.128$ and 0.123, respectively. The standard error of $\hat{\sigma}_I^2$ is given by $S_\varepsilon(\hat{\sigma}_I^2) = \sigma_I^2\sqrt{2/N_I}$ [cf. Eq. (3.98)]. Since σ_I^2 is unknown, we may use $\hat{\sigma}_I^2$, instead, i. e., $S_\varepsilon(\hat{\sigma}_I^2) \simeq \hat{\sigma}_I^2\sqrt{2/N_I}$. For $N_I = 1500$, $S_\varepsilon(\hat{\sigma}_I^2)$ is approximately 3.7 % of the corresponding values of $\hat{\sigma}_I^2$.

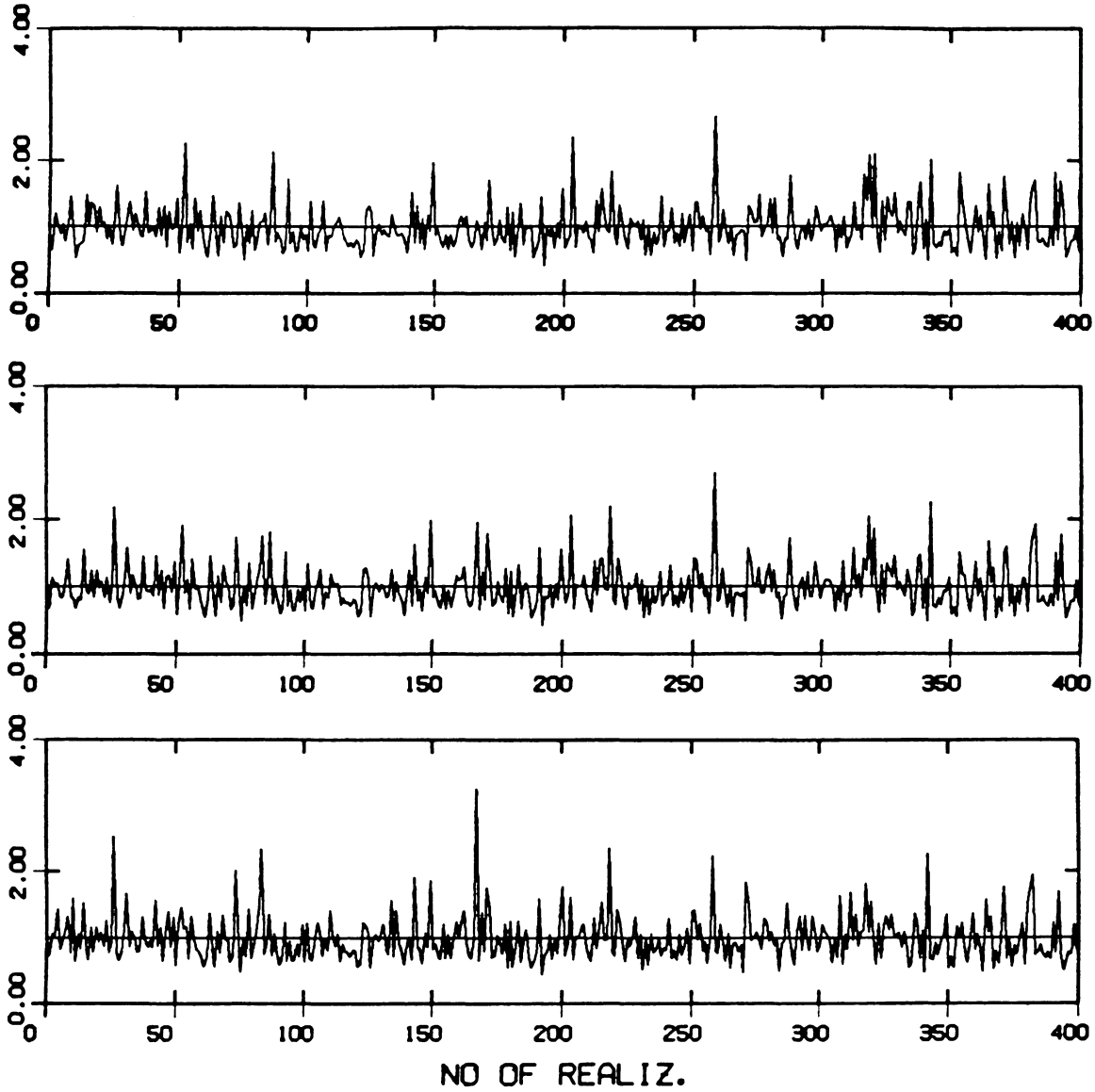

Figure 4.10 Irradiance fluctuations at 3 receivers separated by 0.08ℓ : $\gamma = 13.856$, $\phi_0^2 = 5.0$ ($\zeta = 0.323$); W-K(I).

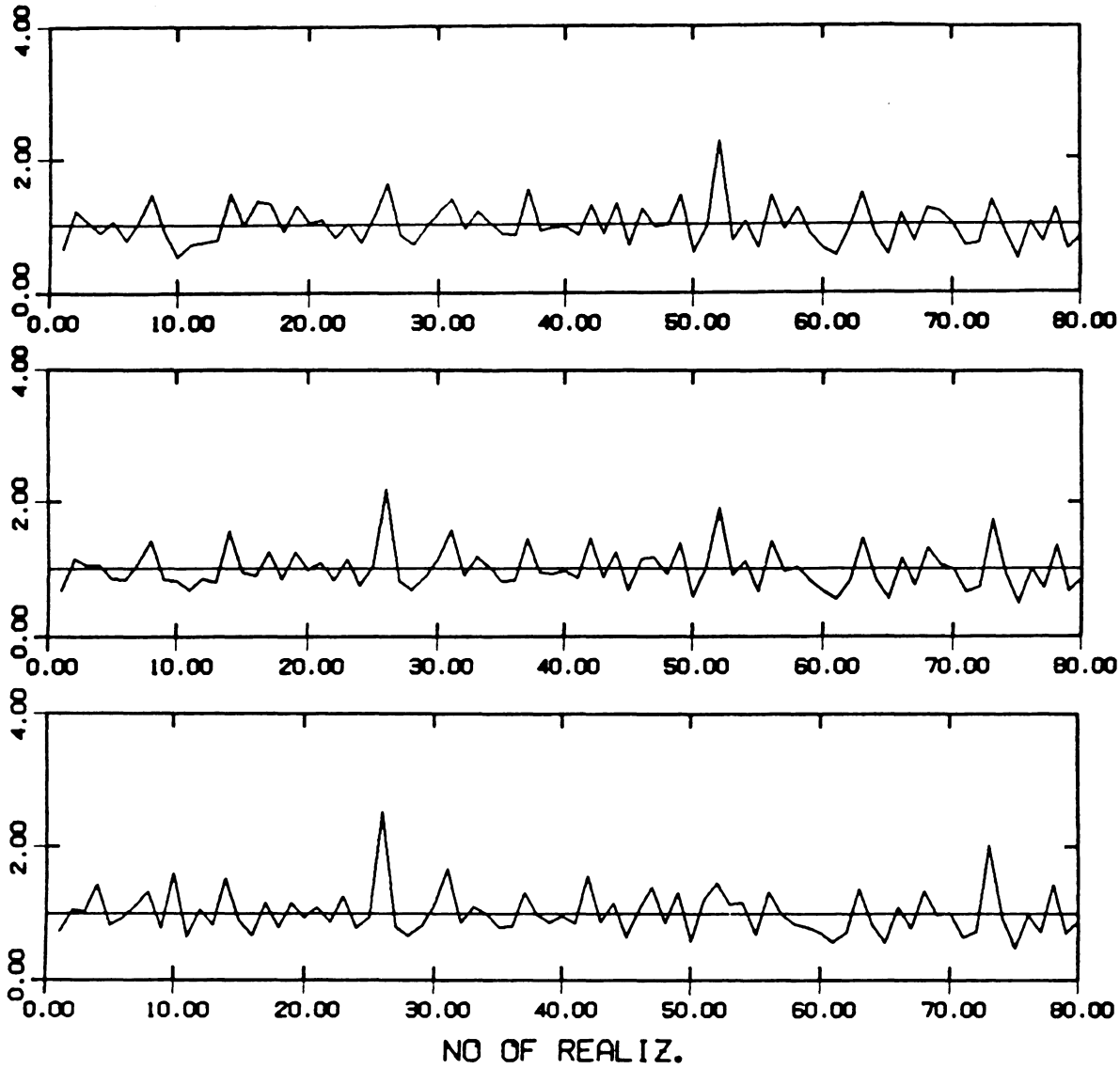

Figure 4.11 Enlarged version of Figure 4.10.

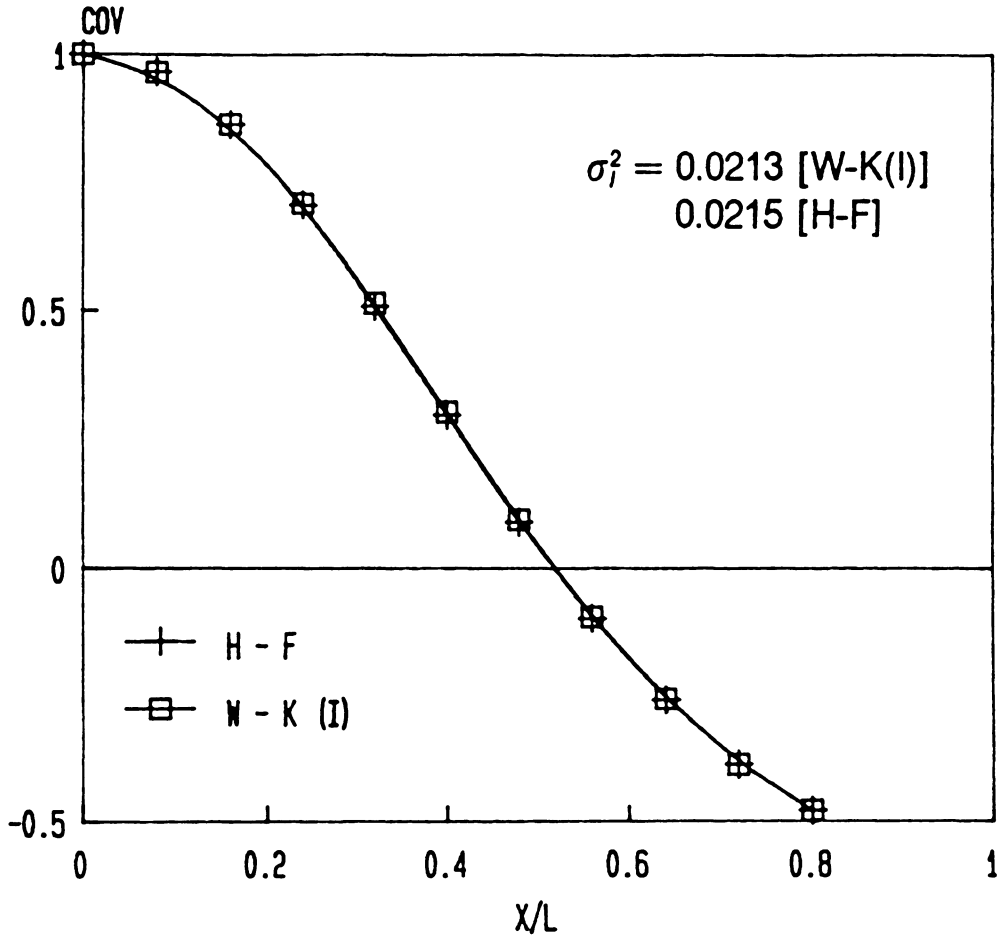

Figure 4.12 Normalized covariance of irradiance vs receiver separation: $\gamma = 13.856$, $\phi_0^2 = 1.0$ ($\zeta = 0.144$); W-K(I) and H-F.

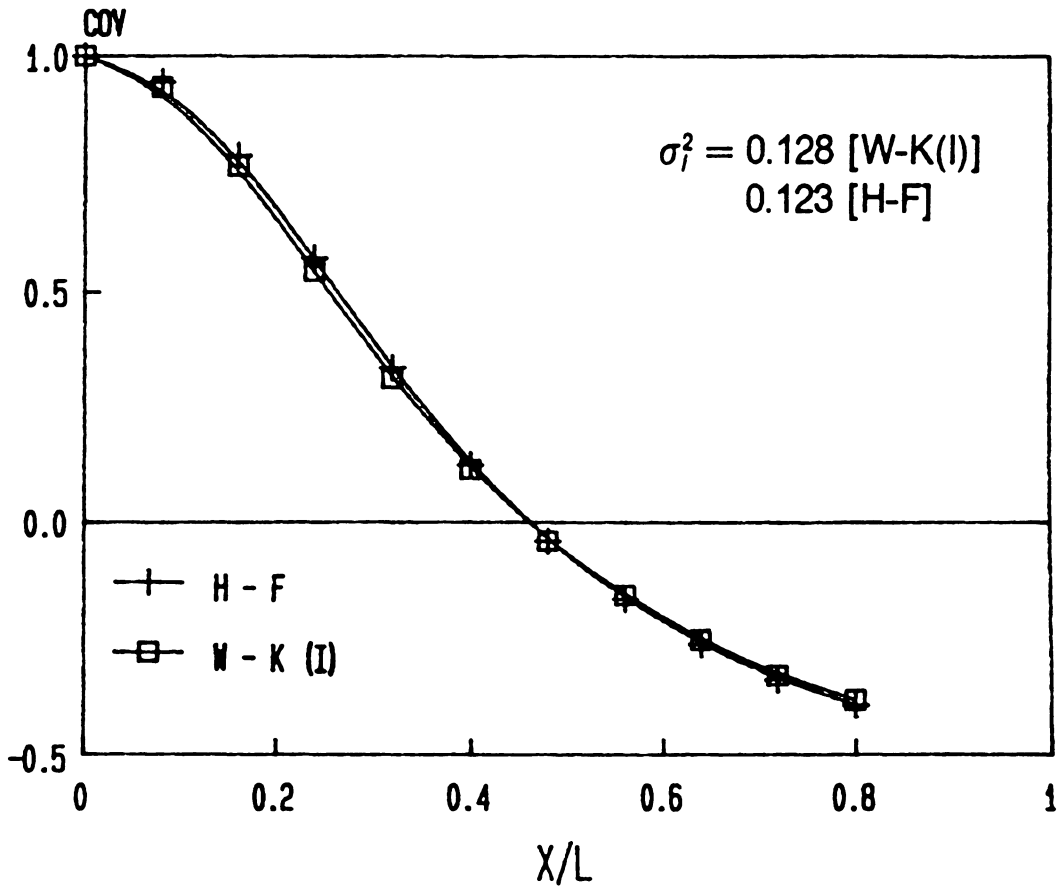

Figure 4.13 Normalized covariance of irradiance vs receiver separation: $\gamma = 13.856$, $\phi_0^2 = 5.0$ ($\zeta = 0.323$); W-K(I) and H-F.

Appendix A4.1 Higher-Order Approximation: W-K(III)

When the number of layers becomes large (say, $N \geq 5$), the resulting expressions for $I_L(\bar{x})$ or $\bar{F}_L(\bar{x},\ \theta)$ can not be manipulated easily. Thus, we first calculate $I_L(\bar{x})$ for three layers, and then generalize the result to N layers.

For convenience, we introduce $\hat{h}_{nl}$ and $\hat{h}_{nl}'$ such that

$$\hat{h}_{nl}(\bar{s}) = h_{nl}(\bar{s})/\bar{k}\ ,\ \hat{h}_{nl}'(\bar{s}) = h_{nl}'(\bar{s})/\bar{k}\ , \tag{A4.1}$$

where

$$h_{nl}(\bar{s}) = h_l(\bar{x} = \bar{x}_{n,l-1},\ \bar{s})\ ,\quad h_{nl}'(\bar{s}) = \frac{\partial}{\partial \bar{x}}\, h_l(\bar{x},\ \bar{s})\big|_{\bar{x}=\bar{x}_{n,l-1}}\ , \tag{A4.2}$$

and $h_l(\bar{x},\ \bar{s})$ is defined by (4.44) [or (4.43)]. From Eqs. (4.60), (4.58) and (4.52) in the text, we have for the second layer [i. e., at $\bar{z} = \bar{z}_3^- = (2\bar{Z})^-$]:

$$\begin{aligned}
\bar{F}_2(\bar{x}_2,\ \theta_2) = \frac{1}{2\pi}\frac{\bar{k}}{2\pi}\sum_n \int_{-\infty}^{\infty} d\bar{s}_1\ e^{i\bar{k}\hat{h}_{n2}(\bar{s}_1)} \int_{-\infty}^{\infty} d\bar{s}_0\ e^{i\bar{k}\hat{h}_{n1}(\bar{s}_0)} \\
\times\ e^{-i\bar{k}\left\{\bar{s}_1\,\delta\theta_2 - [\Delta_{n2}'\bar{s}_1 + \hat{h}_{n2}'(\bar{s}_1)][(\overline{\delta x}_2 - \bar{Z}\,\delta\theta_2)\right\}} \\
\times \int_{-\infty}^{\infty} d\theta_1\ e^{i\bar{k}\bar{s}_1\delta\theta_1}\, e^{-i\bar{k}\left\{\bar{s}_0\,\delta\theta_1 - [\Delta_{n1}'\bar{s}_0 + \hat{h}_{n1}'(\bar{s}_0)][(\overline{\delta x}_2 - \bar{Z}\,\delta\theta_2) - \bar{Z}\,\delta\theta_1]\right\}} \\
\times\ G[(\overline{\delta x}_2 - \bar{Z}\,\delta\theta_2) - \bar{Z}\,\delta\theta_1]\ ,
\end{aligned} \tag{A4.3}$$

where Δ_{nl}' is given by (4.24) and $\overline{\delta x}_l = \bar{x}_l - \bar{x}_{nl}$, $\delta\theta_l = \theta_l - \theta_{nl}$ [for $\bar{x}_{nl}$ and θ_{nl}, see Eq. (4.25)]. Now for the third layer, we can find $\bar{F}_3(\bar{x}_3,\ \theta_3)$ by following exactly the same procedure as for the second layer. The result for $\bar{F}_3(\bar{x}_3,\ \theta_3)$ will not be presented here, since it is too complicated. For simplicity, we use the notations defined by (4.23), i. e.,

$$c_l = -\,\Delta_{nl}'\ ,\quad d_l = 1 + \bar{Z}\,\Delta_{nl}' = 1 + b\,c_l\ ,\quad (b = -\,\bar{Z})\ . \tag{A4.4}$$

Performing wavenumber $(\bar{k}\theta_3)$ integration of $\bar{F}_3(\bar{x}_3,\ \theta_3)$, we obtain

$$
\begin{aligned}
I_L(\bar{x}_3) = \left(\frac{\bar{k}}{2\pi}\right)^3 \sum_n \int_{-\infty}^{\infty} d\bar{s}_2\ e^{i\bar{k}\hat{h}_{n3}(\bar{s}_2)} \int_{-\infty}^{\infty} d\bar{s}_1\ e^{i\bar{k}\hat{h}_{n2}(\bar{s}_1)} \int_{-\infty}^{\infty} d\bar{s}_0\ e^{i\bar{k}\hat{h}_{n1}(\bar{s}_0)} \\
\times\ e^{i\bar{k}\,\overline{\delta x}_3\beta_4} \int_{-\infty}^{\infty} d\theta_3\ e^{-i\bar{k}\,\delta\theta_3\beta_3} \int_{-\infty}^{\infty} d\theta_2\ e^{-i\bar{k}\,\delta\theta_2\beta_2} \int_{-\infty}^{\infty} d\theta_1\ e^{-i\bar{k}\,\delta\theta_1\beta_1} \\
\times\ G[\overline{\delta x}_3 + b\,(\delta\theta_3 + \delta\theta_2 + \delta\theta_1)]\ ,
\end{aligned}
\tag{A4.5}
$$

where the Gaussian function $G(\bar{x})$ is given by (4.47), and

$$
\begin{aligned}
\beta_1(\bar{s}_0,\ \bar{s}_1) &= (d_1\,\bar{s}_0 - \bar{s}_1) - b\,\hat{h}_{n1}'(\bar{s}_0) \\
\beta_2(\bar{s}_0,\ \bar{s}_1,\ \bar{s}_2) &= (b\,c_1\,\bar{s}_0 + d_2\,\bar{s}_1 - \bar{s}_2) - b\,[\hat{h}_{n1}'(\bar{s}_0) + \hat{h}_{n2}'(\bar{s}_1)] \\
\beta_3(\bar{s}_0,\ \bar{s}_1,\ \bar{s}_2) &= (b\,c_1\,\bar{s}_0 + b\,c_2\,\bar{s}_1 + d_3\,\bar{s}_2) - b\,[\hat{h}_{n1}'(\bar{s}_0) + \hat{h}_{n2}'(\bar{s}_1) + \hat{h}_{n3}'(\bar{s}_2)] \\
\beta_4(\bar{s}_0,\ \bar{s}_1,\ \bar{s}_2) &= -(c_1\,\bar{s}_0 + c_2\,\bar{s}_1 + c_3\,\bar{s}_2) + [\hat{h}_{n1}'(\bar{s}_0) + \hat{h}_{n2}'(\bar{s}_1) + \hat{h}_{n3}'(\bar{s}_2)]\ .
\end{aligned}
\tag{A4.6}
$$

Introducing a new integration variable $\xi = -\,b(\delta\theta_3 + \delta\theta_2 + \delta\theta_1)$ for θ_3 and using the fact that $\beta_4 = (\bar{s}_2 - \beta_3)/b$, after a simple manipulation we may rewrite (A4.5) as:

$$
\begin{aligned}
I_L(\bar{x}_3) = \sum_n \int_{-\infty}^{\infty} d\bar{s}_2\ e^{i\bar{k}\hat{h}_{n3}(\bar{s}_2)} \int_{-\infty}^{\infty} d\bar{s}_1\ e^{i\bar{k}\hat{h}_{n2}(\bar{s}_1)} \int_{-\infty}^{\infty} d\bar{s}_0\ e^{i\bar{k}\hat{h}_{n1}(\bar{s}_0)} \\
\times\ J_1\,J_2\,J_3\ ,
\end{aligned}
\tag{A4.7}
$$

where

$$
J_1(\bar{s}_0,\ \bar{s}_1,\ \bar{s}_2) = \frac{\bar{k}}{2\pi} \int_{-\infty}^{\infty} d\theta_1\ e^{-i\bar{k}\,(\beta_1 - \beta_3)}\ , \tag{A4.8}
$$

$$
J_2(\bar{s}_1,\ \bar{s}_2) = \frac{\bar{k}}{2\pi} \int_{-\infty}^{\infty} d\theta_2\ e^{-i\bar{k}\,(\beta_2 - \beta_3)}\ , \tag{A4.9}
$$

and

$$J_3(\bar{x}_3,\ \bar{s}_0,\ \bar{s}_1,\ \bar{s}_2) = \frac{\gamma_L}{2\pi}\frac{1}{\sqrt{2\pi}}\int_{-\infty}^{\infty} d\xi\ \left[e^{-i\gamma_L \bar{s}_2 \xi}\right] \times \left[e^{i\bar{k}\beta_4(\overline{\delta x}_3 - \xi)}\, e^{-(\overline{\delta x}_3 - \xi)^2/2\overline{\Delta x}^2}\right] , \tag{A4.10}$$

with $\gamma_L = \bar{k}/\bar{Z} = k\ell^2/Z$. Substitution of (A4.6) in (A4.8) and (4.9) gives rise to

$$J_1 = \delta[\bar{s}_0 - d_2\,\bar{s}_1 - d_3\,\bar{s}_2 + b\,\hat{h}_{n2}'(\bar{s}_1) + b\,\hat{h}_{n3}'(\bar{s}_2)] , \tag{A4.11}$$

and

$$J_2 = \delta[\bar{s}_1 - (1 + d_3)\,\bar{s}_2 + b\,\hat{h}_{n3}'(\bar{s}_2)] , \tag{A4.12}$$

where $\delta(\bar{s})$ represents the Dirac delta function. We note that J_3 is in the form of a convolution integral. Compare this with (3.58). Applying the convolution theorem to (A4.10) as in Chap. 3 [cf. Eq. (3.60)], we obtain

$$J_3 = \frac{\overline{\Delta x}}{2\pi}\int_{-\infty}^{\infty} d\Omega\ e^{i\Omega(\bar{x}_3 - \bar{x}_{n3})}\,\delta(\bar{s}_2 + \frac{\Omega}{\gamma_L})\, e^{-\overline{\Delta x}^2(\bar{k}\beta_4 - \Omega)^2/2} . \tag{A4.13}$$

We now substitute (A4.11)-(A4.13) in (A4.7). The resulting equation contains three delta functions, and thus after the integration with respect to $\bar{s}_0$, $\bar{s}_1$ and $\bar{s}_2$, the parameters $\bar{s}_{l-1}$, ($l = 1, 2, 3$), are replaced by the corresponding expressions determined from the three delta functions. Let us denote the resulting expressions for $\bar{s}_{l-1}$ by $-\alpha_l$. It follows then that

$$I_L(\bar{x}_3) = \int_{-\infty}^{\infty} d\Omega\ e^{i\bar{x}_3\Omega}\,\tilde{I}_L(\Omega) , \tag{A4.14}$$

with

$$\tilde{I}_L(\Omega) = \frac{\overline{\Delta x}}{2\pi} \sum_n e^{-i\bar{x}_{n3}\Omega} e^{-\overline{\Delta x}^2[\Omega + g_n(\Omega)]^2/2} e^{-i\sum_{l=1}^{3} h_{nl}(\alpha_l)} , \tag{A4.15}$$

where

$$\begin{aligned} g_n(\Omega) &\equiv -\beta_4(\bar{s}_0 = -\alpha_1,\ \bar{s}_1 = -\alpha_2,\ \bar{s}_2 = -\alpha_3) \\ &= -\sum_{l=1}^{3} \bar{k}\,[c_l\,\bar{s}_{l-1} - \hat{h}_{nl}'(\bar{s}_{l-1})] , \end{aligned} \tag{A4.16}$$

and

$$\begin{aligned} \alpha_3 &= \Omega/\gamma_L \\ \alpha_2 &= (1 + d_3)\alpha_3 - b\,\hat{h}_{n1}'(\alpha_3) \\ \alpha_1 &= d_2\,\alpha_2 + d_3\,\alpha_3 - b\,\hat{h}_{n2}'(\alpha_2) - b\,\hat{h}_{n3}'(\alpha_3) . \end{aligned} \tag{A4.17}$$

In the derivation of the above equations, we have used the oddness of $\hat{h}_{nl}(\bar{s})$ $[= h_{nl}(\bar{s})/\bar{k}]$ and $\hat{h}_{nl}'(\bar{s})$ [cf. Eq. (A4.1)] and (A4.2)]. Replacing b and d_l in (A4.17) by $b = -\bar{Z} = -\bar{k}/\gamma_L$ and $d_l = 1 + bc_l = 1 - \bar{k}c_l/\gamma_L$ [cf. Eqs. (4.12) and (A4.4)], and using the definition of $\delta\phi_{nl}'(\bar{s}) = \frac{\partial}{\partial \bar{x}}\,\delta\phi(\bar{x},\ \bar{s})\big|_{\bar{x}=\bar{x}_{n,l-1}}$ [cf. Eqs. (4.43), (A4.1) and (A4.4)], i. e., $\delta\phi_{nl}'(\bar{s}) = \bar{k}\Delta_{nl}'\bar{s} + h_{nl}'(\bar{s}) = -\bar{k}[c_l\bar{s} - h_{nl}'(\bar{s})]$, we may rewrite (A4.16) and (A4.17) as:

$$g_n(\Omega) = \sum_{l=1}^{N} \delta\phi_{nl}'(\alpha_l) , \tag{A4.18}$$

and

$$\begin{aligned} \alpha_3 &= \Omega/\gamma_L \\ \alpha_2 &= \alpha_3 + [\Omega + \delta\phi_{n3}'(\alpha_3)]/\gamma_L \\ \alpha_1 &= \alpha_2 + [\Omega + \delta\phi_{n2}'(\alpha_2) + \delta\phi_{n3}'(\alpha_3)]/\gamma_L . \end{aligned} \tag{A4.19}$$

Now, we generalize this result to the N-layer problem. With the simplified notations, $\bar{x} = \bar{x}_N$ and $\bar{x}_n = \bar{x}_{nN}$, we obtain

$$I_L(\bar{x}) = \int_{-\infty}^{\infty} d\Omega \; e^{i\bar{x}\Omega} \tilde{I}_L(\Omega) \; , \tag{A4.20}$$

with

$$\tilde{I}_L(\Omega) = \frac{\overline{\Delta x}}{2\pi} \sum_n e^{-i\bar{x}_n\Omega} e^{-\overline{\Delta x}^2[\Omega + g_n(\Omega)]^2/2} e^{-i\sum_{l=1}^{N} h_{nl}(\alpha_l)} \; , \tag{A4.21}$$

where

$$g_n(\Omega) = \sum_{l=1}^{N} \delta\phi_{nl}'(\alpha_l) \; , \tag{A4.22}$$

and the recursive relation for α_l is given by

$$\begin{aligned} \alpha_N &= \Omega/\gamma_L \\ \alpha_l &= \alpha_{l+1} + [\Omega + \sum_{p=l+1}^{N} \delta\phi_{np}'(\alpha_p)] \, / \, \gamma_L \; . \end{aligned} \tag{A4.23}$$

[Calculations for $N = 4$ have been carried out, and the resulting expression is consistent with the generalized ones given above.]

Appendix A4.2 Higher-Order Approximation: W-K(II)

For convenience, the definitions for matrices T_{nl} and $\tilde{T}_{nl}$ given respectively by (4.23) and (4.26) in the text will be reproduced here:

$$T_{nl} \equiv \begin{bmatrix} a_l & b_l \\ c_l & d_l \end{bmatrix} = \begin{bmatrix} 1 & -\bar{Z} \\ -\Delta_{nl}' & 1+\bar{Z}\,\Delta_{nl}' \end{bmatrix} , \tag{A4.24}$$

and

$$\begin{aligned} \tilde{T}_{nl} &\equiv \begin{bmatrix} A_l & B_l \\ C_l & D_l \end{bmatrix} \\ &= T_{nl}\, T_{n,l+1} \cdots T_{nN} \ . \end{aligned} \tag{A4.25}$$

We note a few important properties of T_{nl} and $\tilde{T}_{nl}$. First, $|T_{nl}| = a_l d_l - b_l c_l = 1$, and thus $|\tilde{T}_{nl}| = 1$. Next, from the definition, i. e.,

$$\begin{bmatrix} A_l & B_l \\ C_l & D_l \end{bmatrix} = \begin{bmatrix} 1 & b \\ c_l & d_l \end{bmatrix} \begin{bmatrix} A_{l+1} & B_{l+1} \\ C_{l+1} & D_{l+1} \end{bmatrix} , \tag{A4.26}$$

where we simply let $a_l = 1$ and $b_l = b$ $(= -\bar{Z})$, one can show easily that

$$D_l = D_N + \sum_{p=l}^{N-1} c_p\, B_p = 1 + \sum_{p=l}^{N} c_p\, B_p \ , \tag{A4.27}$$

and the recursive relations for B_l and D_l,

$$\begin{aligned} &B_N = b \ , \quad D_N = d_N \\ &B_l = B_{l+1} + b\, D_{l+1} \\ &D_l = \frac{1}{b}\,(d_l\, B_l - B_{l+1}) \ . \end{aligned} \tag{A4.28}$$

Now, let $\delta\phi_{nl}'(\bar{s}) = \bar{k}\Delta_{nl}'\bar{s} + h_{nl}'(\bar{s}) \simeq \bar{k}\Delta_{nl}'\bar{s}$ $(= \bar{k}c_l\bar{s})$ and $\alpha_l = \left(\frac{\Omega}{\gamma_L}\right)\hat{\alpha}_l$ in (4.64) and (4.63). It follows then that

$$\begin{aligned} &\hat{\alpha}_N = 1 \\ &\hat{\alpha}_l = \hat{\alpha}_{l+1} + (1 + b \sum_{p=l+1}^{N} c_p\, \hat{\alpha}_p) \ , \end{aligned} \tag{A4.29}$$

and

$$g_n(\Omega) = (b \sum_{l=1}^{N} c_l \hat{\alpha}_l)\, \Omega \ . \tag{A4.30}$$

After a simple manipulation, we find

$$\hat{\alpha}_l = B_l/b = B_l/(-\bar{Z}) \ , \tag{A4.31}$$

and

$$g_n(\Omega) = (D_1 - 1)\, \Omega = (C_n - 1)\, \Omega \ , \tag{A4.32}$$

where (A4.27), (A4.28) and the definition of C_n, i. e., $C_n = D_1$ [cf. Eq. (4.32)], are used. To find an expression for $\tilde{I}_L(\Omega)$, we substitute (A4.32) and $\hat{\alpha}_l\Omega/\gamma_L$, respectively, for $g_n(\Omega)$ and α_l in (4.62). The result is that

$$\tilde{I}_L(\Omega) = \frac{\overline{\Delta x}}{2\pi} \sum_n \left[e^{-i\bar{x}_n\Omega}\, e^{-\overline{\Delta x}^2 C_n^2 \Omega^2/2} \right] \left[e^{-i\sum_{l=1}^{N} h_{nl}(\hat{\alpha}_l\Omega/\gamma_L)} \right] , \tag{A4.33}$$

where $\bar{x}_n$ is given by (4.33), and C_n ($= D_1$) and $\hat{\alpha}_l$ can be calculated from the recursive relations for D_l and $\hat{\alpha}_l$ [cf. Eqs. (A4.27) and (A4.31)]:

$$\begin{aligned} &\hat{\alpha}_N = 1 \ , \quad D_N = d_N \\ &\hat{\alpha}_l = \hat{\alpha}_{l+1} + D_{l+1} \\ &D_l = d_l\, \hat{\alpha}_l - \hat{\alpha}_{l+1} \ , \quad (d_l = 1 + \bar{Z}\, \Delta_{nl}') \ . \end{aligned} \tag{A4.34}$$

Appendix A4.3 Split-Step-Fourier Algorithm

The parabolic wave equation for a two-dimensional problem is given by [cf. Eq. (2.8)]:

$$\frac{\partial}{\partial \bar{z}} u(\bar{x},\ \bar{z}) = \left[\frac{i}{2\bar{k}} \frac{\partial^2}{\partial \bar{x}^2} + i\bar{k}\ \delta n(\bar{x},\ \bar{z}) \right] u(\bar{x},\ \bar{z}) \ , \tag{A4.35}$$

where the bar notations are used. Using the operator notations A and B such that

$$A = \frac{1}{2\bar{k}} \frac{\partial^2}{\partial \bar{x}^2} \quad , \quad B = \bar{k}\ \delta n(\bar{x},\ \bar{z}) \ , \tag{A4.36}$$

we may rewrite (A4.35) as

$$\frac{\partial u}{\partial \bar{z}} = i\,(A + B)\,u \ . \tag{A4.37}$$

We use the *split-step* algorithm to solve the above equation, i. e.,

$$\begin{aligned} u(\bar{x}, \bar{z} + \overline{\Delta z}) &= e^{\,i \int_{\bar{z}}^{\bar{z} + \overline{\Delta z}} (A+B)\, d\bar{z}'}\ u(\bar{x}, \bar{z}) \\ &\simeq e^{\,i\,\overline{\Delta z}\,(A+B)}\ u(\bar{x}, \bar{z}) \ , \end{aligned} \tag{A4.38}$$

which would be valid for a sufficiently small $\overline{\Delta z}$. If we now take the Fourier transform [cf. definition (3.78), (4.78) or (4.35)] of the above equation with respect to $\bar{x}$, then the operator A can be replaced by $-\,q^2/2\bar{k}$ and the result becomes

$$F_x\{u(\bar{x},\ \bar{z} + \overline{\Delta z})\} = e^{-iq^2 \overline{\Delta z}/2\bar{k}}\ F_x\left\{u(\bar{x},\ \bar{z})\, e^{i\bar{k}\ \delta n(\bar{x},\ \bar{z})\ \overline{\Delta z}}\right\} \ , \tag{A4.39}$$

which is called the *split-step-Fourier* algorithm [90, 91].

5. Concluding Remarks

The propagation of optical plane waves through a one-dimensional Gaussian phase screen and a two-dimensional Gaussian extended medium has been simulated numerically, and wave statistics, i. e., the normalized variance of irradiance σ_I^2 and the normalized covariance of irradiance $c_I(\bar{x})$, have been calculated from the data obtained by the numerical simulation. To realize a random medium instantaneously, we have used a simplified version of the random-motion model [77], and to compute irradiance for each realization of the medium we have used the wave-kinetic numerical method and/or the angular-spectral representation of the Huygens-Fresnel diffraction formula.

Several different levels of approximations are used for the wave-kinetic numerical method. The region of validity of those approximations has been studied by single-realization calculations. The Liouville approximation (the first order approximation) [W-K(LV)] is the simplest and is applicable to any configuration of inhomogeneities, but its region of validity is somewhat limited. It turns out that it is valid for $\zeta \lesssim 0.2$, where $\zeta = 2\phi_0/\gamma$ [see (3.17)]. We are able to introduce higher-order corrections to the first-order approximation. For a phase-screen problem, we can include all the higher-order terms in the phase difference [cf. Eqs. (3.50) and (4.43)], and the resulting expression (W-K) becomes equivalent to the Huygens-Fresnel formulation (H-F), which is exact within the validity of the thin-screen approximation. For an extended medium, however, there is an extra limitation, since we need to introduce an addi-

tional approximation to obtain a closed-form expression for irradiance (or irradiance spectrum). We have derived three different expressions of higher-order approximations, W-K(I), W-K(II) and W-K(III), which have different forms (or levels) of correction factors to the first-order approximation. The higher-order approximations can extend the region of validity about $2 \sim 6$ times (compared to the Liouville approximation): $\zeta \lesssim 0.5$, 0.9 and 1.2 for W-K(I), (II) and (III), respectively. This extension suffices to include strong refractive focusing effects.

For the Gaussian phase-screen problem, the statistical quantities $c_i(\bar{x})$ and σ_i^2 obtained by numerical simulation [with W-K for wave-propagation calculations] show excellent agreement with those from the existing analytical expressions [26] which can be integrated numerically without any difficulty. For the Gaussian extended-medium problem, there exists no analytical solution. However, Tur [50] has computed the fourth-order moment of the field, Γ_4, for several values of the extended-medium parameters, but these are different from the values used in our numerical simulation. The results from the wave-kinetic numerical method [W-K(I)] and the Huygens-Fresnel diffraction formula are compared to each other. Good agreements between the two have been observed.

Computing times for the expressions from the wave-kinetic numerical method and the Huygens-Fresnel formula are comparable. Finally, we note that the simplified model (together with the linear interpolation scheme for phase and angle calculations) reduces computing time considerably. It also allows simpler corrections to the lower-order approximations for the wave-kinetic numerical method, and application of the angular spectral representation of the Huygens-Fresnel diffraction formula to extended media, which turns out to be equivalent to the *split-step-Fourier* algorithm applied directly to the parabolic wave equation (with the simplified model for δn).

High computational costs force us to limit computation of wave statistics only to σ_I^2 and $c_I(\bar{x})$. In principle, we can predict the probability distribution of irradiance for various different values of the random-medium parameters, if sufficient data sets are available. The Gaussian spectrum of refractive-index used in this thesis has little physical significance. It has computational and analytical advantages because it implies the existence of only one scale size of irregularities and because manipulations with Gaussian functions are often analytically tractable. In general, physical irregularities require other spectral models, e. g. various power-law spectra within certain limiting wavenumbers. These imply a continuum of scale sizes, but the analysis may be simplified because such spectra can be approximated well by a weighted sum of Gaussians. Obviously, the number of numerical computations will increase, and this extension is not covered in the present thesis. Likewise, extensions to three-dimensional situations are relatively straight-forward analytically but represent appreciable complications in obtaining useful approximations for numerical computation as well as sizable increases in computer time. Finally, the treatment in this thesis can be extended to space-time correlations for some idealized situations, e. g. when Taylor's *frozen-in* hypothesis is valid.

Bibliography

1. A. Hewish, "The diffraction of radio waves in passing through a phase-changing ionosphere," *Proc. Roy. Soc. London, A 209,* 81-96, 1951.

2. R. P. Mercier, "Diffraction by a screen causing large random phase fluctuations," *Proc. Roy. Soc. London, A 58,* 382-400, 1961.

3. E. E. Salpeter, "Interplanetry scintillations. I. Theory," *Astrophys. J., 147,* 433-448, 1967.

4. R. W. Lee and J. C. Harp, "Weak scattering in random media with application to remote sensing," *Proc. IEEE, 57,* 375-406, 1969.

5. R. Buckley, "Diffraction by a random phase screen with very large r.m.s. phase deviation," *Aust. J. Phys., 24,* 351-371, 1971.

6. R. Buckley, "Diffraction by a random phase screen with very large r.m.s. phase deviation. II. Two-dimensional screen," *Aust. J. Phys., 24,* 373-396, 1971.

7. K. S. Gochelashvily and V. I. Shishov, "Laser beam scintillation beyond a turbulent layer," *Optica Acta, 18,* 313-320, 1971.

8. V. V. Tamoikin and A. A. Fraiman, "The intensity fluctuations of a wave beyond a random phase screen," *Radiofiz., 14,* 1427-1431, 1971.

9. I. G. Yakushkin, "Intensity fluctuations of the field of a plane wave behind a random phase screen," *Radiofiz., 17,* 1350-1356, 1973.

10. V. I. Shishov, "Frequency correlation of scintillations," *Radiofiz., 16,* 423-433, 1973.

11. V. H. Rumsey, "Scintillations due to a concentrated layer with a power-law turbulence spectrum," *Radio Sci., 10,* 107-114, 1975.

12. S. Bonazzola and L. M. Celnikier, "Pulsar scintillation revisited - The physically thin screen model," *Astro. & Astrophys., 45,* 185-192, 1975.

13. S. Bonazzola, L. M. Celnikier, and M. Chevreton, "A full mathematical analysis of the physically thin screen," *Astrophys. J., 219,* 690-699, 1978.

14. V. U. Zavorotnyi, "Strong fluctuations of wave intensity behind a randomly inhomogeneous layer," *Radiofiz., 22,* 508-511, 1979.

15. C. L. Rino, "A power law phase screen model for ionospheric scintillation. 1. Weak scatter," *Radio Sci., 14,* 1135-1145, 1979.

16. C. L. Rino, "A power law phase screen model for ionospheric scintillation. 2. Strong scatter," *Radio Sci., 14,* 1147-1155, 1979.

17. B. J. Uscinski, H. G. Booker, and M. Marians, "Intensity fluctuations due to a deep phase screen with a power-law spectrum," *Proc. Roy. Soc. London, A 374,* 503-530, 1981.

18. S. I. Belousov and I. G. Yakushkin, "Correlation of fluctuations in the intensity of a plane wave behind a strongly refracting chaotic phase screen," *Radiofiz., 24,* 945-951, 1981.

19. D. A. de Wolf, "Wave propagation through quasi-optical irregularities," *J. Opt. Soc. Am., 55,* 812-817, 1965.

20. D. A. de Wolf, "Point-to-point wave propagation through an intermediate layer of random anisotropic irregularities : phase and amplitude correlation functions," *IEEE Trans. Ant. Prop.*, 48-52, 1965.

21. K. C. Yeh and C. H. Liu, "Radio wave scintillations in the ionosphere (Review)," *Proc. IEEE, 70,* 324-360, 1982.

22. S. J. Franke, "The space-time intensity correlation function of scintillation due to a deep random phase screen," *Radio Sci., 22,* 643-654, 1987.

23. E. N. Bramley and M. Young, "Diffraction by a deeply modulated random-phase screen," *Proc. IEE, 114,* 553-556, 1967.

24. Y. I. Al'ber, L. M. Erukhimov, V. A. Ryzhov, and V. P. Uryadov, "Statistical properties of the fluctuations in wave intensity behind a random phase screen," *Radiofiz., 11,* 1371-1376, 1968.

25. M. Marians, "Computed scintillation spectra for strong turbulence," *Radio Sci., 10,* 115-119, 1975.

26. E. Jakeman and J. G. McWhirter, "Correlation function dependence of the scintillation behind a deep random phase screen," *J. Phys. A: Math. Gen., 10,* 1599-1643, 1977.

27. C. L. Rino, "Numerical computation for a one-dimensional power law phase screen," *Radio Sci., 15,* 41-47, 1980.

28. H. G. Booker and G. Majidiahi, "Theory of refractive scattering in scintillation phenomena," *J. Atmos. Terr. Phys., 43,* 1199-1214, 1981.

29. H. Bremmer, "Propagation of electromagnetic waves: (d) Influence of turbulence on wave propagation," in Handbuch der Physik, edited by S. Flugge, Springer-Verlag, Berlin, 1956.

30. L. A. Chernov, *Wave propagation in a random medium,* McGraw-Hill, New York, 1960.

31. V. I. Tatarski, *Wave propagation in a turbulent medium*, McGraw-Hill, New York, 1961.

32. V. I. Tatarski, *The effect of the turbulent atmosphere on wave propagation*, Israel Program for Scientific Translations, Jerusalem, 1971 (available as document TT 68-50464 from U. S. Dept. of Commerce, NTIS, Springfield, VA 22151).

33. J. W. Strohbehn ed., *Laser beam propagation in the atmosphere*, Springer-Verlag, New York, 1978.

34. A. Ishimaru, *Wave propagation and scattering in random media, vol. 2*, Academic Press, New York, 1978.

35. Yu. N. Barabanenkov, Yu. A. Kravtsov, S. M. Rytov, and V. I. Tatarski, "Status of the theory of propagation of waves in a randomly inhomogeneous medium (Review)," *Sov. Phys. Uspekhi, 13*, 551-680, 1971.

36. A. M. Prokhorov, F. V. Bunkin, K. S. Gochelashvily, and V. I. Shishov, "Laser irradiance propagation in turbulent media (Review)," *Proc. IEEE, 63*, 790-811, 1975.

37. R. L. Fante, "Electromagnetic beam propagation in turbulent media (Review)," *Proc. IEEE, 63*, 1669-1692, 1975.

38. P. L. Chow, "Perturbation methods in stochastic wave propagation," *SIAM Rev., 17*, 57-81, 1975.

39. M. Bertolotti, M. Carnevale, A. Consortini, and L. Ronchi, "Optical propagation: problems and trends (Review)," *Optica Acta, 26*, 507-529, 1979.

40. R. Dashen, "Path Integrals for waves in random media," *J. Math. Phys., 20*, 894-920, 1979.

41. R. L. Fante, "Electromagnetic beam propagation in turbulent media: An update (Review)," *Proc. IEEE, 68*, 1424-1443, 1980.

42. I. G. Yakushkin, "Intensity fluctuations during small-angle scattering of wave fields (Review)," *Radiofiz., 28*, 535-565, 1985.

43. J. W. Goodman, *Introduction to Fourier optics*, McGraw-Hill, New York, 1968.

44. D. Marcuse, *Light transmission optics*, Van Nostrand Reinhold, New York, 1979.

45. M. Born and E. Wolf, *Principles of optics*, Pergamon Press, New York, 1980.

46. I. M. Dagkesamanskaya and V. I. Shishov, "Strong intensity fluctuations during wave propagation in statistically homogeneous and isotropic media," *Radiofiz., 13*, 16-20, 1970.

47. W. P. Brown, Jr., "Fourth moment of a wave propagating in a random medium," *J. Opt. Soc. Am., 62*, 966-971, 1972.

48. C. H. Liu, A. W. Wernik, K. C. Yeh, and M. Y. Youakim, "Effects of multiple scattering on scintillation of transionospheric radio signals," *Radio Sci., 9*, 599-607, 1974.

49. V. I. Tatarski, A. S. Gurvich, B. S. Elepov, Vl. V. Pokasov, and K. K. Sabelfeld, "Space structure of strong intensity fluctuations of light in a turbulent medium," *Optica Acta, 26,* 531-542, 1979.

50. M. Tur, "Numerical solutions for the fourth moment of a plane wave propagating in a random medium," *J. Opt. Soc. Am., 72,* 1683-1691, 1982.

51. G. I. Marchuk et al., *Monte Carlo methods in atmospheric optics,* Springer-Verlag, New York, 1980.

52. L. H. Holway, Jr., "Multiple scattering from random plasma inhomogeneities," *Radio Sci., 8,* 681-697, 1973.

53. C. J. Funk, "Multiple scattering calculations of light propagation in ocean water," *Appl. Opt., 12,* 301-313, 1973.

54. H. R. Gordon, O. B. Brown, and M. M. Jacobs, "Computed relationships between the inherent and apparent optical properties of a flat homogeneous ocean," *Appl. Opt., 14,* 417-427, 1975.

55. L. Tsang and J. A. Kong, "Thermal microwave emission from half-space random media," *Radio Sci., 11,* 599-609, 1976.

56. H. L. Wilson and F. D. Tappert, "Acoustic propagation in random oceans using the radiation transport equation," *J. Acoust. Soc. Am., 66,* 256-274, 1979.

57. L. R. Poole, D. D. Venable, and J. W. Campbell, "Semianalytic Monte Carlo radiative transfer model for oceanographic lidar systems," *Appl. Opt., 20,* 3653-3656, 1981.

58. P. Bruscaglioni, G. Zaccanti, L. Pantani, and L. Stefanutti, "An approximate procedure to isolate single scattering contribution to lidar returns from fogs," *Int. J. Rem. Sens., 4,* 399-417, 1983.

59. E. Battistelli, P. Bruscaglioni, A. Ismaelli, and G. Zaccanti, "Use of two scaling relations in the study of multiple-scattering effects on the transmittance of light beams through a turbid atmosphere," *J. Opt. Soc. Am., A 2,* 903-911, 1985.

60. P. Beckmann, *Probability in communication engineering,* Harcourt, Brace & World, New York, 1967.

61. D. A. de Wolf, "Saturation of irradiance fluctuations due to turbulent atmosphere," *J. Opt. Soc. Am., 58,* 461-466, 1968.

62. D. A. de Wolf, "Are strong irradiance fluctuations lognormal or Rayleigh distributed ?," *J. Opt. Soc. Am., 59,* 1455-1460, 1969.

63. E. Jakeman and P. N. Pusey, "The statistics of light scattered by a random phase screen," *J. Phys.A: Math. Gen., 6,* L88-L92, 1973.

64. P. N. Pusey, D. W. Schaefer, and D. E. Koppel, "Single-interval statistics of light scattered by identical independent scatterers," *J. Phys. A.: Math. Nucl. Gen., 7,* 530-540, 1974.

65. D. A. de Wolf, "Waves in turbulent air: A phenomenological model," *Proc. IEEE, 62,* 1523-1529, 1974.

66. J. W. Strohbehn, T. I. Wang, and J. P. Speck, "On the probability distribution of line-of-sight fluctuations of optical signals," *Radio Sci., 10,* 59-70, 1975.

67. R. Barakat, "Sums of independent lognormally distributed random variables," *J. Opt. Soc. Am., 66,* , 211-216, 1976.

68. E. Jakeman and P. N. Pusey, "A model for non-Rayleigh sea echo," *IEEE Trans. Ant. Prop., AP-24,* 806-814, 1976.

69. A. Consortini and L. Ronchi, "Probability distribution of the sum of N complex random variables," *J. Opt. Soc. Am., 67,* 181-185, 1977.

70. D. L. Knepp and G. C. Valley, "Properties of joint gaussian statistics," *Radio Sci., 13,* 59-68, 1978.

71. L. R. Bissonnette and P. L. Wizinowich, "Probability distribution of turbulent irradiance in a saturation regime," *Appl. Opt., 18,* 1590-1599, 1979.

72. G. Parry and P. N. Pusey, "K distributions in atmospheric propagation of laser light," *J. Opt. Soc. Am., 69,* 796-798, 1979.

73. E. Jakeman, "Fresnel scattering by a corrugated random surface with fractal slope," *J. Opt. Soc. Am., 72,* 1034-1041, 1982.

74. G. C. Valley and W. P. Brown, "Intensity statistics for propagation through a turbulent layer," *Appl. Opt., 21,* 3002-3004, 1982.

75. L. C. Andrews and R. L. Phillips, "Mathematical genesis of the I-K distribution for random optical fields," *J. Opt. Soc. Am., A 3,* 1912-1919, 1986.

76. D. J. Link, R. L. Phillips, and L. C. Andrews, "Theoretical model for optical-wave phase fluctuation," *J. Opt. Soc. Am., A 4,* 374-378, 1987.

77. D. A. de Wolf, "A random-motion model of fluctuations in nearly transparent medium," *Radio Sci., 18,* 132-142, 1983.

78. A. Papoulis, *Probability, random variables, and stochastic processes,* McGraw-Hill, New York, 1984.

79. M. J. Levin, "Generation of a sampled Gaussian time series having a specfied correlation function," *IRE Trans. Inf. Theory,* 545-548, 1960.

80. J. N. Franklin, "Numerical simulation of stationary and non-stationary Gaussian random processes," *SIAM Rev., 7,* 69-80, 1965.

81. U. G. Gujar and R. J. Kavanagh, "Generation of random signals with specified probability density functions and power density spectra," *IEEE Trans. Auto. Cont.,* 716-719, 1968.

82. S. C. Liu, "Synthesis of stochastic representations of ground motions," *Bell Sys. Tech. J.,* 521-541, 1970.

83. S. T. Li and J. L. Hammond, "Generation of pseudorandom numbers with specified univariate distributions and correlation coefficients," *IEEE Trans. Sys. Man Cyber. (correspond.)*, 557-561, 1975.

84. P. T. D. Spanos, "Numerical simulation of a Van der Pol oscillator," *Comp. & Maths. with Appls.*, *6*, 135-145, 1980.

85. R. Buckley, "Diffraction by a random phase-changing screen : A numerical experiment," *J. Atmos. Terr. Phys.*, *37*, 1431-1446, 1975.

86. D. L. Knepp, "Multiple phase-screen calculation of the temporal behavior of stochastic waves," *Proc. IEEE*, *71*, 722-737, 1983.

87. C. L. Rino and J. Owen, "Numerical simulations of intensity scintillation using the power law phase screen model," *Radio Sci.*, *19*, 891-908, 1984.

88. S. J. Franke and C. H. Liu, "Space-time statistics of waves propagating through a deep phase screen," 1987.

89. H. A. DeFerrari, "Effects of horizontally varying internal wavefields on multiple interference for propagating through the deep sound channel," *J. Acoust. Soc. Am.*, *56*, 40-46, 1974.

90. S. M. Flatte and F. D. Tappert, "Calculation of the effect of internal waves on oceanic sound transmission," *J. Acoust. Soc. Am.*, *58*, 1151-1159, 1975.

91. R. H. Hardin and D. F. Tappert, "Applications of the split-step Fourier method to the numerical solution of nonlinear and variable coefficient wave equations," *SIAM Rev. (chronicle)*, *15*, 423, 1973.

92. E. Wigner, "On the quantum correction for thermodynamic equilibrium," *Phys. Rev.*, *40*, 749-759, 1932.

93. F. D. Tappert, "Derivation of the collisionless wave kinetic equation," *SIAM Rev. (chronicle)*, *13*, 281, 1971.

94. F. D. Tappert and I. M. Besieris, "Stochastic wave kinetic equation and its application to wave packet spreading," *URSI Symp. on Electromagnetic Wave Theory*, Tbilisi, USSR, Izadatel'stro Nauka, Sibirskoe Otdelenie, Novosibirsk, SSR, 230-234, 1971.

95. I. M. Besieris and F. D. Tappert, "Wave-packet spreading on a random transmission line," *J. Appl. Phys.*, *44*, 2119-2121, 1973.

96. I. M. Besieris and F. D. Tappert, "Properties of frequency modulated pulses in a randomly stratified media," *J. Math. Phys.*, *14*, 704-707, 1973.

97. I. M. Besieris and F. D. Tappert, "Kinetic equation for the quantized motion of a particle in a randomly perturbed potential field," *J. Math. Phys.*, *14*, 1829-1836, 1973.

98. I. M. Besieris and F. D. Tappert, "Stochastic wave kinetic theory in the Louville approximation," *J. Math. Phys.*, *17*, 734-743, 1976.

99. F. D. Tappert, "Diffractive ray tracing of laser beams," *J. Opt. Soc. Am., 66,* 1368-1373, 1976.

100. I. M. Besieris, "The wave-kinetic method, phase-space path integrals, and wave propagation in linear and nonlinear random media," VPI & SU, Tech. Rep. No. VPI-E-79-5, 1978.

101. H. Bremmer, "General remarks concering theories dealing with scattering and diffraction in random media," *Radio Sci., 8,* 511-534, 1973.

102. H. Bremmer, "The Wigner distribution and transport equations in radiation problems," *J. Appl. Sci. and Eng., A 3,* 251-260, 1979.

103. M. J. Bastiaans, "Transport equations for the Wigner distribution function," *Optica Acta, 26,* 1265-1272, 1979.

104. M. J. Bastiaans, "Transport equations for the Wigner distribution function in an inhomogeneous and dispersive medium," *Optica Acta, 26,* 1333-1344, 1979.

105. M. J. Bastiaans, "The Wigner distribution function approach to optical signal and systems," *Opt. Comm., 25,* 26-30, 1978.

106. N. Marcuvitz, "Quasiparticle view of wave propagation," *Proc. IEEE, 68,* 1380-1395, 1980.

107. R. Bamler and H. Glunder, "The Wigner distribution function of two-dimensional signals: Coherent-optical generation and display," *Optica Acta, 30,* 1789-1803, 1983.

108. R. C. Brown and E. J. Heller, "Classical trajectory approach to photodissociation : The Wigner method," *J. Chem. Phys., 75,* 186-188, 1981.

109. D. A. de Wolf, "Computer simulation of electron beams II: low-cost beam-current reconstruction," *J. Appl. Phys., 58,* 3697-3702, 1985.

110. D. A. de Wolf and J. K. Pack, "Wave-kinetic numerical approach to propagation of optical beams," *J. Opt. Soc. Am., A 3,* 532-535, 1986.

111. J. K. Pack and D. A. de Wolf, "A wave-kinetic numerical approach to propagation of optical beams II," *J. Opt. Soc. Am., A 3,* 1766-1771, 1986.

112. J. K. Pack, *A wave-kinetic numerical method for the propagation of optical waves,* MS thesis, VPI & SU, 1985.

113. R. Piessens and M. Branders, "Computation of oscillating integrals," *J. Comp. Appl. Math., 1,* 153-164, 1975.

114. G. M. Jenkins and D. G. Watts, *Spectral analysis and its applications.* Holden-day, San Francisco, 1968.

115. D. A. de Wolf, "Depolarization term of the wave equation," *J. Opt. Soc. Am, 69,* 1313-1314, 1979.

116. F. D. Tappert, "The parabolic approximation method," in Wave propagation and underwater acoustics, edited by J. B. Keller and J. Papadakis, Springer-Verlag, Berlin, 1977.

117. M. Abramowitz and I. A. Stegun, *Handbook of mathematical functions*, Dover, New York, 1972.

118. G. Arfken, *Mathematical methods for physicists*, Academic Press, New York, 1985.

119. C. R. Chester, *Techniques in partial differential equations*, McGraw-Hill, New York, 1971.

120. J. D. Jackson, *Classical electrodynamics*, John Wiley & Sons, New York, 1975.

121. S. Frankenthal, M. J. Beran, and A. M. Whitman, "Caustic corrections using coherent theory," *J. Acoust. Soc. Am.*, *71*, 348-358, 1982.

122. J. J. McCoy and M. J. Beran, "Propagation of beamed signals through inhomogeneous media: A diffraction theory," *J. Acoust. Soc. Am.*, *59*, 1142-1149, 1976.

123. G. E. P. Box and G. M. Jenkins, *Time series analysis*, Holden-day, San Francisco, 1970.

The vita has been removed from the scanned document